

RICE UNIVERSITY

**Regulated Release of a Novel Non-viral Gene Delivery Vector from
Electrospun Coaxial Fiber Mesh Scaffolds**

by

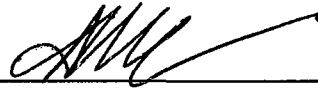
Anita Saraf

A THESIS SUBMITTED

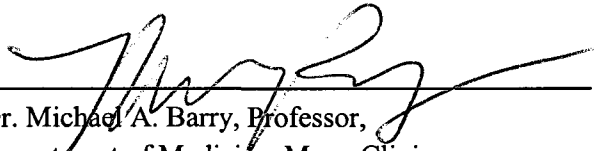
IN PARTIAL FULFILLMENT OF THE
REQUIREMENTS FOR THE DEGREE

Doctor of Philosophy

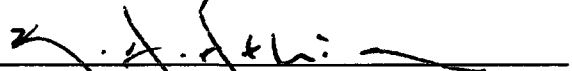
APPROVED, THESIS COMMITTEE:



Dr. Antonios G. Mikos, (Chair), Louis Calder Professor,
Bioengineering, Rice University



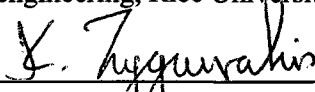
Dr. Michael A. Barry, Professor,
Department of Medicine, Mayo Clinic



Dr. Kyriacos Athanasiou, Karl F. Hasselmann Professor,
Bioengineering, Rice University



Dr. K. Jane Grande-Allen, Associate Professor,
Bioengineering, Rice University



Dr. Kyriacos Zyggourakis, A.J. Hartsook Professor,
Chemical and Biomolecular Engineering, Rice University

Houston, TX
June 2009

UMI Number: 3421194

All rights reserved

INFORMATION TO ALL USERS

The quality of this reproduction is dependent upon the quality of the copy submitted.

In the unlikely event that the author did not send a complete manuscript and there are missing pages, these will be noted. Also, if material had to be removed, a note will indicate the deletion.



UMI 3421194

Copyright 2010 by ProQuest LLC.

All rights reserved. This edition of the work is protected against unauthorized copying under Title 17, United States Code.



ProQuest LLC
789 East Eisenhower Parkway
P.O. Box 1346
Ann Arbor, MI 48106-1346

Abstract

Regulated Release of a Novel Non-Viral Gene Delivery Vector from Electrospun Coaxial Fiber Mesh Scaffolds

by

Anita Saraf

The development of novel strategies for tissue engineering entails the evolution of biopolymers into multifunctional constructs that can support the proliferation of cells and stimulate their differentiation into functional tissues. With that in mind, biocompatible polymers were fabricated into a novel gene delivery agent as well as three dimensional scaffolds that act as reservoirs and controlled release constructs. To fabricate a novel gene delivery agent a commercially available cationic polymer, poly(ethylenimine), PEI, was chemically conjugated to a ubiquitous glycosaminoglycan, hyaluronic acid (HA). The novel polymer, PEI-HA, had significantly reduced toxicity and improved transfection efficiency with multipotent human mesenchymal stem cells. This transfection efficiency could further be modulated by changing the concentration of sodium chloride and temperature used to assemble PEI-HA/DNA complexes. To facilitate the regulated delivery of these complexes in the context of tissue engineering, an emerging technology for scaffold fabrication, coaxial electrospinning was adapted to include PEI-HA and plasmid DNA within the scaffold fibers. Initially, a factorial design

was employed to assess the influence of processing parameters in the absence of gene delivery vectors and plasmids. The study elucidated the role of sheath polymer concentration and core polymer concentration and molecular weight and the presence of sodium chloride on fiber diameters and morphologies. Subsequently, PEI-HA and plasmid DNA were entrapped within the sheath and core compartments of these fibers and the influence of processing parameters was assessed in the context of fiber diameter, release kinetics and transfection efficiency over a period of 60 days. The release of PEI-HA was found to be dependent upon the loading dose of the vector and plasmid. However, the transfection efficiency correlated to the core polymer properties, concentration and molecular weight. The processing parameters could modulate cell transfection for up to 21 days and continue to transfect cells for up to 60 days. Thus, scaffolds with tunable release kinetics and transfection efficiencies can be fabricated using coaxial electrospinning, which can further be used for tissue engineering and gene delivery applications.

Acknowledgements

This thesis is dedicated to my grandparents Prabhakar and Sudha Lingras who inspired my love for science, encouraged me to ask questions – and pushed me to find their answers.

This work was made possible by grants provided by the *National Institutes of Health, the National Science Foundation* and the *Medical Scientist Training Program at Baylor College of Medicine.*

These last five years have been a rich educational experience in academic research. I had the opportunity to formulate my own research plan, design and carry out novel and challenging experiments. In the process, I learned to appreciate the importance of collaboration, networking and grant writing. I profoundly thank *Dr. Antonios Mikos* for the opportunities he has given me. His influence will guide my career for the rest of my life.

I'd also like to extend special thanks to my committee members *Drs. Athanasiou, Zygorakis, Grande-Allen and Barry* who have provided valuable advice to me during my training here

The studies described in this thesis required the collective minds, efforts and instruments of numerous people at Rice and other institutions at the medical center. What follows is a sampling of those that have provided the greatest support and whom I would like to personally thank.

Dr. Michael Barry, who has been my co-advisor as part of the NSF-IGERT grant and helped in the planning and execution of the transfection studies carried out during my thesis-work.

Dr. K. Jane Grande-Allen for personally taking time to teach me experimental techniques and for being so willing to help me with numerous aspects of my experiments.

Drs. Sean Moran and Dr. Lawrence Alemany for their help with running and analyzing NMR spectra.

Dr. Joel Moake for the use of the flow cytometer in his laboratory and for the discussions that helped guide me towards a career in cardiology. *Nancy Turner and Leticia Nolasco* from the Moake research group for their assistance with flow cytometry and for sharing their cell culture facility.

Dr. L. Scott Baggett for his instruction and guidance on statistical analysis and for patiently answering my statistics related questions.

Dr. Robert Raphael for his help with confocal analysis and use of the confocal microscope.

Drs. Junghae Suh and Michael Diehl for eagerly making room for me in their laboratories for plasmid amplification and purification.

Dr. David Engler for allowing the use of his light scattering instruments and for the engaging discussions that accompanied my time in his laboratory.

Dr. Rebecca Richards-Kortum and her laboratory members for allowing the use of their dynamic light scattering instrument.

I would also like to acknowledge the Medical Scientist Training Program at Baylor College of Medicine for giving me the opportunity to study with distinguished faculty of Rice University.

Dr. Sharon Plon for her support and her invaluable role as a mentor throughout my training.

Kathy Crawford and *Vanessa Hathfield* for being ongoing and indispensable sources of support.

While my graduation from the program promises many opportunities, it also saddens me greatly that I will no longer be working as closely with my *friends in the Mikos Laboratory* who are a part of my life in so many ways, and whose friendship and advice I value, respect and trust.

I would like to thank my parents, *Drs. Pradeep and Neelima Saraf*, for providing me with the opportunities that allow me to accomplish all that I can.

Above all, I would like to thank my husband and best friend *Jason Smith*, who has supported and encouraged me unconditionally, continues to support my being “in school” for the indefinite future and knows how to make me smile even when nothing is going right.

Table of Contents

ABSTRACT	II
ACKNOWLEDGEMENTS.....	IV
TABLE OF CONTENTS.....	VII
LIST OF FIGURES	X
LIST OF TABLES	XII
CHAPTER I.....	1
OBJECTIVES AND SPECIFIC AIMS.....	1
CHAPTER II.....	4
BACKGROUND: GENE DELIVERY FOR CARTILAGE REGENERATION: STRATEGIES AND CONSIDERATIONS	4
ABBREVIATIONS.....	5
INTRODUCTION	6
CANDIDATE CELLS FOR GENE DELIVERY.....	8
<i>Autologous Chondrocytes.....</i>	<i>9</i>
<i>Chondroprogenitor Cells.....</i>	<i>10</i>
<i>Cells within the Synovial Cavity.....</i>	<i>12</i>
<i>Transforming Growth Factor β.....</i>	<i>14</i>
<i>Bone Morphogenic Proteins.....</i>	<i>15</i>
<i>Other Anabolic Gene Candidates.....</i>	<i>19</i>
<i>Anti-inflammatory Agents.....</i>	<i>19</i>
CANDIDATE GENE DELIVERY VECTORS.....	20
<i>Viral Vectors.....</i>	<i>20</i>
<i>Non-viral Vectors.....</i>	<i>23</i>
SCAFFOLDS USED FOR GENE DELIVERY	23
<i>Multi-layered Scaffolds</i>	<i>25</i>
CONCLUDING REMARKS	26
FIGURES	27
TABLES	29
CHAPTER III.....	31
SYNTHESIS AND CONFORMATIONAL EVALUATION OF A NOVEL GENE DELIVERY VECTOR FOR HUMAN MESENCHYMAL STEM CELLS	31
ABSTRACT.....	31
ABBREVIATIONS.....	32
INTRODUCTION	34
EXPERIMENTAL PROCEDURES	36
<i>Materials</i>	<i>36</i>
<i>Synthesis of PEI-HA</i>	<i>36</i>
<i>Nuclear Magnetic Resonance Analysis</i>	<i>37</i>
<i>Fluorescence Assisted Carbohydrate Electrophoresis (FACE).....</i>	<i>38</i>

<i>Electrophoresis Band Retardation</i>	39
<i>Dynamic and Static Light Scattering</i>	40
<i>Cell Viability Studies</i>	42
<i>Transfection Studies</i>	42
<i>Statistical Analysis</i>	45
RESULTS	46
<i>Synthesis and NMR Spectroscopy</i>	46
<i>Fluorescence Assisted Carbohydrate Electrophoresis (FACE)</i>	47
<i>Electrophoresis Band Retardation</i>	48
<i>Dynamic Light Scattering</i>	49
<i>Static Light Scattering</i>	49
<i>Cell Viability Studies</i>	50
<i>Transfection Studies</i>	50
DISCUSSION	52
CONCLUSION.....	57
FIGURES	58
TABLES	65
CHAPTER IV	70
FABRICATION OF NON-WOVEN COAXIAL FIBER MESHES BY ELECTROSPINNING.....	70
ABSTRACT.....	70
ABBREVIATIONS.....	71
INTRODUCTION	71
<i>Experimental Procedures</i>	75
<i>Polymer Solution for Fiber Sheath</i>	75
<i>Polymer Solution for Fiber Core</i>	75
<i>Factorial Analysis of Variables</i>	75
<i>Electrospinning Apparatus Setup</i>	76
<i>Analysis of Fiber Morphology</i>	77
<i>Analysis of Fibers on Incubation in Aqueous Medium</i>	79
<i>Statistical Analysis</i>	79
RESULTS AND DISCUSSION.....	80
<i>Variation in the Distribution of Fiber Diameters</i>	81
<i>Influence of Poly(ethylene glycol)Molecular Weight on Fiber Morphology</i>	84
<i>Influence of Poly(ethylene glycol) Concentration on Fiber Morphology</i>	85
<i>Influence of Salt (Sodium Chloride) Concentration on Fiber Morphology</i>	86
CONCLUSION.....	87
FIGURES	89
TABLES	99
CHAPTER V	102
REGULATED NON-VIRAL GENE DELIVERY FROM COAXIAL ELECTROSPUN FIBER MESHES	102
ABSTRACT.....	102
ABBREVIATIONS.....	103
INTRODUCTION	104
MATERIALS AND METHODS	108
<i>Materials</i>	108

<i>Synthesis of Rhodamine Tagged PEI-HA</i>	108
<i>Plasmid Amplification</i>	109
<i>Fabrication of Coaxial Electrospun Scaffolds</i>	110
<i>Scanning Electron Microscopy Analysis of Fiber Diameters</i>	112
<i>Release and Quantification</i>	112
<i>Cell Line and Cell Culture</i>	114
<i>Cell Transfection and Reporter Gene Expression</i>	114
<i>Reporter Gene Expression of Cells Seeded on Coaxial Fiber Meshes</i>	115
<i>Statistics</i>	116
RESULTS	116
<i>Fiber Distribution of Electrospun Coaxial Scaffolds</i>	116
<i>Release of r-PEI-HA</i>	118
<i>Transfection Efficiency of Released pDNA in 2D Cultures</i>	118
<i>Transfection of Cells Seeded onto Coaxial Electrospun Fiber Mesh Scaffolds</i>	119
DISCUSSION	119
CONCLUSIONS	126
FIGURES	127
TABLES	136
SUPPLEMENTAL DATA	139
CHAPTER VI	143
SUMMARY	143
CHAPTER VII	147
BIBLIOGRAPHY	147

List of Figures

Figure 2.1:	Schematic for ex-vivo gene delivery.....	27
Figure 2.2:	Schematic of Knee Joint.....	28
Figure 3.1:	Reaction scheme to conjugate branched polyethyleneimine (PEI) and hyaluronic acid (HA) by the process of reductive amination.....	58
Figure 3.2:	NMR spectra of PEI-HA and HA.....	59
Figure 3.3:	Fluorescence Assisted Carbohydrate Electrophoresis (FACE) of PEI-HA.....	60
Figure 3.4:	Agarose gel electrophoresis representing pDNA binding studies with PEI-HA and PEI.....	61
Figure 3.5:	Dynamic light scattering distribution for PEI-HA/pDNA complexes.....	62
Figure 3.6:	Cell viability at 24 and 72 h after exposure to polymers PEI and PEI-HA.....	63
Figure 3.7:	Transfection efficiency of PEI-HA and PEI on hMSCs represented with expression of green fluorescent protein.....	64
Figure 4.1:	The electrospinning setup.....	90
Figure 4.2:	Confocal microscopy and corresponding SEM images of the coaxial electrospun microfibers.....	92
Figure 4.3:	Distribution of coaxial electrospun PCL/PEG fibers.....	94
Figure 4.4:	Distribution of coaxial electrospun PCL/PEG fibers.....	95
Figure 4.5:	Effect of immersion in PBS on coaxial fibers.....	96
Figure 4.6:	Main effects of processing parameters on fiber diameters.....	98
Figure 5.1:	Main effects of PCL Conc., PEG MW, PEG Conc., and pDNA Conc. on average total fiber diameter of electrospun coaxial fiber meshes.....	127

Figure 5.2:	Fiber diameter distribution within electrospun coaxial meshes immediately after fabrication and after immersion and agitation in PBS for 7 days.	128
Figure 5.3:	Cumulative release of rhodamine-tagged PEI-HA (r-PEI-HA) from electrospun coaxial fiber meshes.....	129
Figure 5.4:	Main effects of PCL Conc., PEG MW, PEG Conc., and pDNA Conc. on r-PEI-HA release.	130
Figure 5.5:	Transfection efficiency of released pDNA in 2D cultures of fibroblast-like cells over a period of 60 days.	132
Figure 5.6:	Main effects of PCL Conc., PEG MW, PEG Conc., and pDNA Conc. on cell transfection efficiency	133
Figure 5.7:	Expression of EGFP by cells seeded on electrospun fiber mesh scaffolds.....	135

List of Tables

Table 2.1:	Comparison of secreted IGF-1 after gene delivery.....	29
Table 2.2:	Cells, gene delivery vectors and genes thus far used for cartilage regeneration.....	30
Table 3.1:	Range and averages of hydrodynamic radii (Rh) obtained with PEI-HA at different salt concentrations	65
Table 3.2:	Distribution and peak intensities describing the range of hydrodynamic radii (Rh) observed with DLS for PEI-HA/pDNA complexes.....	66
Table 3.3:	Representative molecular weights of PEI-HA/pDNA complexes at different salt concentrations and temperatures.....	67
Table 3.4:	Gene delivery efficiency of PEI and PEI-HA.	68
Table 3.5:	Percentage of cells transfected by PEI-HA/DNA complexes at different NaCl concentrations and temperatures.....	69
Table 4.1:	Parameters used in formulating fractional factorial experimental design	99
Table 4.2:	Distribution of coaxial fiber diameters before and after immersion in PBS.....	100
Table 4.3:	Main effects of evaluated parameters on coaxial fiber diameters..	101
Table 5.1:	Fractional factorial experimental design for fabrication of coaxial electrospun fiber mesh scaffolds.....	136
Table 5.2:	Percentage of r-PEI-HA released per day	137
Table 5.3:	Average transfection efficiencies over 60 days for 8 groups of coaxial electrospun fiber mesh scaffolds	138

Chapter I

Objectives and Specific Aims

1. Synthesis and Conformational Evaluation of cationic gene delivery vector PEI-HA and its complexes with DNA.

- Synthesis of chemical conjugate of cationic gene delivery vector branched poly(ethylenimine) (PEI) and hyaluronic acid (HA).
- Evaluation of hydrodynamic radius (Rh) of vector PEI-HA with changing concentrations of NaCl (from 150 mM to 500 mM of NaCl) by dynamic light scattering (DLS).
- Evaluation of the effect of temperature (ambient and physiological) on Rh of PEI-HA/DNA complexes.
- Evaluation of the weight of PEI-HA/DNA complexes with static light scattering at a range of NaCl concentrations and physiological and room temperature.
- Evaluation of cytotoxicity of PEI-HA on human mesenchymal stem cells (hMSCs) and comparison of cytotoxicity with PEI.
- Evaluating the transfection efficiency of PEI-HA/DNA complexes at different NaCl concentrations and temperatures. Correlating the transfection efficiency to Rh data obtained above.

- Comparing transfection efficiency of PEI-HA/DNA with PEI/DNA with hMSCs at different plasmid concentrations.

2. Synthesis and Characterization of Coaxial PCL/PEG Scaffolds with an Aqueous PEG and Organic PCL Sheath.

- Establishing an apparatus and setup for coaxial electrospinning with allows for easy control of the flow rates of solutions of polymers PCL and PEG.
- Determining the range of processing parameters that influence the inner and outer fiber diameters of coaxial fibers.
- Formulating a full factorial design that evaluates the influence of PCL (sheath) polymer concentration, PEG (core) polymer concentration and molecular weight and NaCl concentration within the core.
- Fabricating 16 different groups of coaxial fiber scaffold mats to evaluate the effects of the parameters on inner, outer and total fiber diameter of coaxial scaffolds.
- Evaluation of fiber dimensions (inner, outer and total fiber diameters) using confocal microscopy and scanning electron microscopy (SEM).
- Evaluating the effects of the processing parameters on inner, outer and total fiber diameters using the full factorial design formulated above.

3. Regulated Release of PEI-HA and Plasmid DNA from Coaxial Fiber Meshes.

- Formulation of a fractional factorial design to evaluate the influence of processing parameters on the release of rhodamine tagged PEI-HA. The parameters for evaluation include PCL (sheath) polymer concentration, PEG (core) polymer concentration and molecular weight and the loading dose of PEI-HA and pDNA.
- Fabrication of 8 different groups of coaxial scaffolds with PEI-HA within the fiber sheath and reporter gene green fluorescent protein (GFP) spun into the core of the coaxial fibers.
- Evaluating the influence of processing parameters on fiber diameter.
- Evaluating the release kinetics of PEI-HA from coaxial scaffolds for up to 60 days.
- Evaluating the bioactivity of the plasmid-vector released from coaxial scaffolds by transfecting fibroblast cells in 2D cultures.
- Evaluating the transfection capability on cells directly seeded onto coaxial electrospun scaffolds.

Chapter II

Background: Gene Delivery for Cartilage Regeneration: Strategies and Considerations¹

Abstract

Tissue engineering is a multifaceted technology developed with a purpose of regenerating complex tissues and organs. Cartilage regeneration continues to challenge engineers and a new wave of efforts focus on developing strategies that provide sustained stimulation to cells by growth factors and other biological molecules to promote their differentiation into chondrocytes. Though significant research is dedicated to developing controlled release systems that deliver growth factors directly, a simpler approach to resolving this dilemma involves converting cells into protein producing factories. This is done through gene delivery. Gene therapy studies published for articular diseases such as rheumatoid and osteoarthritis provide valuable information regarding different types of cells, gene delivery vectors and genes that can potentially be used to regenerate cartilage. Tissue engineering approaches provide the opportunity to combine two or more strategies used for gene therapy thus far and create a cohesive system that addresses both cartilage degeneration and synthesis simultaneously. Adopting gene transfer techniques for tissue

¹ Sections of this chapter have been published as follows: Saraf A, Mikos AG. "Gene delivery strategies for cartilage tissue engineering" *Adv Drug Deliv Rev.* 2006 Jul 7;58(4):592-603

engineering is a relatively novel approach, as non-viral gene delivery vectors are continually optimized for therapeutic purposes, and reservations about viral vectors have increasingly dampened their appeal. However, every element involved in gene transfection (i.e., the cell, vector and gene) is a variable which decides the physiological and biomechanical properties of the cartilage produced, and significant work still needs to be done in understanding the contribution of each of these factors to cartilage regeneration.

Abbreviations

BMP-2	Bone Morphogenic Protein 2
BMP-7	Bone Morphogenic Protein 7
CDC	Center for Disease Control and Prevention
cDNA	complementary Deoxyribonucleic Acid
ECM	Extracellular Matrix
GFP	Green Fluorescent Protein
IGF-1	Insulin-like Growth Factor 1
IL- 4	Interleukin 4
IL-1 RA	Interleukin 1 Receptor Antagonist
IL-10	Interleukin 10
IL-13	Interleukin 13
MMP	Matrix Metalloproteinase
MSC	Mesenchymal Stem Cell/ Marrow Stromal Cell

PGA	Poly(glycolic acid)
SMADs	Smooth Muscle Actin (SMA) and Mitotic spindle Assembly checkpoint (MAD) proteins.
TGF- β	Transforming Growth Factor β
TGF- β 1	Transforming Growth Factor β 1
TGF- β 2	Transforming Growth Factor β 2
TGF- β 3	Transforming Growth Factor β 3
TIMP	Tissue Inhibitors of Matrix Metalloproteinase
TIMP-1	Tissue Inhibitor of Matrix Metalloproteinase 1
TIMP-3	Tissue Inhibitor of Matrix Metalloproteinase 3
TNF- α	Tumor Necrosis Factor α

Introduction

Of all the organs targeted for tissue engineering, one could argue that cartilage would be one of the easiest to regenerate. Cartilage is one of the few avascular tissues in the body and is composed of a single cell type – the chondrocyte, which eliminates the need to address two critical problems in tissue engineering – angiogenesis and creation of multilayered tissues derived from cells of multiple lineages. Yet, cartilage tissue engineering is hardly dismissed as trivial and very few successful animal models for cartilage regeneration have progressed to clinical trials. According to the 2002 National Health Interview Survey conducted by the Center for Disease Control and Prevention (CDC), 43 million Americans have some form of arthritis of which 16 million report

related limitations in activity^{1,2} More than 500,000 cartilage repair procedures are performed every year^{3,4,5}. Perhaps nothing reflects the impact of cartilage related diseases to our society as clearly as the \$86 billion that the CDC estimates are annually lost in direct and indirect costs related to their treatment. “Treatment” of these disorders continues to rely heavily on analgesics, although the past few years have seen notable advances in surgical techniques. However, considering the limited regenerative capacity of cartilage, surgical interventions, at best, temporarily mask some of the symptoms without addressing the underlying pathology. This makes it a less viable option for younger patients. In recognition of this, clinicians are trying to incorporate cell transplantation and artificial matrices as treatment options, as they have been clinically proven to give better long term results^{6,7}. Tissue engineering research continues to enhance the effectiveness of these treatments by including the use of growth factors and cytokines with the aim of decreasing damage to the surrounding tissue and regenerating tissue that more accurately resembles native cartilage.

Although various biological factors have been independently identified as necessary for reducing inflammation or promoting regeneration, it is becoming increasingly obvious that careful orchestration of the dose and type of numerous biological factors is essential to optimize this process. The challenge now lies in developing delivery systems that recognize this complexity in delivery of biological agents. The direct delivery of these agents either systemically or locally has numerous limitations. Biological agents have a half life in the order of minutes, which requires high doses of delivery and repeated administration. Furthermore, concentrations that are therapeutic to one organ

may damage another. These problems related to targeting of multiple biological agents and their dose regulation can be solved by creating cells that are modified to transiently over-express certain proteins. *Ex vivo* transfection, where cells are initially isolated from a joint, transfected with the gene of interest and injected back into the joint, cleverly augments autologous cell transplant, a clinical procedure that is approved and widely used (Figure 2.1). Though gene therapy for cartilage regeneration is still in its infancy, one can imagine that in the near future a treatment protocol might involve introduction of multiple cell populations at different time points, each expressing a different protein of interest working in synergy to control inflammation and encourage regeneration. This review article addresses studies related to gene delivery that have thus far been documented, with the aim of understanding the limitations and potential of gene delivery for cartilage regeneration.

Candidate Cells for Gene Delivery

Cartilage defines the skeletal outline of a developing embryo. As the embryo develops most of the cartilage is converted to bone. However, cartilaginous tissue continues to subsist at the ends of bones and functions as a cushion, thus preventing friction between them. Figure 2.2 is a schematic of the knee joint. Not all cartilage tissues are identical and there is just as much heterogeneity within the cartilage as there is between them. Cartilage is classified into three main categories – elastic cartilage found in the external ear, fibrocartilage that is found in the intervertebral discs and hyaline cartilage which is present between articular surfaces. As hyaline cartilage constitutes the

most abundant type of cartilage, and is commonly affected in arthritic disorders, most tissue engineering models focus on regeneration of articular cartilage – which is a type of hyaline cartilage (Figure 2.2). The mechanical and biochemical properties of the cartilage are defined by its extracellular matrix (ECM), all of which is secreted by cells that occupy 2% of the total volume. Consequently, the chondrocytes are immobilized within the thick ECM.

Autologous Chondrocytes

An obvious choice for gene delivery would be chondrocytes, the cells that secrete cartilaginous matrix that defines the cartilage. Gene delivery approaches for tissue engineering of cartilage seldom target the chondrocytes *in vivo*, as these cells are inaccessible to vectors due to the rich matrix that surrounds them. Instead, autologous chondrocytes harvested from joints and expanded *in vitro* in monolayers are preferably used for transfection. The primary drawback to using autologous cells is that they lose their chondrocytic phenotype to become fibroblastic when grown *in vitro* in monolayer as early as after the first passage of cells^{8,9}. This limits the quantity of cells that can be used for transfection and implantation. In arthritic joints, this population of chondrocytes is further limited. Since cartilage is an aneural tissue, initial damage to the cartilage cannot be perceived by the patient. Focal cartilage injuries expand with time and use and lead to a more generalized cartilage loss that reaches the subchondral bone. Only when the damage is significant causing the patient to be immobilized do physicians seek surgical intervention. Furthermore, even during the very early stages of arthritis or other

joint disorders, there is a significant change in the phenotype of the chondrocytes. Chondrocytes undergo significant changes in their cell surface markers as well as accelerate their production of extracellular matrix molecules to keep up with the damage caused to their surrounding tissue¹⁰. Gradually the biosynthetic machinery of the cell fails to keep up with the anabolic demands of the tissue and the chondrocytes undergo apoptosis causing loss of cartilage. Considering the circumstances which lead to the death of the chondrocyte, it would be impractical to further overburden the cells by forcing them to express additional genes.

Chondroprogenitor Cells

Mesenchymal stem cells (MSCs) are increasingly being preferred to autologous chondrocytes as better alternatives for cell transplant. Large quantitative of autologous MSCs can be extracted by minimally invasive techniques from the iliac crest of the patient, and other populations of MSCs are found in blood, and in the periostium. MSCs are multipotent cells with the capacity to regenerate into numerous cells lines including chondrocytes although MSCs from different sources in the body may have different potentials of multipotency. Wakitani et al. pioneered the use of bone marrow derived MSCs for cartilage regeneration when they used cells from New Zealand white rabbits in full thickness cartilage defects¹¹. The cells were saturated in collagen sponges that were embedded into the defect. Even in the absence of additional growth factors, the MSCs secreted a cartilagenous matrix that was converted to bone in subchondral regions of the defect. Although the regenerated cartilage had inferior mechanical properties and

appeared to be discontinuous with the host tissue, the study established that cells other than chondrocytes could be used for cartilage regeneration¹². Subsequent studies have emphasized the need to stimulate MSCs with appropriate chondrogenic factors or inductive material. BMP-2, BMP-7, IGF-1 and a variety of recombinant proteins have produced better results at regeneration than introduction of MSCs into joint spaces alone. A major drawback to most of these models, however, is the absence of joint pathology and most of the experimental models do not reflect the environment of a damaged cartilage¹³. Hence, determining which chondrogenic factors are required for MSCs to undergo true differentiation by imitating the pathways of embryonic development involves more work than mere extrapolation from developmental biology literature. Firstly, there is significant cross talk involved between inflammatory cells present in the joint space, the damaged chondrocytes, and the MSCs that are artificially introduced, and these interactions are absent during normal embryonic development. As a result, genes that stimulate cell differentiation in embryos may not respond the same way in a milieu of inflammatory cells. For example, IGF-1 in developing chondrocytes promotes the synthesis of cartilage specific matrix molecules¹⁴. However, in a milieu of inflammatory cells IGF-1 receptors are severely down-regulated, and thus the required pathways stimulated through IGF-1 remain dormant¹⁵. Furthermore, there is significant inconsistency of response to biological factors between different animal models. For example, when collagen sponges embedded with recombinant BMP-2 and rabbit MSCs were implanted in rabbit knees, the regenerated cartilage was thin and irregular¹⁶. However, when similar sponges containing BMP-2 transfected perichondral cells were

implanted in the knees of rats, the resultant cartilage had a rich collagen I component similar to fibrocartilage¹⁷. The above examples are not indicative of MSCs being poor candidates for cartilage regeneration, but perhaps of the complexities involved in utilizing any multipotent cells in tissue engineering research. MSCs themselves have minimal disadvantages associated with them. MSCs have been shown to inhibit T-cell proliferation through immunosuppressive effects¹⁸. Although this delays immune rejection of transplanted MSCs, thus allowing for use of allogenic cells, it also raises the question of whether the transplanted MSCs can induce tumors in patients receiving them. Preliminary data suggest that such occurrences are rare although an extensive investigation is needed to further address this topic¹⁹.

Cells within the Synovial Cavity

In addition to multipotent stem cells, synovial cells that line the joint cavity are also considered to be promising alternatives for gene therapy. The synovium lines the internal surfaces of a joint cavity and in contrast to the cartilage has a large cell population that covers a significant surface area. Hence, following either direct gene delivery or injection of transplanted cells into the synovial cavity, cell engraftment or transfection is exclusively observed in the synovial lining following simple probability parameters²⁰. This opens the possibility of simplifying gene delivery to an intra-articular injection of gene delivery vectors or cells²¹. Studies by Gouze et al. showed that modified synovial cells continue to express significant amounts of gene product in vivo for up to 42 days after transfection by lentiviruses²². As compared to other models, gene transfer to

synovial cells is significantly more advanced in clinical trials. A phase I clinical trial involving *ex vivo* modification of synovial fibroblasts derived from rheumatoid joints was based on extensive studies on rabbit knees that involved similar modification of synovial cells. In these studies synovial cells were transfected *ex vivo* with IL-1 receptor antagonist cDNA with retroviral vectors. When these cells were transplanted into arthritic rabbit knees it was observed that IL-1 RA was strongly chondroprotective and reduced the number of leucocytes entering the joint space²³. Furthermore, independent studies by Makarov et al. showed that IL-1 RA delivered intra-articularly via gene therapy was four orders of magnitude more effective as an anti-arthritic than recombinant protein delivery systemically²⁴. However, there is some contradiction in reports related to synovial gene transfer. While Evans et al. reported that no IL-1 RA was reported in the peripheral blood of the rabbits, Gouze et al. reported significant amount of protein in the all major organs. This discrepancy can be explained by the technique used for modifying synovial cells. While Evans et al. transfected the cells *ex vivo* and then introduced them into the synovium, Gouze et al. directly injected lentiviruses carrying IL-1 RA into the joint. *Ex vivo* gene transfer has been shown to be similarly successful using other plasmids including IGF-1, and TGF- β . However, current consensus from various studies is that *ex vivo* or direct gene delivery to synovial cells can be toxic resulting in joint fibrosis, osteophyte formation, extensive uncontrolled cartilage growth (in the presence of BMP-2), joint swelling and in some cases cartilage degeneration^{144,25,26,21}.

Candidate Genes

Depending on the choice of cell used for gene delivery, there are a myriad of genes that can potentially be used for gene delivery. As mentioned above, the complexity lies in determining which gene or gene combinations are necessary and sufficient to induce chondrogenesis. Furthermore, the influence of these genes on different cell types in inflammatory environments remains to be determined.

Transforming Growth Factor β

Genes commonly used for cartilage formation include those from transforming growth factor (TGF- β) superfamily including TGF- β 1, which is responsible for initial cell-cell interaction between condensing progenitor cells²⁷. In inflamed joints, TGF- β 1 has anti-inflammatory properties and stimulates new matrix synthesis by chondrocytes^{128,28,5}. TGF- β 2 mediates hypertrophic differentiation of chondrocytes by regulating Indian hedgehog (Ihh) and Parathyroid Growth Hormone (PTHrP) expression²⁹, however, it has not been used as extensively as TGF- β 1 for gene delivery. During development TGF- β 1-3 are involved in inhibiting formation of blood vessels in cartilage³⁰. When Lee et al. transfected a monolayer of intervertebral disc cells with TGF- β 1 cDNA and grew them in 3 dimensional pellet cultures, they found a 375-475% increase in proteoglycan synthesis as compared to pellets containing cells not transfected with TGF- β 1³¹. Irrespective of the number of cells used to grow these pellets, Lee et al. could not grow pellets larger than 5-7 mm in diameter. It is yet unclear whether the size of the pellet could be increased using different genes or a combination of genes including

TGF- β 1. It is crucial to regulate the dose of TGF- β 1 secreted into the joints space. Mi et al. have shown that low doses of intra-articular injection of adenoviruses containing TGF- β cDNA have no therapeutic or harmful effect on arthritic joints³². However, high levels of TGF- β , when transfected into the joints, increase production of nitric oxide (indicating inflammation), muscle edema and reduced movement of the joint. These effects were absent in control joints that received the similar concentration of virus vector with luciferase cDNA.

Bone Morphogenic Proteins

Within the TGF superfamily are also included Bone Morphogenic Proteins (BMPs), BMP-2 and BMP-7 being most commonly used in gene delivery studies for cartilage. One of the first studies involved growing modified periosteal mesenchymal stem cells by transfection with BMP-7 cDNA³³. When the modified cells were embedded in Poly(glycolic acid) (PGA) scaffolds and placed in full thickness defects within the rabbit knee, Grande, et al. found that transduced cells placed in PGA scaffolds did significantly better than non-transduced cells placed in scaffolds. They had a larger amount of hyaline cartilage, and quicker restoration of the subchondral bone (as early as six weeks)³³. However, BMPs must be used with caution for cartilage regeneration as they are potent stimulators of ossification.

Insulin-like Growth Factor -1

IGF-1, a growth factor recognized to induce cartilage proteoglycan synthesis and collagen matrix production has also been studied in animal models with positive results. Since recombinant IGF-1 has a very short half life, researchers are keen upon developing a gene delivery system that can modify cells to synthesize their own IGF-1 for extended periods of time. Nixon et al. compared the effects of modifying pristine equine chondrocytes, bone marrow derived chondroprogenitor cells, and synovial cells with IGF-1 cDNA¹⁵. They found that these cells were capable of maintaining therapeutic levels of IGF-1 expression for up to 28 days in *in vitro* monolayer cultures. Transfected chondrocytes were able to maintain their morphology and secrete significantly greater amounts of proteoglycans and collagen II. However, independent experiments by Mandry et al. found that when IGF-1 is transfected into articular chondrocytes, there is no significant increase in collagen II expression by these cells, although histologically the constructs score higher than untreated controls². This discrepancy can be attributed to one or more of the differences in setup between the two experiments. While Nixon et al. were performing their studies *in vitro*, using adenoviruses with transfection efficiencies of 40-50%, Mandry et al. were using FuGene 6, a non-viral vector *in vivo*, where transfection efficiency was at 35%. Transfection of rat articular chondrocytes *ex vivo* with IGF-1 cDNA containing adenoviral vectors and their subsequent implantation in partial thickness articular cartilage defects resulted in preservation of the chondrocytic morphology and formation of a structure that resembled hyaline cartilage 8 weeks into the study. Similar results were obtained when rabbit articular chondrocytes were

modified after transfection³⁴. Further characterization of these constructs for mechanical properties is needed to enhance our understanding of the variables that dictate the outcome of long term expression of IGF-1 on various cell lines. Table 1 lists the various delivery systems and their efficiencies at secrete IGF-1.

Transcription factors

Transcription factors are regulatory proteins that bind to specific regions on the genome and control their expression. Such modulated gene expression can potentially be used to generate the differential ECM composition in each zone. A noteworthy advantage offered by transcription factors over expression proteins such as TGF β or IGF is that a significantly small amount of protein expression is required activate numerous downstream pathways that can stimulate the differentiation of multipotent cells along a particular cell line. However, to date, transcription factors have not been used for tissue engineering applications and hence provide a new forefront for creating novel tissue engineering strategies. One of the transcription factors which has repeatedly been marked as essential and non-redundant for promoting cells into the chondrocytic lineage is Sox-9³⁵. Sox-9 is one of the first transcription factors that gets activated during skeletogenesis to generate a chondrocytic mold which is later replaced by endochondral ossification. Furthermore, endochondral ossification cannot occur without down regulation of Sox-9 expression, and hence Sox-9 is essential for both promoting and preserving the chondrocytic phenotype. Sox-9 is a typical transcription factor containing a transcription activation domain that binds to enhancers of collagen IIa^{36,37} and

collagen IXa³⁸. In addition, when cells engineered to suppress Sox-9 expression are introduced in chondrogenic fields, they are distinctly devoid of collagen II, collagen X, collagen XI and aggrecan. The further lack of chondrogenic condensates in these fields confirms the integral role Sox-9 in chondrogenesis³⁹. In an elegant series of experiments conducted by Ikeda et al⁴⁰, it was reported that without Sox-5 and Sox-6, induction of chondrogenesis by Sox-9 alone was delayed and not as robust as in the presence of all three transcription factors (together called the Sox-trio). Furthermore, chondrocyte specific markers remained high for at least three weeks post transfection and the chondrocytes did not convert into a prehypertrophic or hypertrophic phenotype. Collagen II reached peak expression levels when hMSCs were transfected with the Sox-trio and cultured in the presence of chondrogenic medium (comprising of TFG- β 3, BMP-2 and dexamethasone) and was reasonably high when transfected with the Sox-trio alone. However, when hMSCs were transfected with Sox-9 alone, the expression of aggrecan dominated over the expression of collagen II. Several of these findings were later confirmed in vivo by Lefebvre et al.⁴¹ At the molecular level, Sox-5 and Sox-6 act to modulate the structure of DNA so as to facilitate recruitment of other transcription factors including Sox-9. When Sox-9 acts in conjunction with Sox-5 and Sox-6, the synthesis of cartilage specific ECM is upregulated multifold. Therefore, it may be concluded that the Sox trio can be used to induce and preserve a robust chondrocytic phenotype from hMSCs.

Other Anabolic Gene Candidates

Although TGF- β 1, IGF-1 and BMPs are commonly targeted in experiments involving gene delivery for cartilage regeneration, up regulation of some other biological molecules such as transcription factors, intracellular signaling molecules and growth factors is also considered to be promising. Studies have shown that fibroblast growth factor (FGF-3) receptor signaling is sufficient to induce chondrogenic differentiation⁴². Signal transduction molecules SMADs are also important intracellular regulators of chondrocytic differentiation. As these molecules function intracellularly, they cannot be delivered to cells in a soluble form. Gene therapy is perhaps the only effective technique to utilize these molecules for cartilage regeneration²¹. The success of this strategy is limited by the transfection efficiency of the gene delivery vector and the survivability of the cells undergoing transfection.

Anti-inflammatory Agents

Although cartilage regeneration mainly involves enhancing the anabolic activity of cells to either synthesize extracellular matrix molecules or imitate the differentiation observed in embryonic development, tissue engineering of damaged cartilage cannot be a complete success without addressing the inflammatory agents that overwhelm the joint space. Most of the work with anti-inflammatory agents has been performed in animal models where arthritis is induced using collagen or other stimulatory molecules. Studies have involved the use of IL-1 receptor antagonist, soluble TNF-alpha receptors, anti-inflammatory cytokines such as IL-10, IL-4 and IL-13, all of which have been successful

at decreasing inflammatory response in animal models^{146,43-45,23}. Other effective strategies involve using tissue inhibitors of matrix metalloproteinases (TIMPs). Following induction of arthritis, synovial cells secrete matrix metalloproteinase (MMPs) that cause severe destruction of the cartilage ECM. In addition, MMPs are also responsible for the cellular invasion of the joint by inflammatory cell. Tissue engineering strategies have been applied to curtail the destruction caused by MMPs by modifying arthritic synovial cells to over express TIMPs. Gelfoam sponges were seeded independently with synovial cells transfected with TIMP-1 and TIMP-3. The studies showed a 25% and 13% decrease respectively in the number of invading cells. Significant reduction in cell proliferation was also observed in addition to reduced levels of active MMPs. A possible extrapolation of this approach could involve the creation of a dual system, one containing synovial cells that overexpress anti-inflammatory agents and the other system containing chondrocytes or stem cells over expressing one or more anabolic factors – thus addressing both cartilage destruction and regeneration observed in articular diseases.

Candidate Gene Delivery Vectors

Viral Vectors

There are two main classes of gene delivery vectors – those involving viruses and those involving non-viral agents, such as polymers and liposomes. Viral vectors seem to be overwhelmingly preferred to non-viral vectors in most documented studies involving gene delivery for cartilage regeneration. The question of using viral versus non-viral

vectors for any kind of gene delivery has caused intense debate since the inception of the idea of gene therapy. Viral vectors have been preferred in all avenues of gene delivery simply because they are better at successfully transfecting cells. While viral vectors can attain transfection efficiencies of around 80-90%, non-viral vectors can at most transfect 40-50% of the cell population. This continues to be a major obstacle in the use of non-viral vectors for gene delivery. However, non viral vectors are receiving increasing attention on the basis of their ease of synthesis, low immunogenicity and unrestricted plasmid size. The apprehension that envelopes the use of viral vectors for gene therapy has been justified based on many factors. Firstly, viral vectors induce an inflammatory response, which can cause a myriad of side effects ranging from mild edema to multi-system organ failure. The immune system's enhanced response to the now recognized virus makes it difficult to administer gene therapy repeatedly. At a more cellular level, transfection of a virus causes significant changes in cell surface markers of transfected cells, decreasing the possibility of reusing the same population of cells for a second round of gene delivery. Furthermore, cells that synthesize proteins encoded in the transgene express some viral markers and the duration of protein synthesis is limited by the ability of inflammatory cells to identify these cells and eliminate them. Modifications of virus genomes where minimal amounts of viral genes are retained have helped address many of these issues. Some of these modifications have extended expression of transgenes carried by the viruses for as long as 84 days⁴⁶.

However, direct injection of viral vectors is considered to be harmful as independent studies have shown dose dependent inflammatory response in joints of various animals⁴⁷.

Another disadvantage to intra-articular injection of viruses is that the viruses spread to other organs, however this dispersion of the virus has not been confirmed in larger animals such as rabbits and rhesus monkeys⁴⁸. *Ex vivo* gene delivery is a novel method that circumvents most problems related to viral gene delivery while providing all of its benefits. The technique involves *in vitro* gene delivery to extracted cells after expanding the cells in culture. The transfected cells are then reintroduced into the body where they function as factories producing high quantities of the protein of interest. This technique, also coined cell mediated gene transfer, is ideal for introducing a variety cell populations transfected with different types of genes, at different time points without bringing the virus in direct contact with the body. There is some contention that viral genomes may be left behind in such *ex vivo* transfected cells, but that is currently being investigated. Studies prove that there is significant increase in the duration of protein expression with *ex vivo* gene delivery as compared to direct injection of viral vectors⁴⁸. Nixon, et al. observed expression of marker Green Fluorescent Protein (GFP) beyond 60 days in chondrocytes transfected *ex vivo* with adenovirus. Rabbit synovial cells transfected *ex vivo* with a retrovirus maintained IL-1RA expression for up to 6 weeks²³. Furthermore, recent work has shown that in the absence of immune recognition of transgene product cells lining the synovial cavity can transcribe the transfected cDNA at relevant levels for up to 6 months²². Other advantages of *ex vivo* gene delivery include the possibility to transfect cells other than those that line the synovial membrane. Articular chondrocytes as well as chondroprogenitor cells that are modified to secrete higher amounts of proteins

can be directly injected within joints, where they are shown to preferentially adhere to damaged cartilage⁴⁸.

Non-viral Vectors

FuGene 6² and modified cationic liposomes⁴⁹ are two non-viral gene delivery methods that have so far been utilized for gene delivery for cartilage regeneration. FuGene 6 is a non-liposomal lipid formulation which has been shown to successfully transfect a variety of cell-lines. After transfection with FuGene 6, Mandry et al. encapsulated the transfected articular chondrocyte into alginate spheres. The mean transfection efficiency was around 35% and 60% of the transfected chondrocytes expressed the transgene IGF-1 for as long as 6 weeks. IGF-1 expression peaked at day 5, and was sustained above therapeutic levels for 32 days. Transfection using the poly-L-lysine lipids designed by Goomer et al. involved a multi-step process where transfection was optimized by introducing cells in a detergent (lysolethicin) to permeabilize the cell membrane. Furthermore, transferrin was covalently attached to the polycationic backbone to promote electrostatic interaction with DNA. Transfection efficiency by this method was reported at 71% *in vitro*. The transgene expression was maintained up to 13 days after transfection and no immune response was observed *in vivo* in animal models. Future studies will undoubtedly incorporate novel non-viral gene delivery vectors, including polymeric vectors that are currently being developed.

Scaffolds used for Gene Delivery

Scaffolds provide a way to localize cells to an area in the defect while supporting the joint mechanically during the formation of novel tissue. Furthermore, since chondrocytes need a three dimensional configuration to preserve their morphology, scaffolds are ideal for cartilage regeneration as they provide spatial communication between cells while providing a infrastructure of fibers that provide mechanical support to the cells and healing tissue. Numerous natural and artificial materials have been used for cartilage regeneration including fibrin and collagen matrices, hydroxylapatite, synthetic hyaluronic acid sponges, and numerous polymers. However, scaffolds also introduce new limitations to the experimental design. When cells are seeded onto scaffolds, a good portion of them fail to attach to the scaffold fibers. The cells that eventually populate the scaffolds are produced from repeated cell duplications of the existing cells. Considering that in most practical scenarios transfection efficiency is significantly less than 100%, the actual number of transformed cells that continue to grow on scaffolds is very small. Furthermore, most viruses (and non-viral vectors) only transiently transfect cells and the expression of the transgene is lost after the cell replicates. Due to some of these reasons, previous experiments involving gene delivery to scaffolds have had limited success. When Baragi et al. used *ex vivo* transfected chondrocytes to populate collagen scaffolds and subsequently transplanted these scaffolds into articular cartilage defect, they noticed that over 90% of the cells were lost during the first 24 hours after seeding⁵⁰. Polyglycolic acid sponges have provided more promising results. Separate populations of periosteal stem cells that were transduced *ex vivo* with BMP-7 and sonic hedgehog respectively and seeded onto PGA scaffolds showed remarkable healing of full thickness cartilage defect

as early as 6 weeks³³. Similarly, Mason et al. transfected rabbit derived mesenchymal stem cells with BMP-7 and obtained complete osteochondral healing in defects implanted with cell seeded PGA scaffolds at 8 and 12 weeks⁵¹. Hence, most strategies involving the use of scaffolds undergo *ex vivo* transfection of cells before being placed onto scaffolds. A few studies conducted thus far involve the incorporation of plasmids (with or without gene delivery vectors) into the scaffold meshes, but these models have mainly been used for bone and vascular tissue engineering. Hence, a significant amount of work needs to be done in optimizing scaffold technology to promote or preserve the chondrocytic phenotype.

Multi-layered Scaffolds

One of the challenges involving the use of scaffolds in cartilage regeneration involves the variability in cell type and extra cellular matrix present between the different layers of cartilage. To regenerate the multilayered cartilage structure, stackable scaffolds containing layers with distinctive properties need to be fabricated such that they can stimulate desired phenotypic characteristics in cells enmeshed within them. For example, Ng et al.⁵², formulated a bilayered scaffold from agarose, whereby each layer was fabricated with from a different concentration. The differences in concentration stimulated different mechanical properties in the tissues produced initially; however, these properties could not be sustained for prolonged durations.

Creation of such multilayered constructs does provide the versatility required in creating tissues with layered compositions. However, limitations in differentiating and

preserving such cultures is attributed to the fact that neither gene delivery agents nor growth factors can be effectively delivered such that they can be confined to the specific regions of interest within the scaffold. Hence, it is essential to develop new processing techniques that allow the fabrication scaffolds that can house specific biological factors within confined layers.

Concluding Remarks

Table 2 summarizes the various cells, scaffolds and gene delivery vectors that have thus far been used for cartilage tissue engineering. It is evident that new strategies need to be developed to allow the integration of gene delivery with three dimensional scaffolds. Such strategies can translate not only to seemingly simple tissues such as cartilage, but also to more complex tissues present in the body. Development of novel biomaterials and novel processing methods for translating existing biomaterials into better non-viral gene delivery vectors or versatile scaffolds will be imperative in creating new strategies in tissue engineering.

Figures

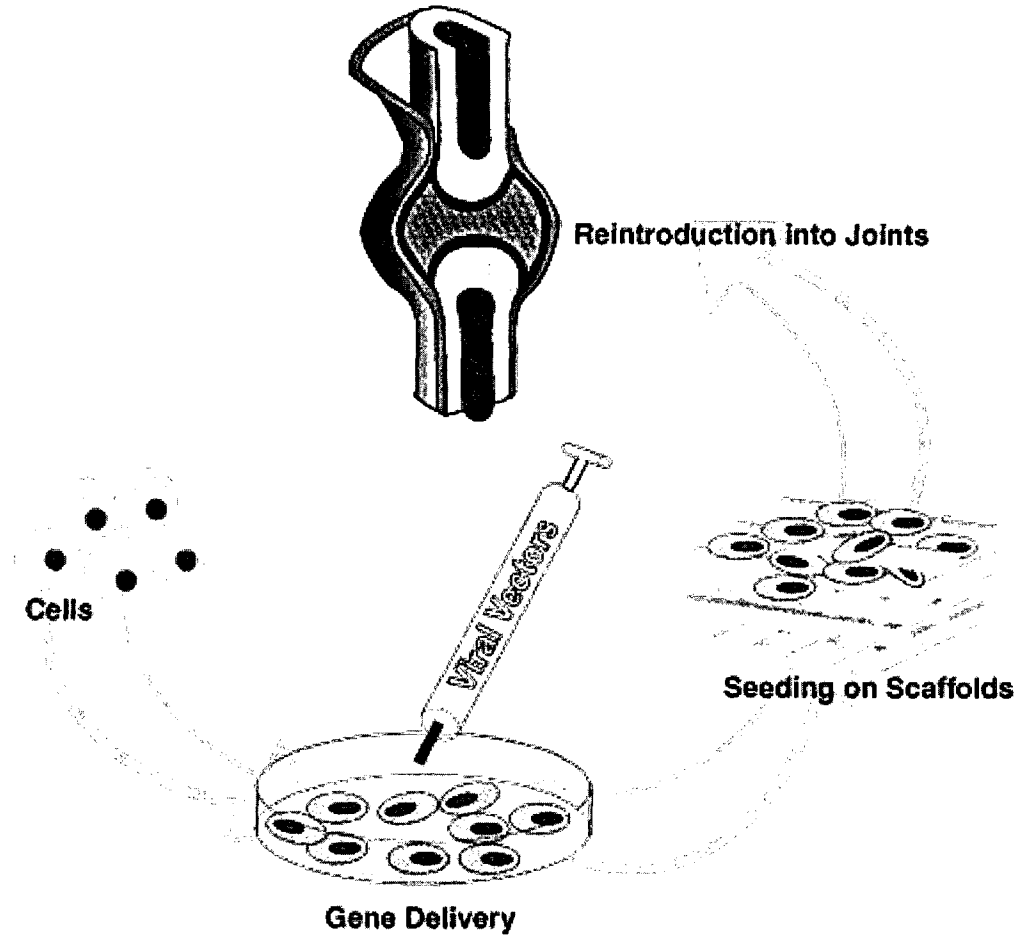


Figure 2.1: Schematic for ex-vivo gene delivery

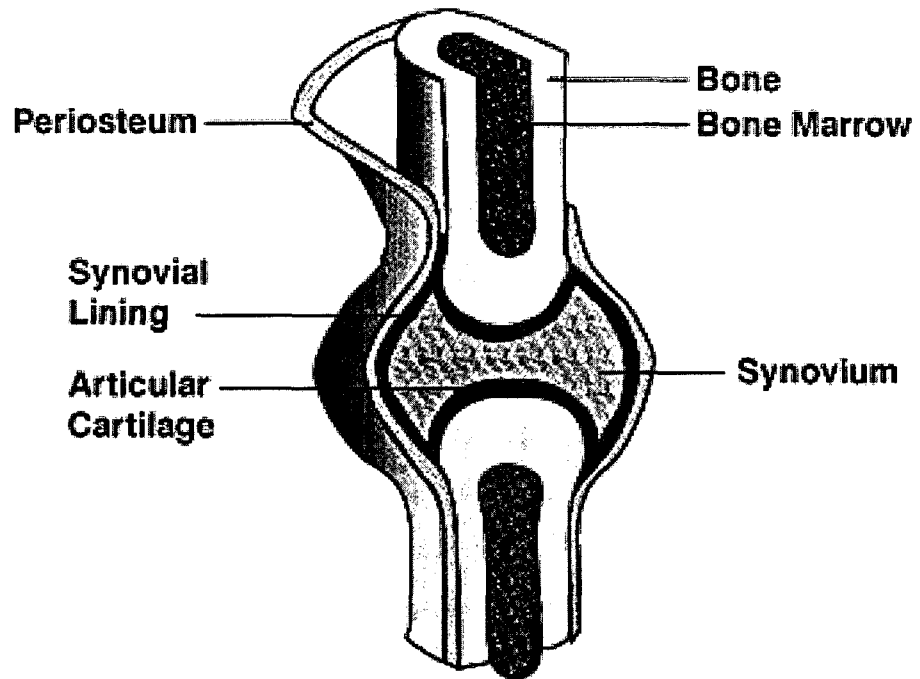


Figure 2.2: Schematic of Knee Joint

Tables

Gene of interest	Method of transfection, cells & vectors employed	Concentration of protein secreted	Duration protein was detected	Reference
IGF-1	<i>Ex vivo</i> synovial cells Adenovirus	Maximum: 246±43 ng/ml	All 8 days evaluated	53
IGF-1	<i>Ex vivo</i> chondrocytes FuGENE 6	123±22 ng /10 ⁷ cells	All 36 days evaluated	2
IGF-1	<i>Ex vivo</i> chondrocytes, MSCs synovial cells Adenovirus	<i>Chondrocytes</i> : max: 70 ng/ml <i>MSCs</i> : max:115 ng/ml <i>Synovial cells</i> : max: 246 ng/ml	All 28 days evaluated	15

Table 2.1: Comparison of secreted IGF-1 after gene delivery.

Cells	Vectors	Genes	Scaffolds	Reference
<i>In vitro transfection</i>				
<i>Chondrocytes</i>				
Rabbit	Reterovirus	LacZ	Collagen	54
Horse	Adenovirus	IGF-1 GFP	-	15
	Adenovirus	IGF-1	-	14
Rat	Baculovirus	GFP		55
Lapine	FuGENE6	IGF-1 LacZ	Alginate beads	2
Cow	Adenovirus	GFP	Alginate beads	56
Human	Adenovirus	B- galactosidase	Alginate beads	57
<i>Chondroprogenitor cells</i>				
Rabbit MSCs	Retroviruses	BMP-7	Polyglycolic Acid	5
Rabbit Periosteal cells	Retroviruses	BMP-7 Shh	Polyglycolic Acid	33
	Cationic lipids	TGF- β 1 PTHrP B-galactosidase	-	58
<i>Synovial cells</i>				
Horse	Adenovirus	IGF-1	-	15
<i>Other Cells</i>				
NIH/3T3	Reterovirus	IL-1 RA	-	59
Rat fibroblasts	Adenovirus	IGF-1	-	
		BMP-2	-	
Rat muscle cells	Reterovirus	LacZ	Collagen	54
<i>In vivo transfection</i>				
Rat	Lentivirus	B-galactosidase IL-1 RA	-	22
Rabbit	Adenovirus	TGF- β 1	-	32
	Adenovirus	IL-10	-	43
Cow	Adenovirus	TGF- β 1	-	25

Table 2.2: Cells, gene delivery vectors and genes thus far used for cartilage regeneration.

Chapter III

Synthesis and Conformational Evaluation of a Novel Gene Delivery Vector for Human Mesenchymal Stem Cells²

Abstract

We have synthesized a novel gene delivery vector by covalently combining branched polyethylenimine (PEI) and hyaluronic acid (HA) with the aim of improving transfection of PEI into human mesenchymal stem cells (hMSCs), while maintaining cell viability. Because of the opposite charges on PEI and HA, the PEI-HA vector forms a zwitterionic polymer capable of inter- and intra-molecular interactions. We have characterized the hydrodynamic radius of PEI-HA and PEI-HA/pDNA complexes at ambient and physiological temperatures, as well as at a range of salt concentrations using light scattering, and investigated the effect of the size of transfecting complexes on gene delivery. We found that by increasing the salt concentration from 150 to 1000 mM of NaCl, the mean hydrodynamic radius (Rh) of PEI-HA increases from 2.0 ± 1.1 nm to 366.0 ± 149.0 nm. However, increasing the salt concentration decreases the mean Rh of PEI-HA/pDNA complexes from 595.0 ± 44.6 nm to 106.0 ± 19.2 nm at 25°C and from

² This chapter has been published as follows: Saraf A, Hacker MC, Sitharaman B, Grande-Allen KJ, Barry MA and Mikos AG "Synthesis and Conformational Evaluation of a Novel Gene Delivery Vector for Human Mesenchymal Stem Cells," *Biomacromolecules*, 2008 Mar; 9(3):818-27

767.0 ± 137.2 nm to 74.0 ± 23.0 nm at 37°C. hMSCs transfected with smaller complexes showed a significant increase in transfection from 3.8 ± 1.5% to 19.1 ± 4.4%. Similarly, PEI-HA performed significantly better than PEI in terms of cell viability (86.0 ± 6.7% with PEI-HA versus 7.0 ± 2.8% with PEI, 24 hours post exposure at the highest concentration of 500 mg/ml) and maximum transfection efficiencies (12.0 ± 4.2 % with PEI/pDNA complexes and 33.6 ± 13.9 % with PEI-HA/pDNA complexes). Thus, modifying PEI by covalent conjugation with HA improves its performance as a gene delivery vector in hMSCs. This presents a promising approach to altering hMSCs for tissue engineering and other applications.

Abbreviations

Acryl/bis: Acrylic Acid/ Bis-acrylamide

AMAC: 2-Aminoacridone

α-MEM: Alpha Modified Eagle's Medium

BMP: Bone Morphogenetic Protein

N:P ratios: Primary and Secondary Cations (from PEI) to Anions (from pDNA) Ratio
(in moles)

CD44: Clusters of Differentiation 44

CMV: Cytomegalovirus

DLS: Dynamic Light Scattering

DMSO: Dimethyl Sulfoxide

pDNA: Plasmid Deoxyribonucleic Acid

ECM:	Extracellular Matrix
eGFP:	Enhanced Green Fluorescent Protein
EthBr:	Ethidium Bromide
FACE:	Fluorescence Assisted Carbohydrate Electrophoresis
FACS:	Fluorescence Activated Cell Sorter
FID:	Free Induction Decay
GFP:	Green Fluorescent Protein
HA:	Hyaluronic acid
hMSCs:	Human Mesenchymal Stem Cells
M_w :	Weight Average Molecular Weight
MSCs:	Mesenchymal Stem Cells
MWCO:	Molecular Weight Cut Off
NNLS:	Non-Negative Least Squares
PEI:	Poly(ethylenimine)
PEI:	Branched Poly(ethylenimine)
PBS:	Phosphate Buffered Saline
pCMV-BMP-2:	Plasmid-Cytomegalovirus-Bone Morphogenetic Protein - 2
pCMV-eGFP:	Plasmid-Cytomegalovirus-Enhanced Green Fluorescent Protein
rMSCs:	Rat Marrow Stromal Cells
SLS:	Static Light Scattering
TBE:	Tris-Borate-EDTA
TEMED:	N,N,N',N'-(tetramethyl)-(ethylenediamine)

UV: Ultraviolet

Introduction

Polymeric gene delivery vectors have been developed over the past 30 years toward an increased specificity to many different cell types. Polyethylenimine (PEI) continues to be the preferred cationic polymeric gene delivery vector with its mechanism extensively studied and tested amongst various cell types⁶⁰. Furthermore, PEI has also been covalently and electrostatically bound to many different biological molecules to improve targeting^{61, 62, 63} of primary cells and cell lines. Since mesenchymal stem cells (MSCs) are becoming an increasingly important cell source for tissue engineering^{64, 65}, it is essential to evaluate the potential of polymers as transfection vectors in these cells in order to advance the field of tissue engineering. Since most polymers are tested in cell lines, data on transfection of MSCs (including hMSCs) with non-viral agents are scarce. Poly-L-lysine-palmitic acid derivatives⁶⁶ demonstrated transfection of 15% of rMSCs, whereas similar studies with PEI/pDNA complexes achieved efficiencies of 5%⁶⁶ to 13%⁶⁷. Adenoviruses continue to be the gene delivery agent of choice for MSCs. Commercial lipid based agents such as FuGENE 6 and Dotap (both from Roche Pharmaceuticals) have transfection efficiencies of less than 6%⁶⁸ in hMSCs, whereas non-vector mediated transfection methods such as electroporation have gene delivery efficiencies in the range of 27% to 41%⁶⁹. Furthermore, cell mortality is significant with electroporation, limiting the successful translation of these techniques to tissue engineering purposes.

Here we describe the synthesis and characterization of a novel gene delivery vector, a chemical conjugate of branched PEI (PEI, $M_w = 25$ kDa) and hyaluronic acid (HA, $M_w = 2.3$ kDa), the later of which is a natural ligand for receptors CD 44, CD 54 and CD 168 on hMSCs^{70, 71, 72}. Previous PEI-ligand polymers have shown increased targeting and higher transfection efficiencies^{63, 73, 74} as compared to unmodified PEI alone. Between 80 – 90% of hMSCs express CD 44 receptors that can bind to HA oligomers, and the density of these receptors can be increased with biological stimuli including the presence of HA⁷⁵. In addition to improving cell targeting, we hypothesized that HA would also mitigate the toxicity notoriously associated with the cationic amine groups of PEI^{76, 77} by countering them with the carboxylic groups present on HA. Recent studies where PEI/pDNA complexes were coated with HA have shown improved gene delivery due to easier dissociation of pDNA from PEI⁷⁸. Similarly, PEI/pDNA complexes immobilized on HA crosslinked hydrogels successfully transfected T3T cells⁷⁹. Furthermore studies have shown that HA oligomers are involved in angiogenesis^{80, 81}, modulate proteoglycan synthesis⁸², and activate cell signaling pathways⁸³, which are vital for tissue engineering applications.

The studies presented here describe the synthesis and characterization of PEI-HA as a gene delivery vector. The specific goals involve determining the influence of salt concentration on the size of the vector as well as the vector/plasmid complex at ambient and physiological temperatures. We further investigate the influence of the size of these complexes on transfection efficiency in hMSCs. The studies also investigate the

performance of vector PEI-HA as compared to PEI in terms of cell viability and transfection efficiency in hMSCs.

Experimental Procedures

Materials

Chemicals used for synthesis, namely sodium borate, sodium cyanoborohydrate and PEI ($M_w = 25$ kDa) were purchased from Sigma-Aldrich (St. Louis, MO). Sodium hyaluronate ($M_w = 2.3$ kDa) was generously provided by Genzyme. hMSCs were purchased from the laboratory of Dr. Darwin Prockop at the Tulane Center for Gene Therapy and grown using protocols established by Prockop et al.⁸⁴. Materials for cell culture including α - Modified Eagle's Medium (α -MEM), glutamine, trypsin and PBS were obtained from Gibco (Carlsbad, CA). Plasmid DNA with cytomegalovirus (CMV) promoter and enhanced Green Fluorescent Protein (eGFP) as the reporter gene (pCMV-eGFP, 4.7 kb, cat # 6085-1) from Clontech, Palo Alto, CA, USA, and CMV promoter induced Bone Morphogenic Protein - 2 (BMP-2), (pCMV-BMP-2, 6.7 kb, cat # SC108987) from Origene, Rockville, MD.

Synthesis of PEI-HA

PEI-HA was synthesized by the process of reductive amination. PEI (250 mg) and HA (500 mg) were added to a three-neck round bottom flask in the presence of 0.1 M sodium borate buffer (pH 8.5). Sodium cyanoborohydrate (0.2 mg) was added as a reducing agent at the beginning of the reaction and the mixture was heated to 40°C with

constant stirring. An additional 0.15 mg of sodium cyanoborohydrate was added at 30 h into the reaction. The reaction was maintained for 48 h. The products were dialyzed against 0.02 M of sodium borate buffer in a VivaSpin centrifuge tube (Molecular weight cut-off (MWCO) 30 kDa) (Sartorius Corp., Edgewood, NY) and the dialysate was transitioned to pure water. The dialyzed products were then lyophilized resulting in a dry powder that was used for subsequent analysis.

Nuclear Magnetic Resonance Analysis

Proton NMR spectra were acquired using a 400 MHz spectrophotometer (Bruker Avance 400, Zurich, Switzerland). DEPT-135 ^{13}C NMR spectra were acquired using a Bruker Avance 500 spectrometer. Samples of PEI, HA and PEI-HA were prepared by dissolving the materials in D_2O at 37°C on a shaker table. NMR spectra were recorded at ambient temperature and processed using the MestRe-C software (Mestrelab Research S.L., Spain). To improve signal-to-noise, line broadening of 2 Hz and 10 Hz was used to process the forward induction decay (FID) of the proton and carbon spectra respectively. Chemical shifts in the spectra obtained were expressed as parts per million using HDO ($\delta = 4.79$ ppm) as an internal reference. By integrating the peaks corresponding to the protons of the CH_2 groups of PEI and CH_3 groups of HA, the percentage conjugation of PEI and HA was established.

Fluorescence Assisted Carbohydrate Electrophoresis (FACE)

To confirm the amount of HA attached to PEI, FACE with 2-aminoacridone (AMAC) was performed^{85, 86, 87}. 10 mg of HA and PEI-HA were separately dissolved in 150 mM NaCl solution and the pH was adjusted to 5.5. The samples (5 μ l each) were mixed with 80 μ l of 0.1 M ammonium acetate and treated with 15 μ l of chondroitinase AC II (cleaves galactosaminidic linkage)⁸⁸ overnight at 37°C. The following day the samples were lyophilized and reconstituted with 0.1 M AMAC solution (85% of total volume) in glacial acetic acid-DMSO (3:17, v/v, 15% of total volume) and freshly prepared sodium cyanoborohydride solution (3×10^{-5} M per sample). The mixtures were centrifuged for 5 min at 13,000 rpm and incubated at 37°C overnight to allow derivatization with AMAC. Fluorescent standards were prepared by diluting known quantities of maltotriose and performing the same fluorescent labeling. After derivatization samples were mixed with 20 μ l of glycerol and protected from light for FACE analysis.

A two layered polyacrylamide gel was used to isolate the HA bands. The layers consisted of: i) resolving gel (final concentration 20% acrylamide/bis-acrylamide (acryl/bis) (37.5 : 1), 2.5% glycerol and 44.8 mM tris acetate (pH 7.0)); total volume 5 ml and ii) stacking gel (final concentration 8% acryl/bis (37.5 : 1), 2.5% glycerol, 44.8 mM tris acetate (pH 7.0) and PEG (M_w 8000, 4.4% w/v)); total volume 5 ml. These solutions were made freshly each time. 28 μ l of 10% ammonium persulfate and 7.5 μ l TEMED were added to facilitate cross-linking of the gels. The solution was mixed rapidly and placed between glass plates such that the resolving gel formed the bottom layer and the

stacking gel formed the top layer, where an 8-10 well comb was inserted before the stacking gel was formed. 8 μ l of each sample (experimental samples along with the maltotriose samples for quantification) were loaded in each well. Electrophoresis was performed at 500 V until satisfactory resolution of the bands was obtained (60-75 min). The gels were illuminated with UV light and digitally imaged using a Kodak Gel Logic 100 imaging system and Kodak 1D software (Kodak, Rochester, NY, version 3.6.0). Quantitative analysis was performed with densitometry on Gel Pro Analyzer software (Media Cybernetics, Silver Spring, MD; v 4.5.0).

Electrophoresis Band Retardation

PEI-HA/pDNA (pCMV-eGFP) complexes at nitrogen : phosphate (N:P) ratios of 2:1, 7.5 : 1 and 13.5:1 were assembled in NaCl solutions of molarities ranging from 150 mM to 1000 mM. Total number of nitrogens at physiological pH were determined by the total moles of primary and secondary amines in PEI-HA and the total number of phosphates were determined as the total moles of phosphate groups contributed by pDNA^{62 89}. PEI/pDNA complexes were also assembled at N:P ratios 2:1, 7.5:1 and 13.5:1. PEI/pDNA complexes at 2:1 showed some precipitation and hence were not used for analysis. The samples were vortexed and incubated for 1 h. The samples were then loaded on 0.5% agarose gels synthesized in 0.5X Tris-borate-EDTA (TBE) buffer. 5 μ l of ethidium bromide (EthBr) was added to 50 ml of agarose solution during the assembly of the gels to visualize free pDNA. 10 μ l the sample (containing either 1 μ g free DNA or vector complexed with 1 μ g pDNA) were added to the wells in the presence of 5 μ l of 1X

loading dye. Electrophoresis was performed for 50 min at 80 V in 0.5X TBE buffer, after which the migration of free DNA towards the anode was assessed under a UV light.

Dynamic and Static Light Scattering

(A) Creating PEI-HA and PEI-HA/pDNA complex solutions

PEI-HA was dissolved in 150, 300, 500, 700 and 1000 mM NaCl solutions to make a 0.1 M PEI-HA solutions. pH was adjusted to 7.4 using 0.1 N HCl dissolved in 150 - 1000 mM NaCl solutions respectively and filtered with a 0.2 μm filter (Whatman, NJ). The solutions were introduced drop-wise into plasmid DNA pCMV-BMP-2 at N:P ratio of 7.5 : 1. For dynamic light scattering (DLS) and static light scattering (SLS) experiments, the above solutions were freshly made and distributed into 250 μl batches at 25°C.

(B) DLS

For measuring the hydrodynamic radii (R_h), dynamic light scattering (DLS) results were obtained using a 90PLUS Particle Size Analyzer (Brookhaven Instruments), the laser operating at 659 nm wavelength. The solutions were allowed to equilibrate at 25°C for 10 min in cuvettes prior to acquiring the readings. The temperature was then raised to 37°C and allowed to equilibrate with the solution for 10 min prior to acquiring additional readings. Similarly, readings were performed at both 25°C and 37°C with PEI-HA/pDNA complexes at NaCl concentrations of 150, 500, and 1000 mM. The cumulant method was used to derive information about the R_h distribution and Laplace inverse program Non-Negative Least-Squares (NNLS) was used to determine the intensity weighted aggregate

particle size in the form of Rh. The dust-cut off was set at 1000 nm and values higher than 1000 nm were not accounted for during processing.

(C) SLS

Using toluene as the reference solvent, scattering intensities were recorded for the samples and toluene in batch mode using a DAWN-EOS instrument (Wyatt Technology, equipped with a 30 mW GaAs laser at $\lambda = 690$ nm) for SLS. Measurements were carried out at both 25°C after letting the solutions equilibrate for 10 min and 37°C after letting the solutions equilibrate for 10 - 15 min. dn/dC ratios were calculated to be 0.1 mg/ml using toluene as the reference solvent on a Wyatt Technologies optilab device. Each SLS measurement was repeated at least three times and one representative measurement was used to obtain the Zimm plot. This plot allows the determination of the weight average molecular weight (M_w) and the second virial coefficient (A_2) using the Zimm equation:

$$\frac{2\pi^2(\tilde{n}(dn/dC))^2}{\lambda^4 \times Na} \times \frac{C}{R(\theta)} = \frac{1}{M_w} + 2A_2C$$

where \tilde{n} is the refractive index of the solvent, dn/dC is the refractive index of the polymer, λ is the wavelength of the laser beam used, Na is Avogadro's number, C is the concentration of the polymer in solution, and $R(\theta)$ is the Reyleigh ratio. M_w is to be derived.

Cell Viability Studies

The toxicity of the synthesized PEI-HA was compared to the toxicity of PEI on hMSCs. hMSCs were seeded on 96-well, clear bottom plates at a density of 4×10^4 cells/cm². Cells were allowed to attach to the surface overnight then exposed to PEI, or PEI-HA at concentrations ranging from 10 to 500 $\mu\text{g}/\mu\text{l}$. PEI and PEI-HA solutions were prepared by dissolving the respective polymers in α -MEM followed by filtration through a 0.2 μm filter. hMSCs were exposed to the polymer solutions for 24 h then washed with PBS and complete media (α -MEM, 20% FBS, 10% glycine, 10% penicilline-streptomycine) in the wells. Cells were tested for viability at 24 and 72 h post exposure to the polymers using a Live/Dead Viability/Cytotoxicity assay for mammalian cells (Molecular Probes, Carlsbad, CA; 4 μM Ethidium homodimer-1 (EthD-1) and 2 μM of Calcein-AM). Cells were washed with PBS prior to addition of 100 μl Live/Dead reagent, then incubated for 30 min. Untreated hMSCs grown in complete medium were used as live controls. Fluorescence was measured using a fluorescent microplate reader (FLx800 Bio-TEK instruments) equipped with a 485/582 (excitation/emission) filter to measure calcein (green fluorescence). The fraction of live cells was calculated as described by Temenoff et al.⁹⁰. Furthermore, live and dead cells were visualized by fluorescence microscopy using Nikon-Eclipse E600 and Image-Pro Plus software v 5.1 (Media Cybernetics Inc., Bethesda, MD, v 5.1).

Transfection Studies

Cell culture

hMSCs were plated on 6-well plates at a density of 5×10^3 cells/cm². hMSCs were allowed to attach overnight in the presence of complete medium after which the medium was replaced by α -MEM. Before the cells were transfected with the plasmids, the cell cycles were synchronized with the assumption that the doubling time of hMSCs is ~ 30 h⁹¹. To this end, the cells were incubated in serum free medium (α -MEM) for 30 h. Once synchronized, cells were incubated in complete medium for 6 h to allow reactivation of the normal cell cycle.

Assembly of PEI-HA/pDNA and PEI/pDNA complexes

PEI and PEI-HA were each separately dissolved in 150 and 500 mM of NaCl solution and filtered through a 0.2 μ m filter. Each of the solutions was divided into two batches; one batch was placed at room temperature for dissolution, the other was placed in a 37°C incubator. On complete dissolution of the two polymers, 0.1 N HCl dissolved in 150 or 500 mM NaCl were used to titrate the polymer solutions to physiological pH (7.4). Additional NaCl solutions were used to bring the final concentration of the two polymers to 1 mg/ml upon which they were returned to the incubator or room temperature overnight. The following day, 1.0, 2.5 and 3.8 μ l reporter plasmid (concentration 4 μ g/ μ l) was aliquoted into tubes and the volume was adjusted to 50 μ l with NaCl solutions. These solutions were then independently combined with vectors either in a 37°C water bath or at room temperature. PEI or PEI-HA was added drop-wise with frequent mixing such that the N:P ratio in each case was preserved at 7.5 : 1. The samples were briefly centrifuged and returned either to the incubator or left at room temperature to stand for 2 h.

Transfection of hMSCs with PEI/pDNA and PEI-HA/pDNA complexes

hMSCs were allowed to attach overnight in 6-well plates and their cell cycles were synchronized as described above. Complexes assembled at 37°C were kept in the water bath until they were introduced drop-wise onto the cells, and after transfection the cells were immediately returned to the incubator. Complexes assembled at room temperature were introduced onto cells similarly and then returned to the incubator as well. Two groups served as controls; one treated only with complete medium and the other group treated with pDNA alone. Flow cytometry was used to determine the percentage of transfected cells.

Flow cytometry

(a) Fixing cells: Cell-wells were washed three times with sterile PBS to remove any dead cells, then treated with 0.5 ml of 0.5 X trypsin (Gibco, Bethesda, MD) at 37°C for 3 minutes. Trypsinization was terminated with the addition of complete medium. The cells were collected in suspension and centrifuged for 10 min at 10,000 rpm. The medium was aspirated and replaced with chilled 1% formaldehyde solution for 1 h on ice. The cells were centrifuged again and the formaldehyde solution was replaced with PBS.

(b) Counting cells: The cells were counted using flow cytometry (Becton Dickenson FACS Scan) at high flow using CellQuest Pro software (BD Biosciences, San Jose, CA, v 5.1). To determine the location of hMSCs on the graph, sterile PBS (background signal) followed by hMSCs suspension in PBS was run through the flow cytometer. The location

of hMSCs was gated and this gate used to identify cells in experimental samples. The FACS machine was further calibrated to register green fluorescence emitted by cells that were successfully transfected, while a separate channel recorded the total number of cells passing through the capillary of the FACS. A maximum limit of 5×10^3 cells per sample was implemented on the gated population of all experimental groups. In cases where cell mortality was too high to obtain the set cell-count, the reading terminated if no new cells were registered after 3 min. The total number of cells counted up to that point was used to calculate the transfection efficiency⁹²

$$\text{Absolute Transfection Efficiency} = \frac{\text{Cell Count of Experimental Cells}}{\text{Cell Count of Control Sample}} \times (\% \text{ Cells Transfected})$$

While analyzing transfection percentage, markers were placed at 1% of control samples (untreated cells) to determine the population of cells with a relative rightward shift.

Statistical Analysis

Statistical analysis was performed between groups for the live/dead assay and flow cytometry transfection studies. Groups were analyzed with ANOVA using a *p-value* <0.05 and pair-wise comparisons were performed using the Tukey's Honestly Significant test.

Results

Synthesis and NMR Spectroscopy

The conjugates of HA and PEI were synthesized in aqueous buffer by reductive amination according to the scheme shown in Figure 3.1. This reaction involves the formation of an imide intermediate at the anomeric C1 of HA, which is reduced to a secondary amine by sodium cyanoborohydride. The PEI-HA conjugate was then purified by ultrafiltration and finally lyophilized to form a dry powder.

The ^1H NMR spectrum of HA showed a signal of $\delta \sim 5.15$ ppm for the anomeric carbon C1 of HA, which did not appear in the spectrum for the purified PEI-HA conjugate (Fig. 3.2a). Signals corresponding to all other functional groups of HA and PEI were found in the NMR spectrum of the conjugate as follows (Figs.1 and 2a): $\delta \sim 2.0$ ppm (H of $-\text{NCOCH}_3$ from HA); $\delta 2.5 - 3.2$ ppm (H of $\text{N-CH}_2\text{-CH}_2\text{-N}$ from PEI); $\delta \sim 3.35$ ppm (H of C2' from HA); $\delta 3.4 - 3.7$ ppm (H of C4, C5, C3', C4' from HA); $\delta 3.7 - 4.0$ ppm (H of C2, C3, C6a, C4', C5' from HA); $\delta \sim 4.15$ ppm (H of C6a from HA); $\delta \sim 4.45$ ppm (H of C1' from HA); $\delta \sim 4.55$ ppm (H of C1 from HA).

The DEPT-135 ^{13}C NMR spectrum of PEI-HA further confirmed the presence of PEI and HA in the conjugate (Figs. 3.1 and 3.2b). The peaks of the expected functional groups can be assigned as follows^{93, 94}: $\delta \sim 25$ ppm (NCOCH_3 from HA); $\delta 40 - 55$ ppm (methylene $\text{N-CH}_2\text{-CH}_2\text{-N}$ from PEI); $\delta \sim 57$ ppm (methine C2 from HA); $\delta \sim 63$ ppm (methine C6 from HA); $\delta \sim 71$ ppm (methine C4 from HA); $\delta 74 - 76$ ppm (methine C3, C3' from HA); $\delta 78 - 80$ ppm (methine C5, C5' from HA); $\delta \sim 82$ ppm (methine C4'

from HA); $\delta \sim 88$ ppm (methine C3 from HA); $\delta \sim 103$ ppm (methine C1 from HA); $\delta \sim 106$ ppm (methine C1' from HA). The C1 signal of α - and β -anomer was only found in the spectrum of HA at $\delta \sim 94$ ppm and $\delta \sim 98$ ppm, respectively. Due to a low signal-noise ratio in the PEI-HA spectrum the absence of the anomeric C1 signal could not be confirmed as clearly as for the ^1H spectrum. To quantify the amount of HA attached to PEI by ^1H NMR, the peaks corresponding to H of $-\text{NCOCH}_3$ from HA at $\delta \sim 2.0$ ppm and H of $\text{N-CH}_2\text{-CH}_2\text{-N}$ from PEI at $\delta 2.5 - 3.2$ ppm were integrated and the ratios of ^1H atoms were compared to determine the amount of HA incorporated into PEI. This analysis showed that between 11.4 to 13.0 % of primary amines of PEI had reacted with HA to form PEI-HA via reductive amination.

Fluorescence Assisted Carbohydrate Electrophoresis (FACE)

A sample gel containing HA and PEI-HA, before and after treatment with chondroitinase ACII is shown in Figure 3.3. As seen in lane 5 of the gel, the undigested HA sample has a mixture of oligomers within the sample obtained from the manufacturer. When treated with chondroitinase AC II, which cleaves galactosaminidic linkages, HA multimers reduce to dimers as shown in lane 6. Lane 3 contains untreated PEI-HA and does not show the presence of HA, even at high exposures, indicating that the polymer does not contain non-covalently attached HA contributing to the stoichiometry of the polymer. When the same samples were treated with chondroitinase ACII however, we can see HA dimers in lanes 2 and 4, suggesting that HA has been cleaved from the parent molecule, PEI-HA. The amount of HA attached to PEI was

calculated using densitometry on the bands of HA in the gels. Relative ratios of the oligomers within the HA used were determined from lane 5. These ratios were then applied to the HA band in lanes 2 and 4, while standards were used to quantify the total HA in these lanes. FACE studies were repeated two additional times to confirm the average amount of HA.

Calculations showed that taking into account the various “mers” present within the reactant HA, $13 \pm 1\%$ of the primary amine groups of PEI were substituted with HA via reductive amination. This is in good agreement with the data obtained from NMR analysis.

Electrophoresis Band Retardation

To determine whether salt concentration would facilitate pDNA packing within the vector, PEI-HA and pDNA complexes were assembled after PEI-HA was equilibrated in NaCl solutions of various concentrations ranging from 150 to 1000 mM. As seen in Figure 3.4, the amount of unbound pDNA detected on the agarose gel decreased with increasing salt concentrations at N:P ratios of 2:1 and 7.5:1. At NaCl concentrations equal to or greater than 500 mM, the amount of unbound pDNA decreased at N:P ratio 2:1 and was absent, even at high exposures, at N:P ratio 7.5:1. However, at N: P ratio of 13.5:1 none of the samples showed unbound pDNA. No free pDNA was observed with PEI/pDNA complexes assembled at 7.5:1 and 13.5:1.

Dynamic Light Scattering

(A) PEI-HA

In pure water, PEI-HA has limited solubility and forms visible aggregates. These aggregates can dissipate completely when the solution is incubated at 37°C for 3 days or alternatively if the vector is dissolved in 150 mM NaCl solution. Once the polymer was completely dissolved in NaCl solutions, DLS studies on PEI-HA showed a range in Rh of the vector with increasing salt concentrations. The Rh distribution of PEI-HA shifted significantly to higher Rh as higher molarity NaCl solutions were used (Table 3.1). As seen in Table 3.1, the peak intensity occurred at 2.0 ± 1.1 nm for the vector dissolved in 150 mM of NaCl, 11.4 ± 5.2 nm in 500 mM of NaCl, and 366.0 ± 149.0 in 1000 mM NaCl.

(B) PEI-HA/pDNA Complexes

At 25°C PEI-HA/pDNA complexes assembled in all salt solutions displayed a bimodal distribution. Increasing the salt concentrations resulted in more complexes with smaller Rh. After increasing the temperature to 37°C most populations with smaller Rh shifted slightly towards higher Rh while their size distribution became narrower (Figure 3.5 and Table 3.2).

Static Light Scattering

The scattering intensity of the polymer complexes at 25 and 37°C was used to construct Zimm plots. Data points for the Zimm plots were obtained by diluting the

sample with their respective salt solutions then measuring light intensities at eighteen different scattering angles. Using regression analysis, data points were fitted to a trend line (not shown) in order to determine the A_2 as well as molecular weight. Representative molecular weights of the complexes at 25 and 37°C were similar for complexes assembled at 150, 300 and 500 mM of NaCl solution as seen in Table 3.3.

Cell Viability Studies

As shown in the plot in Figure 3.6(a), at both 24 and 72 h for all tested concentrations, PEI was extremely toxic to hMSCs with $7.0 \pm 2.8\%$ of hMSCs cells surviving after exposure to PEI alone. In contrast, PEI-HA exhibited reduced toxicity to hMSCs even at the highest concentration tested (500 $\mu\text{g/ml}$), where an average of $86.0 \pm 6.7\%$ of cells remained viable. With longer exposure for 72 h to PEI-HA, cell mortality was higher, where on average $61.6 \pm 2.7\%$ of cells survived. However, at concentrations used for transfection ($<50 \mu\text{g/ml}$), cell viability was high at $87.6 \pm 4.6\%$ at 24 h and even higher at 72 h ($101.6 \pm 11.6\%$). Fluorescent microscopy images reflect the quantitative findings. hMSCs treated with PEI-HA display normal morphology and are prevalent throughout the wells. However, cells treated with PEI are fewer in number and present as cell clusters with abnormal morphology indicative of dead or dying cells (Figure 3.6(b)).

Transfection Studies

(A) Dose response of PEI-HA vs. PEI as transfection agents

Preliminary studies showed that maximum transfection with PEI-HA and PEI can be achieved within a 24 h incubation period. Also, PEI-HA/pDNA complexes assembled in

500 mM of NaCl solution exhibited improved transfection over those complexes assembled in 150 mM NaCl solution. However, higher transfection efficiencies and cell viability were achieved when PEI/pDNA complexes were assembled in 150 mM of NaCl. Hence, these salt concentrations were used to form complexes to transfect hMSCs with 20 µg/ml, 50 µg/ml or 75 µg/ml of plasmid DNA. As shown in Table 3.4, cells transfected with PEI had significantly reduced cell counts as compared to those transfected with PEI-HA. Transfection efficiencies decreased with increasing pDNA amounts due to reduced cell counts from PEI associated toxicity. With PEI-HA, a maximum transfection efficiency of $33.6 \pm 13.9\%$ was observed with 50 µg/ml of pDNA (Figure 3.7 and table 3.4). However, with increasing the concentration to 75 µg/ml of pDNA, the transfection efficiency decreased to $22.9 \pm 4.3\%$. Nevertheless, the transfection efficiency of PEI-HA/pDNA complexes was still higher than that of PEI/pDNA complexes even at 50 µg/ml ($7.25 \pm 2.9\%$) and 75 µg/ml of pDNA, where the cell count was too low to assess transfection.

(B) Effect of NaCl concentration and temperature on transfection efficiencies

To establish a correlation between light scattering data and transfection efficiencies, PEI-HA was dissolved in 150 and 500 mM NaCl solution complexed with pDNA at either 25 or 37°C. PEI-HA dissolved in 150 mM NaCl solution and complexes assembled at both temperatures exhibited low transfection efficiencies, ($3.8 \pm 1.5\%$ and $4.3 \pm 3.8\%$ respectively) (Figure 3.7 and table 3.5). However, when PEI-HA was dissolved in 500

mM of NaCl, transfection efficiency significantly improved to $12.7 \pm 4.3\%$ and $19.1 \pm 4.4\%$ at 25 and 37 °C respectively.

Discussion

PEI-HA is a novel polymeric gene delivery vector designed with the objectives of (i) reducing the toxicity of PEI and (ii) increasing specific interactions with hMSCs^{95, 96}. Experiments described here focus on the synthesis of covalently conjugated PEI-HA and the dynamic behavior of the vector in ionic (NaCl) solutions of different concentrations in ambient versus physiological temperatures. The two temperatures studied here are most commonly used to assemble and transfect vector/plasmid complexes to cells respectively. Experimenting with these variables provides an insight into utilizing ions and temperature to optimize transfection efficiencies.

PEI-HA is synthesized by covalently linking PEI to HA via reductive amination (Figure 3.1) and the resulting zwitterionic polymer is purified by repeated dialysis. ¹H and ¹³C NMR spectrometry of the PEI-HA conjugate revealed characteristic signals from both precursors (Figure 3.2) and a conversion of 11.4-13.0 % primary PEI amines into secondary amines. These results were further confirmed with FACE, which showed that $13 \pm 1\%$ of primary amines were conjugated to HA.

One of the objectives for conjugating anionic HA with PEI was to reduce the toxicity associated with PEI. A major drawback associated with PEI as demonstrated here with hMSCs and elsewhere with rat MSCs⁹⁷ (rMSCs), as well as cell lines⁷⁶ is the toxicity associated with the polymer. This toxicity has been attributed to the cationic charges on

PEI^{77, 98} that cause cell death by disrupting the cell membrane and organelles⁹⁹. In hMSCs, even low concentrations of PEI (10 µg/ml) cause significant mortality (<10% viability), which is persistent even after PEI is complexed to pDNA (Table 4). However, at PEI-HA concentrations relevant to transfection studies performed here (< 50 µg/ml), cell viability is consistently high at $87.0 \pm 4.6\%$ after 24 h of exposure and $101.7 \pm 11.6\%$ 48 hours after the cells are returned to complete medium (Figure 3.5).

The objective of increasing transfection efficiency of PEI by using HA as a ligand to hMSCs receptors was also achieved in studies described here. Transfection efficiencies in the range of 7.3 to 12.0 % were obtained with PEI/pDNA complexes, which are similar to values reported in literature^{66, 67}. As shown in Table 4, a maximum transfection efficiency of $33.6 \pm 13.9\%$ was obtained for PEI-HA complexed with 50 µg/ml of pDNA. Although at lower concentrations of pDNA (20 µg/ml) PEI and PEI-HA performed similarly, the toxicity associated with PEI/pDNA complexes was significantly higher than that seen with PEI-HA/pDNA complexes as evident in the cell counts shown. At still higher concentrations of pDNA, the transfection efficiency dropped to $22.9 \pm 4.3\%$ for PEI-HA/pDNA complexes. This could be attributed to an increase in complex size or complex aggregation in small transfection volumes (200 µl), although the experiments described here do not provide any conclusive evidence.

We further evaluated the influence of salt and temperature on the size of the vector and its complexes with pDNA with the objective that we can optimize the transfection efficiency of PEI-HA by modulating these parameters. Based on the ligand and the mechanism of uptake (receptor-associated versus receptor free), various groups have

associated the influence of complex size on gene delivery. Due to opposite charges on PEI and HA, the zwitterionic polymer PEI-HA is capable of inter- and intra-molecular bonds that can induce aggregation. Transferrin-PEI vectors, also formed by conjugating anionic and cationic molecules have better transfection efficiencies when pDNA complexes are as large as 500 nm in diameter¹⁰⁰. This has been attributed to improved uptake due to “increased sedimentation of larger particles on cell surfaces” and better endosomal release of larger complexes due to the proton sponge effect¹⁰¹. However, ligand conjugated vectors associated with receptor-mediated endocytosis, have performed better with smaller pDNA complexes¹⁰². In this case, formation of aggregates in PEI-HA/pDNA complexes due to electrostatic interactions would limit transfection¹⁰³. Hence, we modulated salt concentrations to study its influence on the vector and the vector’s ability to pack pDNA. Furthermore, we modulated salt and temperature to understand their influence on the size of the vector/plasmid complex and understand how size relates to transfection efficiency.

As vector PEI-HA was dissolved in NaCl solutions of increasing ionic strength, the Rh of the molecule increases by at least an order of magnitude. While the vector had a mean Rh of 2.0 ± 1.1 nm at 150 mM NaCl, the Rh increased to 11.4 ± 5.2 nm at 500 mM NaCl and further to 366.0 ± 149.0 nm at 1000 nM NaCl solution (Table 3.1). This suggested that the polymer continues to unfold as the ionic concentration increases due to the shielding effect on intra-molecular bonds¹⁰⁴. In addition, increasing ionic strength also allows for better pDNA packing as observed in the band retardation studies (Figure 3.4). The appearance of pDNA as shown in the gel in Figure 3.4 is dependent on the

number of free phosphate groups in the pDNA backbone available to intercalate with EthBr. Hence, the absence of EthBr staining within the lanes suggests the absence of free pDNA in those lanes. While complexes assembled at 150 mM and 300 mM NaCl solutions show residual unbound pDNA at N:P ratios of 2:1 and 7.5:1, solutions greater than 500 mM NaCl have very little residual pDNA within their respective lanes. When these results are considered together, a larger Rh of PEI-HA vectors correlates to improved pDNA packing. Previous studies have shown that when pure cationic polymers such as PEI are bound to pDNA at increasing NaCl concentrations, the binding affinity between the plasmid and vector decreases significantly¹⁰⁵. However, the complete retardation of pDNA with increasing ionic concentration suggests a possible mechanism whereby the ions in solution unravel the PEI-HA vector thus allowing pDNA to better interact with the cationic backbone of the vector. Improved packing of the plasmid within the vector indicates protection of the plasmid DNA from degradation by lysosomal enzymes⁴⁵, thus leading to better gene delivery^{76, 106}.

Light scattering studies further elucidate the dynamic behavior of PEI-HA/pDNA complexes at increasing ionic concentrations. At both 25 and 37°C, higher ionic concentrations significantly reduced the mean hydrodynamic radius of the complexes as shown in Figure 3.5 and Table 3.2. The mean complex size did not decrease below 100 nm at 500 mM of NaCl (used for transfection), while complexes assembled at 150 mM NaCl were largest with an average Rh of 595.0 ± 44.6 nm (25°C) and 766.5 ± 137.2 nm (37°C). Furthermore, at 37°C the complexes exhibited a narrower distribution range with increasing ionic concentration. Two possible explanations for larger hydrodynamic radii

at the higher temperatures are that¹⁰⁷: (a) the pDNA complexes formed aggregates driven by thermal energy, or (b) the individual PEI-HA/pDNA complexes themselves experienced a changing conformational expansion due to the thermal energy introduced. To test these hypotheses, SLS data were analyzed using Zimm equations to determine the average molecular weight of the complexes. As seen in Table 3.3, the data obtained by batch method suggest that complexes assembled at similar ionic concentrations but at different temperatures did not differ in molecular weights, indicating that the increase in Rh may not be due to the formation of larger aggregates.

Subsequent transfection studies examined the influence of complex size on gene delivery. Results show that, in general, larger complexes with $R_h > 500$ nm do not perform well as gene delivery agents. Hence, complexes assembled at 150 mM of NaCl at both ambient and physiological temperatures showed very low transfection despite relatively high exposure periods to cells (24 h). However, as the ionic strength was increased and the pDNA complexes reduced in mean Rh, gene delivery efficiencies improved significantly. Maximum GFP expression was obtained with complexes assembled in 500 mM of NaCl at physiological temperature. Although these complexes showed a significantly larger Rh than those assembled at ambient temperatures, this population had a narrower standard deviation in complex sizes. The improvement in gene delivery could be attributed to a variety of factors including, (i) a narrower population distribution of the complexes, (ii) an improved proton sponge effect due to a more open conformation of PEI-HA, subsequently causing an earlier release of the complex from endosomes, or (c) improved release of plasmid DNA from the complexes due to their

association with HA as observed by Yoshihiro et al.¹⁰⁴. The current studies cannot sufficiently identify any one of these factors as being responsible for improved transfection and further studies will be needed to elucidate the mechanisms involved in gene delivery with this vector.

Conclusion

The synthesis of PEI-HA, a novel gene delivery vector, via reductive amination was described in this study. We show that by modulating the NaCl concentration and temperature, we can control the hydrodynamic radius of PEI-HA/pDNA complexes. Results indicate that increasing the ionic concentration reduces the Rh of the PEI-HA/pDNA complexes and increases the transfection efficiency. Complexes at a higher temperature have a more narrow Rh range, which further improves transfection. The studies performed here demonstrate transfection efficiencies as high as $33.6 \pm 13.9\%$, with a mean cell viability of $86.0 \pm 6.7\%$. PEI-HA is comparable with other commercial, non-viral gene delivery agents while being more cytocompatible and feasible for tissue engineering applications.

Figures

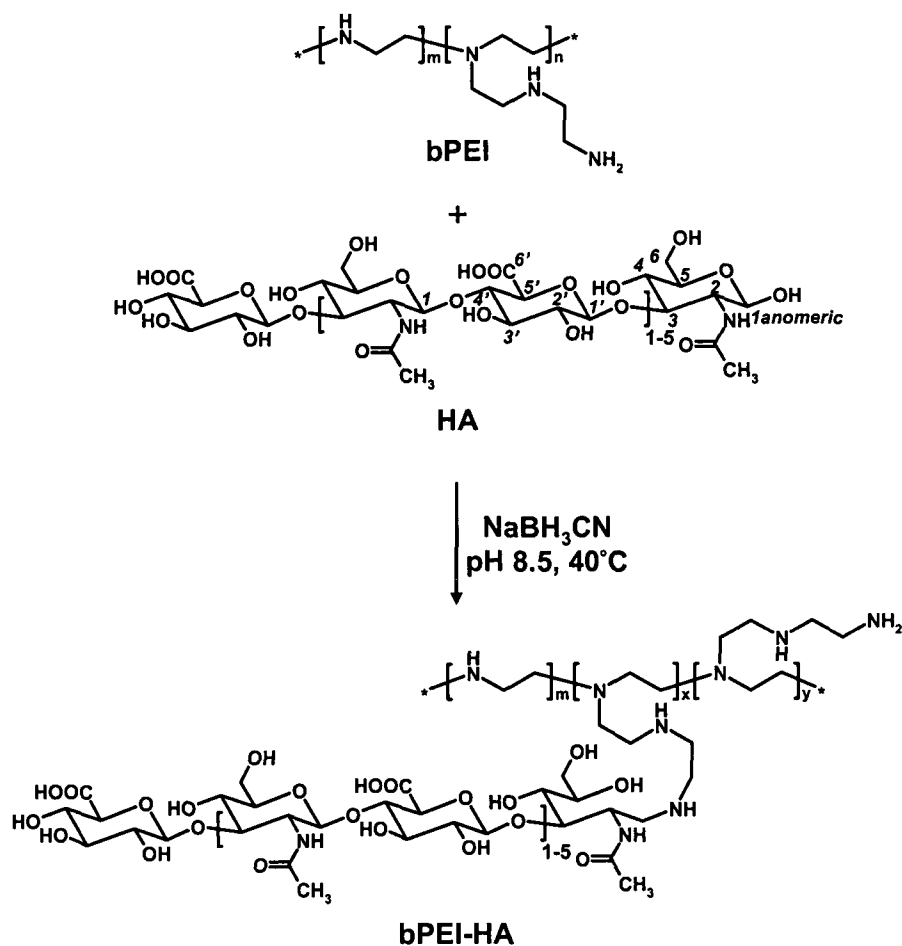


Figure 3.1: Reaction scheme to conjugate branched polyethylenimine (PEI) and hyaluronic acid (HA) by the process of reductive amination. Note that the structure of PEI has been simplified for brevity. All structures are depicted in the undissociated state. The carbon atoms of the structural subunits of HA, N-acetylglucosamine (C1 - C6) and glucuronate (C1' - C6'), are numbered for reference. PEI represented in the reaction products contains two different forms of primary amines, those that participate in the chemical bond with HA and those that do not.

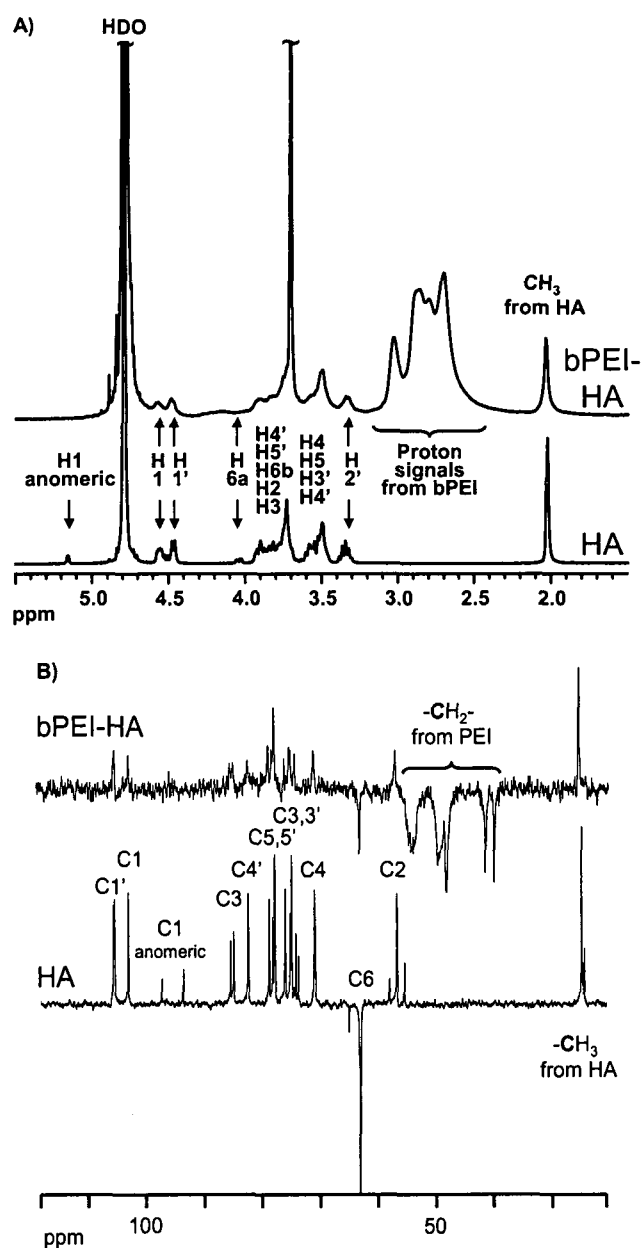


Figure 3.2: ^1H NMR spectra of PEI-HA and HA (A). DEPT-135 ^{13}C NMR spectra of PEI-HA and HA. DEPT-135 ^{13}C NMR spectra of PEI-HA and HA. The corresponding structures are depicted in Figure 3.1 (B).

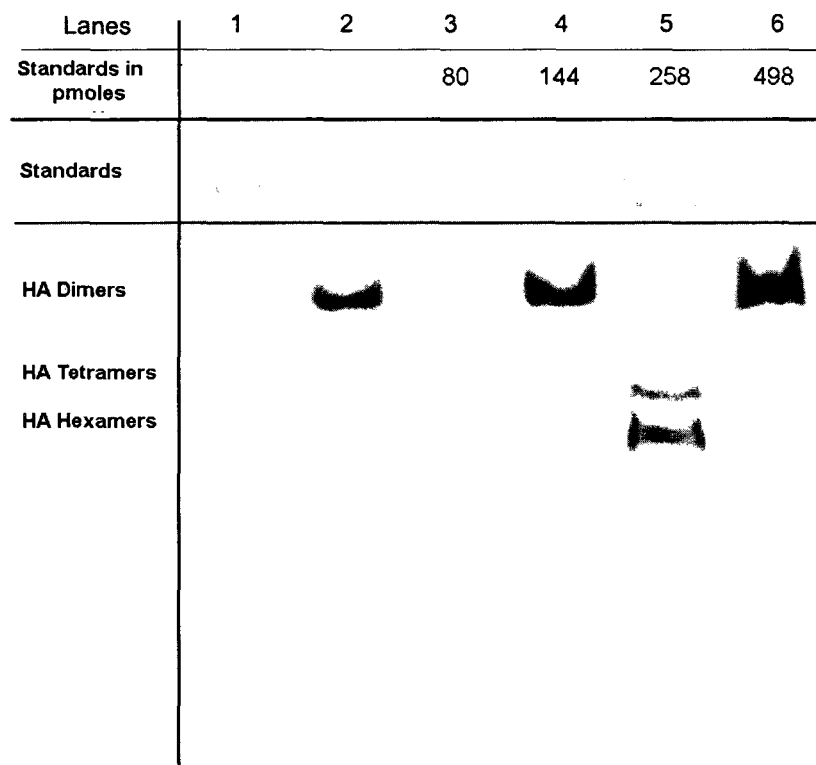


Figure 3.3: Fluorescence Assisted Carbohydrate Electrophoresis (FACE) of PEI-HA. Lanes represent ladder (1); PEI-HA treated with the enzyme chondroitinase AC II (2) and (4); PEI-HA not treated with the enzyme (3); pure undigested HA as obtained from the manufacturer (5) and pure HA digested with chondroitinase AC II (6). The enzyme was delivered in excess of the sample (>100X) and cleaves galactosaminidic linkages within the sugar molecule. Standards of maltotriose used to quantify HA are shown at the top.

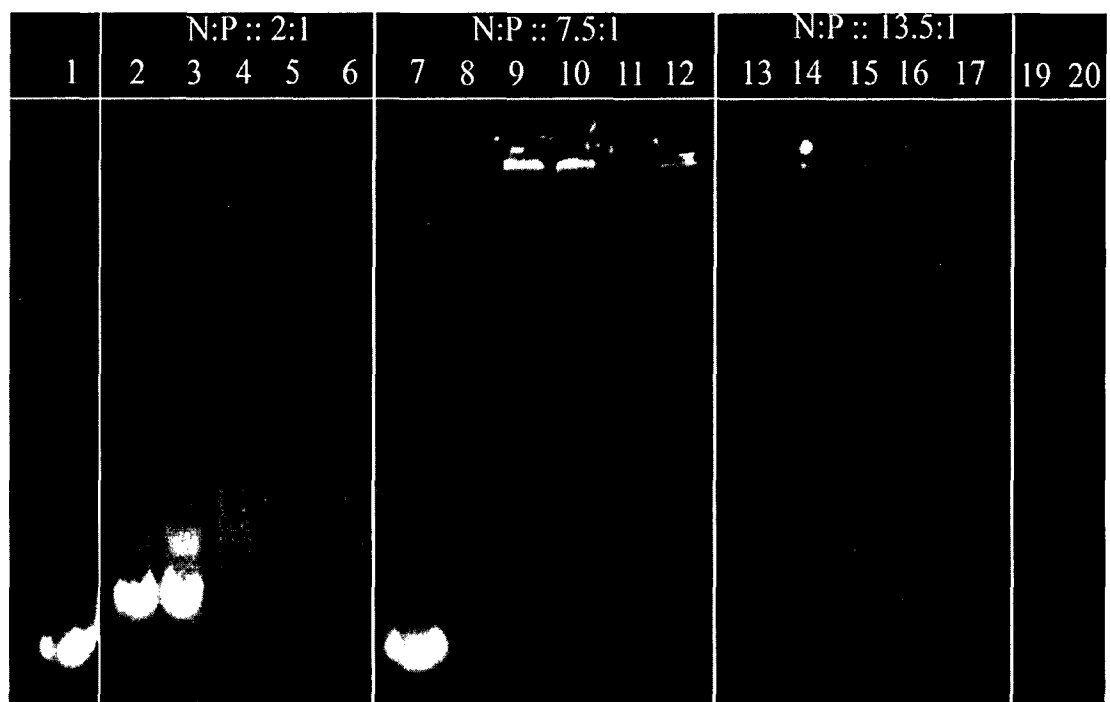
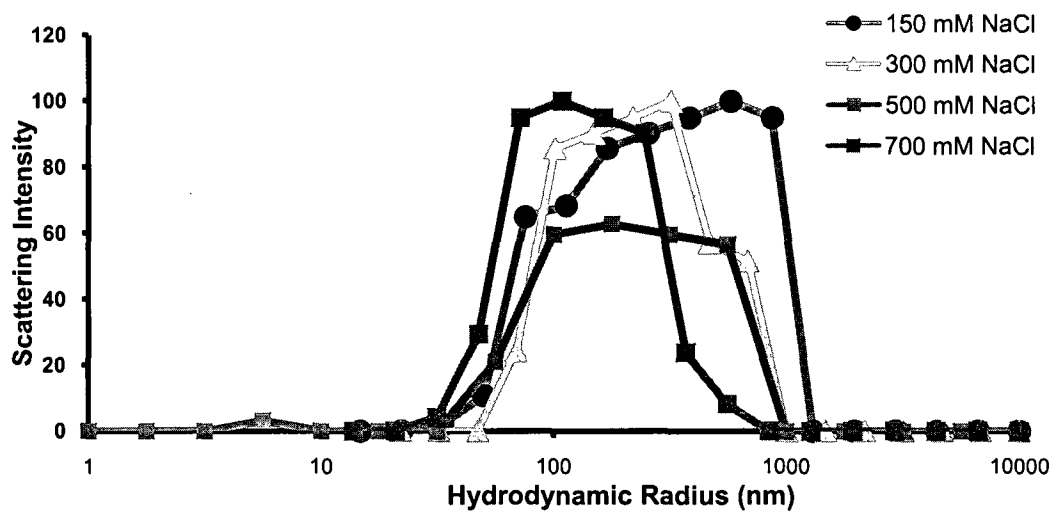
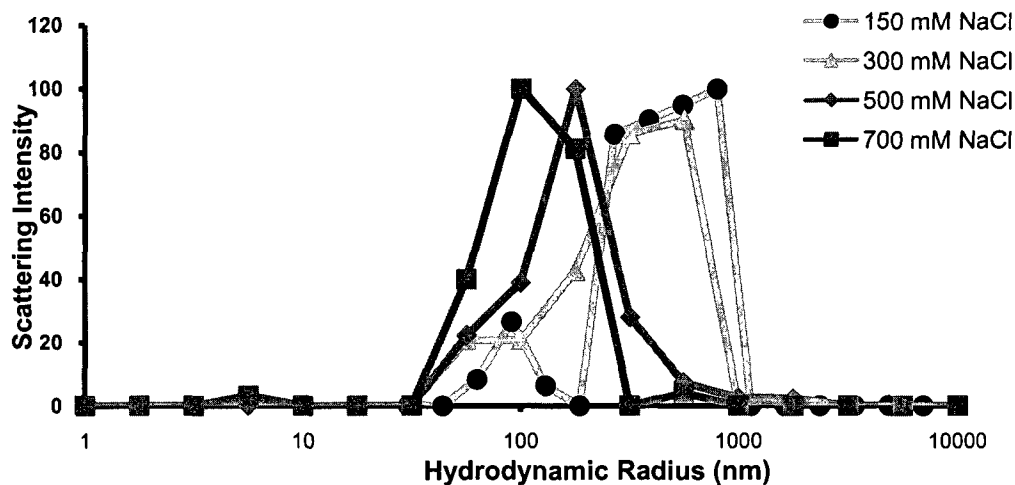


Figure 3.4: Agarose gel electrophoresis representing pDNA binding studies with PEI-HA and PEI. 1 μ g of pCMV-eGFP plasmid was combined with PEI-HA at N:P ratios of 2:1, 7.5:1 and 13:1 and with PEI at ratios 7.5:1 and 13.5:1. The lanes represent the following: Lane 1: 1 μ g uncomplexed pDNA, Lanes 2-6: PEI-HA/pDNA complexes at N:P :: 2:1, assembled in 150 mM NaCl (2); 300 mM NaCl (3); 500 mM NaCl (4); 700 mM NaCl (5); 1000mM NaCl (6); 1 μ g uncomplexed pDNA (7); Lanes 8-12: PEI-HA/pDNA complexes at N:P :: 7.5:1, assembled in 150 mM NaCl (8); 300 mM NaCl (9); 500 mM NaCl (10); 700 mM NaCl (11); 1000 mM NaCl (12); Lanes 13-17: PEI-HA/pDNA complexes at N:P ratios 13.5:1, assembled in 150 mM NaCl (13); 300 mM NaCl (14); 500 mM NaCl (15); 700 mM NaCl (16); 1000mM NaCl (17). PEI/pDNA complexes at N:P ratios 7.5:1 (19) and 13.5:1 (20).

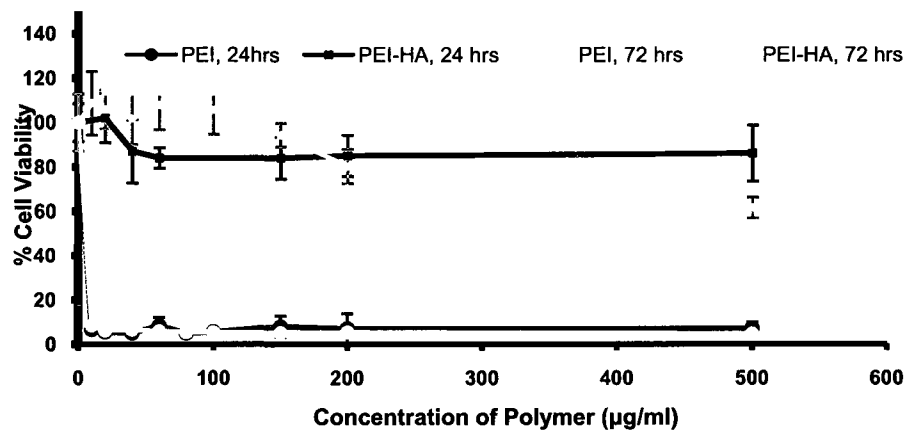


(A)

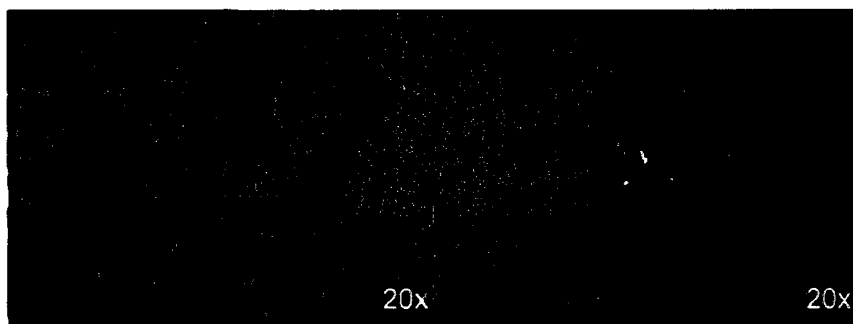


(B)

Figure 3.5: Dynamic light scattering distribution for PEI-HA/pDNA complexes assembled at N:P ratios of 7.5 : 1 at (A) 25°C and (B) 37°C. Mean Rh shifts to the left (smaller values) with increasing salt concentrations. However, at higher temperature (37°C) the Rh shifts to the right, (larger Rh) while exhibiting a narrower size distribution.



(A)



(B)

Figure 3.6: Cell viability at 24 and 72 h after exposure to polymers PEI and PEI-HA.

(A) hMSCs were treated with a range of PEI and PEI-HA concentrations ranging from 10 µg/ml to 500 µg/ml. Cells were exposed to the polymers for 24 h after which transfection medium was replaced with complete medium. Error bars indicate 1 standard deviation with $n = 4$.

(B): Cells treated with PEI-HA (left) and PEI (right) after 8 h of exposure to the respective gene delivery vectors. Green represents uptake of calcein dye by live cells, whereas the red dye represents binding of the ethidium homodimer to the nucleic acid of damaged cells.

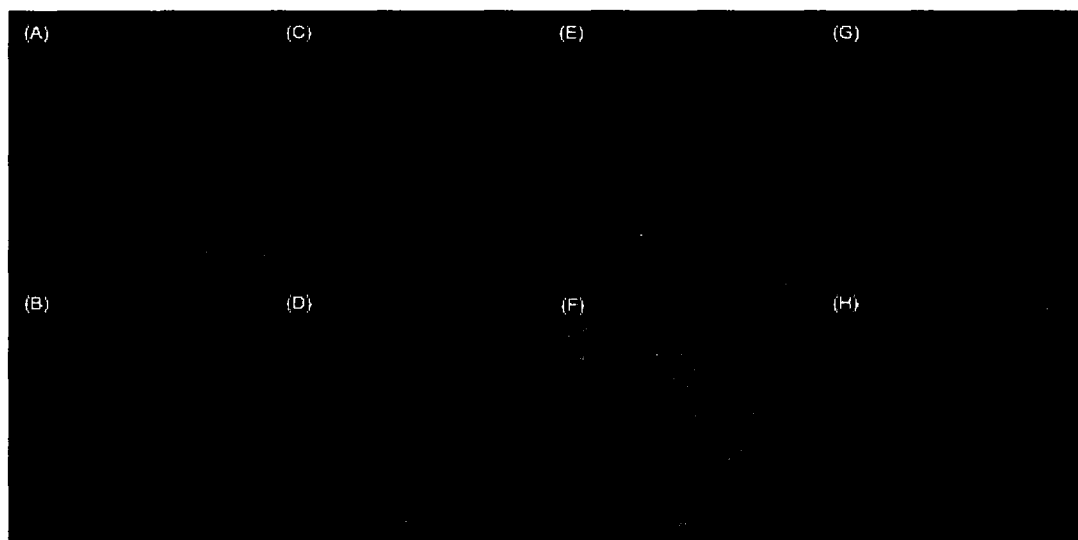


Figure 3.7: Transfection efficiency of PEI-HA and PEI on hMSCs represented with expression of green fluorescent protein. Representative fluorescence images of MSCs treated with 200 μ l of transfecting solutions containing (A) 20 μ g/ml pDNA alone; (B) PEI complexes with 20 μ g/ml of pDNA; PEI-HA complexes with (C) 20 μ g/m μ g and (D) 50 μ g/m of pDNA at 25°C in 150 mM NaCl solution; PEI-HA complexes with (E) 20 μ g/ml and (F) 50 μ g/ml of pDNA at 25°C in 500 mM NaCl solution; PEI-HA complexed with (G) 20 μ g/ml of pDNA at 37 °C in 500 mM NaCl solution; and (H) 75 μ g/ml of pDNA at ambient temperature in 500 mM NaCl solution. Expression of green fluorescent protein (GFP) is represented in green in the cells. Bar represents 100 μ m for all images.

Tables

NaCl concentration	150 mM	500 mM	1000 mM
Range of Rh (nm)	1.0-3.2	4.0-27.0	212.0-556.0
Mean Rh (nm)	2.0 ± 1.1	11.4 ± 5.2	366.0 ± 149.0

Table 3.1: Range and averages of hydrodynamic radii (Rh) obtained with PEI-HA at different salt concentrations; 150, 500 and 1000 mM NaCl solution.

NaCl concentration	150 mM	300 mM	500 mM	700 mM
25 °C				
Distribution (nm)	33.4-1000	47.3-1000	3.2-1000	2.9-847
Mean Rh (nm)	595.0 ± 44.6	295.0 ± 25.0	119.9 ± 35.6	105.9 ± 19.2
37 °C				
Distribution (nm)	187-1140	40-1000	30-1000	32-1000
Mean Rh (nm)	766.5 ± 137.2	517.2 ± 44.7	193.5 ± 13.7	74.2 ± 23.0

Table 3.2: Distribution and peak intensities describing the range of hydrodynamic radii (Rh) observed with DLS for PEI-HA/pDNA complexes at ambient (25°C) and physiological temperature (37°C).

NaCl concentration	150 mM	300 mM	500 mM	700 mM
MW at 25°C	4.04×10^7	4.33×10^7	1.68×10^7	1.07×10^7
MW at 37°C	4.19×10^7	4.05×10^7	1.95×10^7	8.9×10^6

Table 3.3: Representative molecular weights of PEI-HA/pDNA complexes at different salt concentrations and ambient (25 °C) versus physiological (37 °C) temperatures. Molecular weight is reported as g/mol. The values were obtained by using SLS data and Zimm equations.

Vector	PEI			PEI-HA		
DNA amount	20 µg/ml	50 µg/ml	75 µg/ml	20 µg/ml	50 µg/ml	75 µg/ml
Cell Count (max. 5000)	1974.0 ± 780.0	1087.0 ± 333.7	Cell count ≤ 500	4957.0 ± 10.2	4999.0 ± 120.6	4885.0 ± 59.3
Transfection Efficiency	12.0 ± 4.2	7.3 ± 2.9		12.7 ± 4.3	33.6 ± 13.9*	22.9 ± 4.3**

*All groups had a sample size of n= 4 – 6 and were assessed for statistical difference at p< 0.05. * and ** represent statistical difference between the corresponding PEI/DNA complexes.*

Table 3.4: Gene delivery efficiency of PEI and PEI-HA in 200 µl of transfecting solution at 20 µg/ml, 50 µg/ml and 75 µg/ml of DNA in hMSCs after exposure for 24 h to the gene delivery complexes. The table represents the maximum cell counts obtained after transfection with PEI/DNA or PEI-HA/DNA complexes (population limit is set at 5000 cells). The percentage of transformed cells obtained after transfection with PEI/DNA and PEI-HA/DNA complexes. Transfection efficiencies noted here have been corrected for cell viability.

Amount of DNA delivered	DNA only	150 mM at 25 °C	500 mM at 25 °C	150 mM at 37 °C	500 mM at 37 °C
20 µg/ml	1.8 ± 0.4	3.8 ± 1.5*	12.7 ± 4.3	4.3 ± 3.8	19.1 ± 4.4**

*All experimental groups (n=4) were assessed for statistical difference at $p < 0.05$. * represents statistical difference between samples transfected with DNA alone, whereas ** represents statistical difference between samples transfected at 25°C in 150mM NaCl.*

Table 3.5: Percentage of cells transfected by PEI-HA/DNA complexes at different NaCl concentration and temperature. Total volume of the transfecting solution was 200 µl. Complexes assembled at 150 mM NaCl showed a significantly decreased gene delivery rate as compared to those assembled at 500 mM NaCl. Complexes assembled at physiological temperatures also showed significantly increased transfection efficiency as compared to those assembled at ambient temperatures for higher NaCl concentrations.

Chapter IV

*Fabrication of Non-woven Coaxial Fiber Meshes by Electrospinning*³

Abstract

There is a great need for biodegradable polymer scaffolds that can regulate the delivery of bioactive factors such as drugs, plasmids and proteins. Coaxial electrospinning is a novel technique that is currently being explored to create such polymer scaffolds by embedding within them aqueous based biological molecules. In this study we evaluated the influence of various processing parameters such as sheath polymer concentration, core polymer concentration and molecular weight, and salt ions within the core polymer on coaxial fiber morphology. The sheath polymer used in this study was poly(ϵ -caprolactone) (PCL) and the core polymer was poly(ethylene glycol) (PEG). We examined the effects of the various processing parameters on core diameters, total fiber diameters and sheath thicknesses of coaxial microfibers using a 2⁴ full factorial statistical model. The maximum increase in total fiber diameter was observed with increase in sheath polymer (PCL) concentration from 9 to 11 wt % ($0.49 \pm 0.03 \mu\text{m}$) and salt concentration within the core from 0 to 500 mM ($0.38 \pm 0.03 \mu\text{m}$). The core fiber diameter was most influenced by the sheath and core polymers (PCL and PEG,

³ This chapter has been published as follows: Saraf A, Lozier G, Kasper FK, Baggett LS, Raphael RM, Mikos AG, "Fabrication of Non-Woven Coaxial Fiber Meshes by Coaxial Electrospinning" *Tissue Engineering, C.* 2009, doi:10.1089/ten.tec.2008.0422.

respectively) concentrations, the latter of which increased from 200 to 400 mg/ml ($0.40 \pm 0.01 \mu\text{m}$ and $0.36 \pm 0.01 \mu\text{m}$, respectively). The core polymer (PEG) concentration had a maximal negative effect on sheath thickness ($0.40 \pm 0.03 \mu\text{m}$), while salt concentration had the maximal positive effect ($0.28 \pm 0.03 \mu\text{m}$). Molecular weight increases in core polymer (PEG) from 1.0 kDa to 4.6 kDa caused moderate increases in total and sheath fiber diameters and sheath thicknesses. These experiments provide important information that lays the foundation required for the synthesis of coaxial fibers with tunable dimensions.

Abbreviations

BSA:	Bovine Serum Albumin
CH ₃ OH:	Methanol
CHCl ₃ :	Chloroform
FITC:	Fluoresceine Isothiocynate
NaCl:	Sodium Chloride
PCL:	Poly(ϵ -caprolactone)
PDGF:	Platelet Derived Growth Factor
PEG:	Poly(ethylene glycol)

Introduction

The fabrication of non-woven fiber meshes with electrospinning is becoming increasingly popular in numerous fields. This technology is now being adapted in

textiles^{108, 109, 110, 111}, drug delivery^{112, 113, 114, 115, 116, 117}, surgical and wound dressings^{118, 119, 120, 121, 122, 123}, tissue engineering^{124, 125, 126, 127, 128} as well as in the field of electronics^{129, 130}. A modification of the well-known single polymer-solvent electrospinning technique (hereafter referred to as conventional electrospinning) is coaxial electrospinning; a fabrication method that produces fibers with a coaxial core and sheath component, where each component can have different solubilities in organic and aqueous solvents. In this case the core is hydrophilic to facilitate the loading and preservation of bioactivity of biological molecules, whereas the sheath is hydrophobic to allow fiber formation after evaporation of the volatile organic solvent. The advantages of such a technique to the tissue engineering community are significant; it allows for the creation of scaffolds that act as reservoirs, and fibers that allow for controlled release of aqueous based biological molecules. Although biological molecules such as plasmids¹³¹, growth factors^{121, 132, 133} and drugs^{117, 134, 135} have been incorporated into conventional electrospun fibers, coaxial fibers have shown greater potential in maintaining bioactivity and extended release. For example Zhang et al.¹³⁶ and Jiang et al.¹³⁷ amongst others have demonstrated that when proteins such as bovine serum albumin (BSA) and lysozyme were incorporated into the cores of coaxial fibers, they exhibited minimal burst release, an extended duration of sustained release, and significantly less aggregation of the bioactive compound as compared to their incorporation by conventional blend and emulsion electrospinning techniques. Additionally, experiments by Liao et al.¹³⁸ have demonstrated that platelet derived growth factor (PDGF), when released from coaxial fiber meshes over a period of 20 days, is as potent as fresh PDGF in promoting proliferation of NIH 3T3 fibroblasts.

An increasing number of attempts are being made to determine the parameters that control the morphology and dimensions of the coaxial fibers. These parameters can play an integral role in the rate of degradation of coaxial fiber scaffolds as well as diffusion and release of the compounds embedded within them. Thus far, there has been a reasonable understanding of the mechanism behind conventional electrospinning and the factors that control the fiber morphology. For example, numerous studies have shown that an increase in polymer viscosity by increasing either the molecular weight or concentration increases the average fiber diameter and decreases bead formation within fibers^{139, 140, 141}. Furthermore, increasing the dielectric constant of the electrospun solvents causes the fiber diameter to decrease^{142, 143, 144}. Other factors such as humidity¹⁴⁵, flow rates¹⁴⁶, voltage¹³⁹, distance between the polymer outlet and collecting plate¹⁴⁷ and diameter of the polymer ejecting orifice¹⁴⁸ also play significant roles in determining fiber morphology. However, similar data on coaxial fiber morphology is more limited. Initial studies by Zhang et al. have shown a positive correlation between the core polymer (gelatin) concentration¹⁴⁹ as well as core flow rates¹³⁷ on overall fiber diameters. In other studies Wang et al.¹⁵⁰ reported that increases in core and sheath polymer flow rates increase the inner and outer diameters of the fibers. Some of the limitations in identifying these relationships come with a limited understanding of the complex electrohydrodynamic interactions between the core and sheath solutions during the electrospinning process, which in turn contributes to limitations in designing coaxial fibers with specific dimensions.

In this study the following four factors and their role in coaxial fiber morphology were evaluated: (i) sheath polymer concentration, (ii) core polymer concentration (iii) core polymer molecular weight, and (iv) sodium chloride (NaCl) ionic concentration in the aqueous core polymer solution. This study describes the variability in fiber morphology within a scaffold based on the factors mentioned above. Furthermore, this study also describes the influence of the factors mentioned above upon core, sheath and total fiber diameters using a full factorial statistical model. This model is a powerful method for determining the influence of each of the processing parameters upon fiber dimensions. Although other biodegradable polymers can be used to manufacture similar coaxial fiber scaffolds, we have used poly(ϵ -caprolactone) (PCL) in an organic (hydrophobic) solvent as the sheath polymer and poly(ethylene glycol) (PEG) in an aqueous solvent as the core polymer. These polymers were selected as model polymers because they have been used and characterized extensively for various applications, both in our laboratory as well as by the research community in general. To differentiate the location of the PCL sheath and the PEG core fibers, fluorescent markers were added to each of the polymer solutions, which allowed their visualization with confocal microscopy. The red fluorescence (associated with DiI, mixed with the PCL sheath solution) and green fluorescence (associated with fluorescein isothiocyanate (FITC) mixed with the aqueous PEG core solution), facilitated distinction of the sheath and core morphology of the fibers. This methodology has elucidated the parameters necessary for the fabrication coaxial fibers of desired dimensions.

Experimental Procedures

Polymer Solution for Fiber Sheath

For the fabrication of sheaths for the microfibers, poly(ϵ -caprolactone) (PCL, MW = 80 000, Sigma, St. Louis, MO) was dissolved overnight in 3:1 w/v chloroform (CHCl_3): methanol (CH_3OH) at 9 or 11 wt %. Immediately before electrospinning, Vibrant[®] DiI (Molecular Probes, Carlsbad, California; Cat. # V-22885) was mixed with the PCL solution at 1.33 μL of DiI per 1 ml of PCL solution followed by thorough mixing with the vortexer. Aluminum foil was wrapped around the vials containing the solutions to protect them from light.

Polymer Solution for Fiber Core

For fabricating the cores of the coaxial microfibers, poly(ethylene glycol) (PEG, 1.0 kDa or 4.6 kDa) (Sigma, St. Louis, MO) was mixed with water or 500 mM NaCl solution at 200 mg/ml or 400 mg/ml concentration. The solutions were vortexed and placed on a shaker table until complete dissolution was achieved. 0.05 wt % FITC (Sigma, St. Louis, MO) was added to the PEG solutions immediately before electrospinning. After addition of FITC, the solutions were mixed with the vortexer for homogeneity. Aluminum foil was wrapped around the vials containing the solutions to protect them from light.

Factorial Analysis of Variables

A 2⁴ factorial design was formulated followed by Analysis of Variance (ANOVA) to evaluate the influence of PCL concentration, PEG molecular weight, PEG concentration,

and NaCl concentration on total fiber diameters and sheath thicknesses as noted in Table 1. “High” and “low” concentrations of PCL were synthesized at 11 wt % and 9 wt % respectively. PEG molecular weights with a “high” value of 4.6 kDa and a “low” value of 1.0 kDa were similarly used. PEG solutions from each of the two molecular weights were mixed at a “high” PEG concentration of 400 mg/ml and a “low” concentration 200 mg/ml. The PEG polymers were dissolved either in water (“low” value for NaCl concentration) or 500 mM of NaCl solution (“high” value for NaCl concentration).

Electrospinning Apparatus Setup

The schematic in Figure 4.1 represents the electrospinning setup for the electrospun non-woven coaxial fibers. The setup consisted of two syringe pumps (Cole Parmer, Vernon Hills, IL) set to different flow rates (15 ml/hr for the sheath flow rate and 0.6 ml/hr for the core flow rate), a power supply (Gamma High Voltage Research, Ormond Beach, FL), and a square grounded copper plate (11 × 11 × 0.3 cm). Two 10 mL syringes were filled with the core solution (PEG) and sheath solution (PCL), respectively. The syringes were connected to the reservoir via silicon tubes attached to luers (Small Parts Inc. Miramar, FL) that screwed into a steel reservoir. The reservoir had three luers, two of which were connected to needles; a 22 gauge (ID = 0.0464 mm) inner needle and a 16 gauge (ID = 1.3589 mm) outer needle, respectively, (Brico Medical Supplies, Metuchen, NJ) placed concentric to each other (Figure 4.1, inset b). The needles were locked into their respective luers, after which the luers were threaded into the reservoir (C) as shown in figure 4.1(b). This fixed the needles in a concentric conformation during the process of

electrospinning. The third luer lead into the reservoir and provided an inlet for the PCL solutions. The positive lead from the power supply was attached to the needle, whereas the negative lead was connected to the copper plate placed at a distance of 22 cm from the tips of the concentric needles. The reservoir, needles and the copper and glass plates were set-up in a plexi-glass box as shown in Figure 4.1 with the syringes and power supply directly outside for easy manipulation. The non-woven coaxial fibers were collected onto a glass plate (0.22 cm thick) placed above the copper plate in a vertical setup. Prior to use, the glass plates were washed with warm water and soap and dried with Kimwipes.

A voltage between 19-21 kV was applied between the needle and copper plate to induce electrospinning of the polymer solutions for 3 minutes. After electrospinning, the electrospun sheets were dried overnight in a chemical fume hood. For confocal analysis, the sheets were cut into sections (3.5 cm × 1.5 cm, cut from the periphery towards the center of each mat) and placed between two glass cover slips (Fisherbrand, Pittsburgh, PA). For SEM analysis, the sheets were cut into 1 cm × 1 cm squares and placed on a stage lined with non-conducting tape. Three non-woven mats were spun for each of the parameters and used for analysis.

Analysis of Fiber Morphology

(A) Scanning Electron Microscopy (SEM)

SEM analysis on the fibers was performed as previously described¹⁵¹. Briefly, electrospun scaffolds were sputter-coated with gold for 1 min and observed with an FEI-

XL 30 environmental scanning electron microscope (Mawah, NJ) at an accelerating voltage of 20 kV. For quantification of fiber diameter, measurements were made on the first eight fibers that intersected from left to right, a line drawn horizontally across the middle of an image (at 2500× magnification). Images from four random locations (selected blindly at 50× magnification) from each of the 3 scaffold mats were used for a total of 96 measurements.

(B) Confocal Microscopy

Sections of non-woven electrospun scaffolds were placed between glass cover slips as noted above and were mounted on the stage of a Zeiss LSM 510 (Thornwood, NY) confocal microscope. The scaffolds were excited with argon (488 nm, 6% power) or helium-neon (543 nm, 25% power) lasers configured for multi-track imaging and imaged with a 63×/1.4NA objective. The emission of FITC was detected using a 510 to 550 nm bandpass filter and the emission of DiI was detected using a low pass 560 nm filter. This configuration was used to prevent overlap between the two emission wavelengths.

The cover slips were scanned along the long axis moving from the right edge to the left. Four independent visual fields were selected randomly on each of the samples at approximately 20, 40, 60 and 80% of the total length from the right most edge of the cover slips. All fibers within a focal plane in that field were scanned and recorded. The focal plane was then reconfigured to record additional fibers in that location. A total of 30 fibers were imaged per mat. The core and total fiber diameters were measured using

Zeiss LSM 5 Image Browser (v. 3,2,0,115) by two independent observers. Sheath thicknesses were calculated as a difference between the total and inner fiber diameters:

$$\text{Sheath thickness} = \text{Total fiber diameter} - \text{Core fiber diameter}$$

Readings by both observers were incorporated and evaluated by statistical software (JMP® software, SAS Institute Inc., v 5.1) to determine the influence of the various processing parameters on fiber morphology.

Analysis of Fibers on Incubation in Aqueous Medium

To determine if the submicron fibers had a thin PCL sheath that surrounded the fibers, 5 scaffolds each of 8 mm diameter from two groups of scaffolds made from 9 wt % PCL were incubated in 2 ml phosphate buffer solution (PBS) for a period of 3 days. The fibers were placed on a shaker table operating at 115 rpm in a warm room (37°C). The polypropylene tubes holding these scaffolds were covered with aluminum foil to prevent photo-bleaching. After 3 days, 2 scaffolds from each group were analyzed using confocal microscopy as previously described. Three scaffolds were analyzed with SEM for fiber diameter measurements as described above.

Statistical Analysis

The resultant data of inner and total fiber diameters and the sheath thickness were analyzed using Analysis of Variance (ANOVA) with the SAS JMP software. The total diameter, inner diameter and sheath thickness were selected as response variables, whereas PCL concentration, PEG molecular weight, PEG concentration and NaCl

concentration were selected as predictors. The analysis provided least squares mean diameters at each of the “high” and “low” levels of the predictors. To estimate the influence of each of the factors at “high” versus “low” values the “high” least squares mean diameter was subtracted from the “low” least squares mean diameter value and the resultant standard errors were calculated using the following formula:

$$\text{Resultant Standard Error} = ((\text{Standard Error of "high" values})^2 - (\text{Standard Error of "low" values})^2)^{1/2}$$

Results and Discussion

The specific objective of this study was to understand the influence of sheath polymer concentration, core polymer concentration and molecular weight and NaCl concentration within the core solution on coaxial fiber morphology. The factors used to study the influence of these processing parameters are shown in Table 4.1. These parameters were selected based on preliminary studies that established concentration and molecular weight ranges that resulted in a stable Taylor cone and produced continuous fibers without apparent defects (such as beading or clumping).

The study evaluated transverse dimensions of coaxial fiber morphology, i.e. outer sheath of the fibers made from PCL and inner core made from PEG using confocal microscopy. These were clearly distinguished with the fluorescent markers used in the study as shown in Figure 4.2. Other methods of analysis such as Transmission Electron Microscopy (TEM) did not provide sufficient visualization of the core/sheath morphology in coaxial microfibers, although it has successfully been used previously for

visualization of coaxial nanofibers¹⁵². The sheath fibers appeared red due to the incorporation of DiI in the PCL solution whereas the core fibers appeared green due to the incorporation of FITC in the PEG solution. Although the fluorescent markers were not covalently tagged to the polymers, evidence in the literature strongly indicates that mixing between the sheath and core solutions is minimal, thus confining the dyes to their respective polymers^{153, 154}.

Variation in the Distribution of Fiber Diameters

SEM analysis of the coaxial fiber meshes shows a significant change in the distribution of the fiber diameters as the sheath polymer (PCL) is increased in concentration from 9 wt % to 11 wt % as indicated in Figures 4.2 and 4.3. Fibers made from 9 wt % PCL had a significant increase in the percentage distribution of submicron fibers (diameters < 1 μm). The average population of submicron fibers increased from 3.0 ± 2.9 % to 25.7 ± 8.1 % when PCL concentration across all groups dropped from 11 wt % to 9 wt %. Similarly, intermediate fibers with diameters between 1.1 and 2.0 μm increased from 4.8 ± 3.3 % to 13.8 ± 5.0 %. The prevalence of a population of significantly smaller fibers within coaxial fiber meshes have been widely reported in literature⁴⁶. Thus far, however, the composition of these fibers has been unknown. However, two theories have been proposed. Yu et al.¹⁵³ suggested that these fibers are mainly composed of the core polymer and are formed when the charge density of the polymer solutions is high. The core polymer is extruded at a higher rate than the sheath polymer feed line can provide for entrainment. The other hypothesis states that sub-jets

are formed from the sheath polymer solution during the process of electrospinning due to Maxwell's stresses¹³⁶ acting on the polymer jet due to the surrounding electric field. This creates fibers that do not exhibit core/shell morphology and are composed of the shell polymer.

Confocal microscopy images of these fibers, as in Figure 4.4, show that the fibers less than 1 μm in diameter appear to be predominantly PEG (core) polymer. The potential presence of an undetected thin PCL sheath surrounding the predominantly PEG fibers could not be excluded due to the limited resolution of optical microscopy. Hence, two of the synthesized groups of 9 wt % PCL polymer fiber scaffolds were incubated in phosphate buffer solution (PBS) for 3 days at 37°C on a shaker. SEM analysis of the fibers showed that there was on average a decrease in the population of submicron fibers (pWCn scaffolds decreased from 17.78 ± 2.34 to 11.44 ± 1.72 % whereas the pwcn scaffolds decreased from 30.11 ± 2.11 to 20.5 ± 1.68 %) as noted in Table 4.2. Confocal microscopy analysis further suggests that the submicron fibers observed after 3 days of incubation in PBS had both PCL and PEG present within them as shown in Figure 4.5.

The intermediate fibers with diameters between 1.1 and 2.0 μm had a significantly increased PEG content as compared to the coaxial microfibers > 2.0 μm (46.1-85.0% versus 25.2-52.7%). The mechanism behind the formation of these submicron and intermediate fibers cannot be explained by the experiments described here. However, these data suggest that by increasing the sheath polymer concentration, the prevalence of submicron and intermediate fibers decreases significantly.

Influence of PCL Sheath Concentration on Fiber Morphology

An additional goal of this study was to evaluate the influence of the different parameters listed in Table 4.1 on total and core diameter and sheath thickness. The “high” and “low” values of the parameters were selected on the condition that they produced continuous, uniform coaxial fibers. PCL concentration was evaluated at a “low” value of 9 wt % and a “high” value of 11 wt %, as shown in Table 4.1. Figure 4.6 and Table 4.3 show the influence of the PCL sheath concentration on total and core diameters, as well as sheath thicknesses with dimensions at “low” concentration treated as baselines. Hence, increasing the PCL concentration contributed to an increase in the total and core fiber diameters as well as the sheath thickness. The total diameter increased by $0.49 \pm 0.03 \mu\text{m}$ whereas the sheath diameter increased by $0.11 \pm 0.03 \mu\text{m}$. The data suggest that the core fiber diameters were also affected by the increase in PCL concentration; the mean increased by $0.40 \pm 0.01 \mu\text{m}$. The increase in thickness of the fiber sheaths due to an increase in sheath polymer concentration can be explained as an effect of increasing the viscosity of the polymer. However, the relatively greater effect on the overall fiber diameter as well as on the core fiber diameter requires further discussion.

The increase in core diameters due to increase in PCL concentration could be an indirect effect related to the decreased prevalence of submicron fibers in meshes made from 11 wt % PCL formulations. Since the flow rate, and hence the total core polymer supplied to the meshes remains constant, the core polymer either becomes part of submicron fibers (with 9 wt % PCL formulations) or gets embedded within the coaxial fibers (with 11 wt % PCL formulations). Thus there is a significant increase in average

core diameters (by 5.91 ± 0.22 %) of fibers made from 11 wt % PCL. This increase in the core diameters further translates to an increase in the total diameter of the coaxial fibers.

Influence of Poly(ethylene glycol)Molecular Weight on Fiber Morphology

Increasing the molecular weight of the core polymer moderately increases the total and core diameters as well as the sheath thickness. Molecular weight is a contributing factor to the viscosity of the polymer solution and possibly increases the overall viscosity of the polymer jets. For example, in our experience when the molecular weight of PEG is increased to 10,000 kDa the polymers precipitate at the coaxial needle outlet. Upon increasing the PEG molecular weight, the total diameter of the fibers increases by 0.12 ± 0.02 μm , whereas the core diameter increases by 0.06 ± 0.01 μm , or 0.63 ± 0.31 %. There is also a comparable increase in the sheath thickness (0.08 ± 0.03 μm) of the fibers. To our knowledge, thus far, studies have not looked at the influence of polymer molecular weights on coaxial fiber morphology. However, we can draw upon few studies that have addressed the influence on conventional fibers. A study by Koski et al.¹⁵⁵ reported that increasing the molecular weight of poly(vinyl alcohol) increased the fiber diameter of conventional fibers from 200 nm to 2 μm . A similar study published by Eda et al.¹⁵⁶ investigated the influence of a wider range (44,100, 393,400, and 1,877,000 g/mol) of molecular weights. Although none of the above concentrations produced uniform, bead-free fibers, the study reported a change in the electro-hydrodynamic cone jet properties

that further resulted in the change in morphology of the polymer jet as well as the morphology of the fibers. Influences of a smaller range of molecular weights such as the ones tested here may be more subtle but still significant in affecting fiber diameters as reported here.

Influence of Poly(ethylene glycol) Concentration on Fiber Morphology

Increasing the PEG concentration from 200 mg/ml to 400 mg/ml caused a significant effect on the morphology of the fibers. The total diameter of the fibers decreased by $0.05 \pm 0.03 \mu\text{m}$. The core fiber diameter increased by $0.36 \pm 0.01 \mu\text{m}$ ($9.89 \pm 0.30 \%$), whereas the sheath thickness decreased by $0.4 \pm 0.3 \mu\text{m}$. A study by Zhang et al.¹⁴⁷ reported a similar increase in core diameters in coaxial fibers, however, they also reported an increase in the total diameters contrary to the results reported here. The main difference between these two studies is the dimensions of the fibers analyzed; while the study by Zhang et al. was testing nanofibers between 277 and 378 nm, this study is examining microfibers with average sheath thicknesses of $2.50 \pm 0.35 \mu\text{m}$. Zhang et al. have explained their results with the help of the “swell effect” of viscoelastic polymers, whereby the core fluid diameter enlarges after it is extruded from a narrow space, such as a needle. This swell effect of the core polymer translates to the fiber sheaths, which in turn increases the total diameter. The elasticity of the PEG and PCL may translate differently in microfibers than in nanofibers. In the case of fibers that have sheath thicknesses in the micrometer range, the swell effect may translate only to a few layers within the wall of the sheath polymer, causing their compression, which in turn provides

more volume for the core polymer to expand. The finding that the sheath thickness decreases with an increase in the core polymer concentration further supports the theory that the core polymer compresses the inner sheath layers. The resulting sheath thickness versus the structural density profile of the coaxial sheath may play a significant role in the degradation kinetics of the fibers and the release of the molecules embedded within them.

Influence of Salt (Sodium Chloride) Concentration on Fiber Morphology

The influence of charge density on the behavior of polymer jets and consequently on fiber morphology is relatively well characterized in the literature in the context of conventional electrospinning^{141, 142}. Charge densities of electrospun jets are attributed to the dielectric permittivity of the solvents or the conductivity of the polymers within them⁴⁸. Increasing the charge density by using a solvent with a higher dielectric constant, using a more conducting polymer, or increasing the electric current applied causes a decrease in the resultant fiber diameter^{157, 140}. Adding salts such as palladium diacetate¹⁵⁷ or NaCl¹⁴⁰ also decreases the fiber diameter by increasing the conductivity and charge density. However, similar data on coaxial fibers is limited.

Contrary to results with conventional electrospinning, when 500 mM NaCl was added to the aqueous core PEG solution of the coaxial jet, the total and core diameters, as well as the sheath thicknesses increased. The average increase in total diameter was $0.38 \pm 0.03 \mu\text{m}$, the core diameter increased by $0.12 \pm 0.01 \mu\text{m}$ whereas the sheath thickness increased by $0.28 \pm 0.03 \mu\text{m}$. Although these results seem counterintuitive, consideration

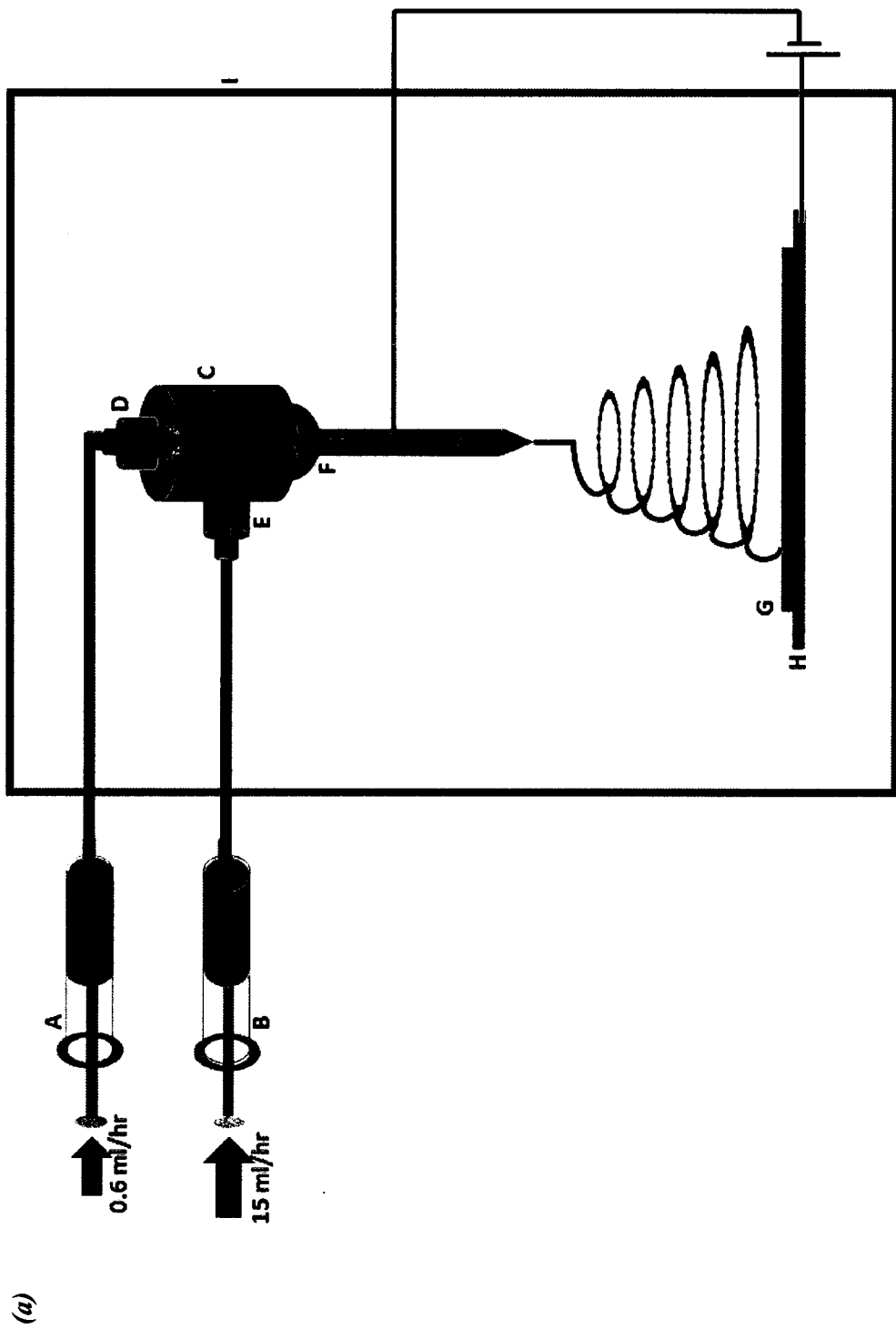
of the theories proposed thus far with regards to conventional electrospinning can offer some insight. It is well known that the addition of salt increases the conductance of solvents thereby increasing the dielectric constant of the solution. With conventional electrospinning models, increasing the conductance of the polymer increases the bending instability of the polymer jet. When radial Maxwell forces cause sufficient repulsion between the charges, the resultant jet splits, consequently forming fibers with smaller diameters¹⁵⁸. However, the electro-hydrodynamics in coaxial systems are more complex. Although similar Maxwell repulsive forces may be present within the charged core polymer, a less conductive PCL polymer sheath may mitigate these forces. Thus, in coaxial systems the charge repulsion may not overcome the cohesive forces and instead translates to larger fiber diameters. Characterization of the complex interactions involved in a coaxial system that are responsible for this phenomenon is beyond the scope of this study. Further elucidation with theoretical models for coaxial spinning, similar to those provided for conventional electrospinning by Reneker et al.^{139, 159} and Rutledge et al.^{142, 143, 144, 147, 160} amongst others will be required to appreciate the complex electro-hydrodynamic interactions involved in coaxial systems.

Conclusion

The experiments described here evaluate the influence of various processing parameters on coaxial fiber morphology. The influence of sheath polymer (PCL) concentration, core polymer (PEG) concentration and molecular weight, and NaCl concentration within the core polymer on total and core fiber diameters and sheath

thickness were tested using confocal microscopy. The results show that increasing PCL concentration and NaCl concentration have the most influence of total fiber diameters. Core diameters are most influenced by PCL and PEG concentrations. Core polymer concentrations have a negative influence on sheath thicknesses, whereas NaCl concentration has maximal positive influence on sheath thickness. The information generated by these studies has the potential to facilitate the synthesis of coaxial fibers with tunable dimensions, which consequently may affect the release kinetics of the compounds embedded within them.

Figures



(b)

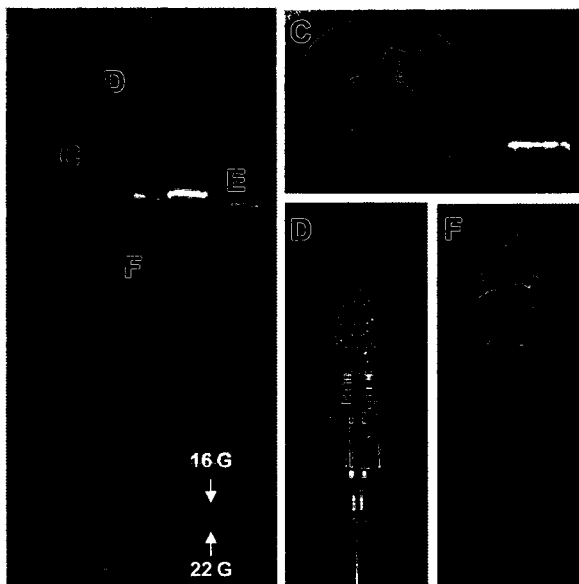
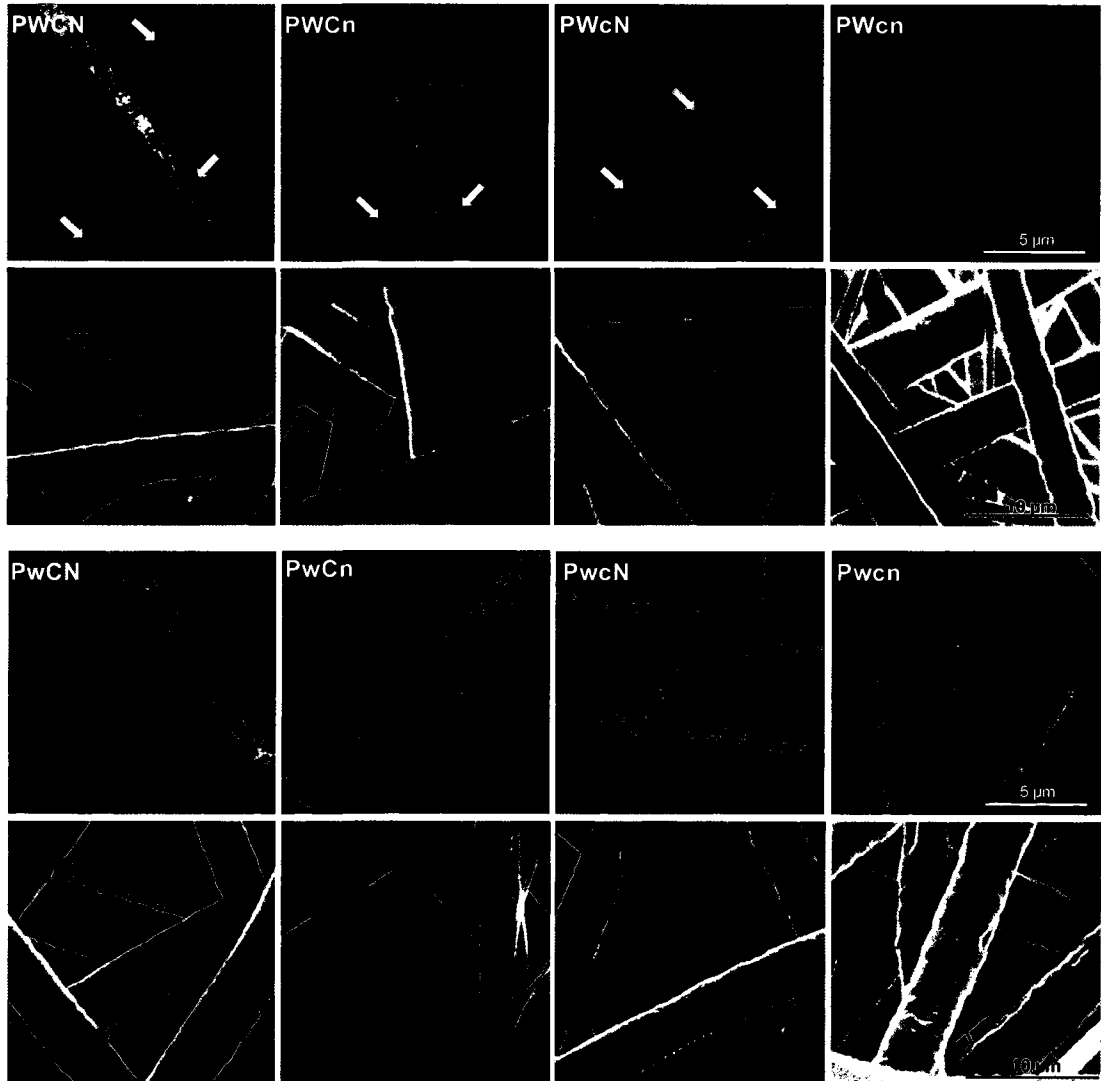


Figure 4.1: The electrospinning setup.

(a) The device involves two syringes (A and B) that contain the aqueous and organic phase of the coaxial solutions, respectively. The solutions are independently fed to a reservoir (C). The reservoir contains an opening at the top that allows for attachment of a male luer (D) with a 22 gauge needle. Similarly, another male luer (E) screws into the side of the reservoir which carries the organic solution into the

reservoir. The reservoir empties into an 16 gauge needle (F) attached to the bottom of the reservoir. The 22 gauge needle passes coaxially through the reservoir and the 16 gauge needle and its tip is flush with the 16 gauge needle. Potential difference is applied between a copper plate and the 16 gauge needle as indicated. Fibers are collected on a glass plate (G) placed on top of the copper plate (H). This setup is housed in a plexi-glass box (I) as indicated. (b) The actual reservoir used for these experiments is made from stainless steel. The inset shows the concentric needle tips. Outer needle is 16 gauge and inner needle is 22 gauge. The setup can be assembled and disassembled easily due to the screw threads that have been designed into the reservoir and luers as shown. The threads as well as the luers help lock the needles in a concentric position.



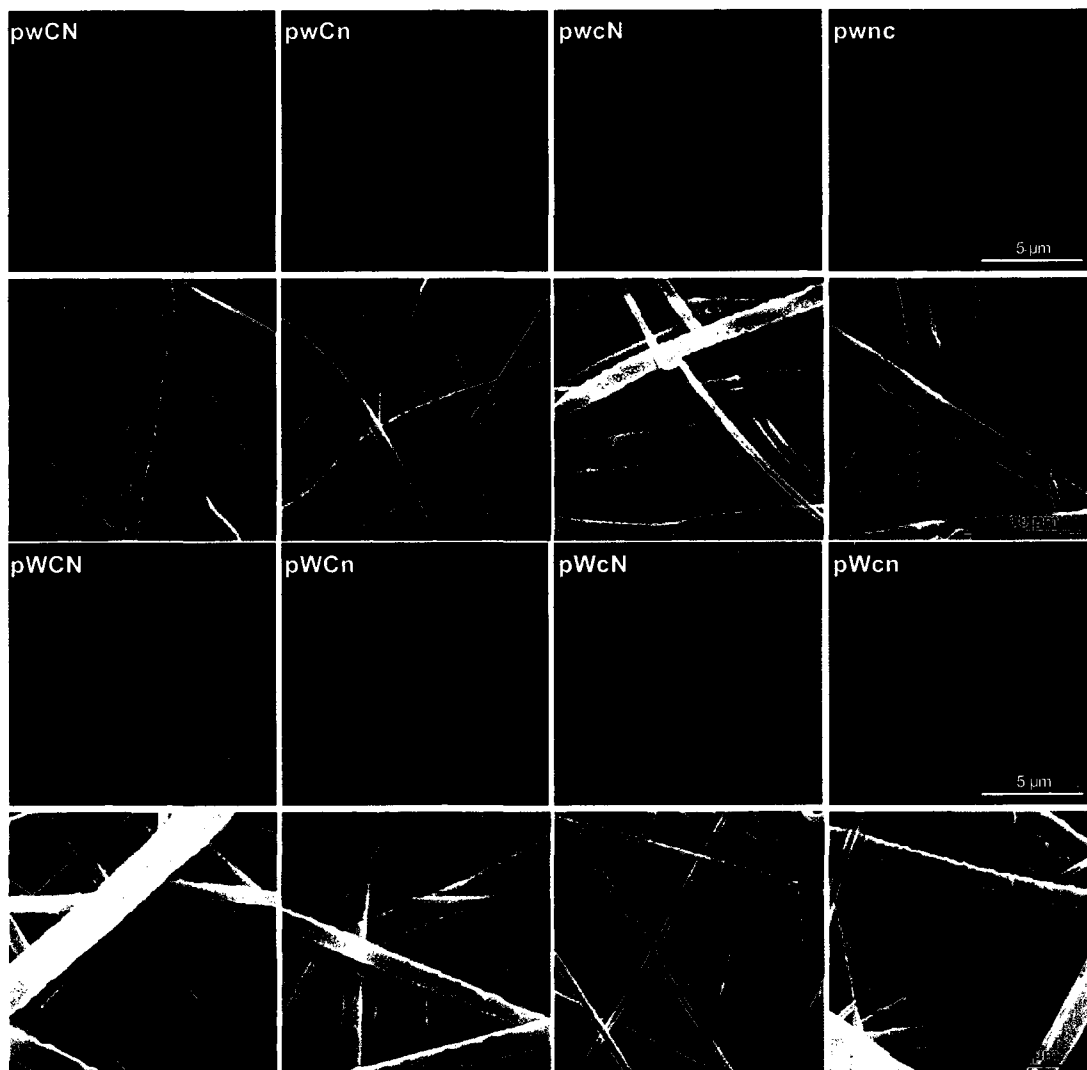


Figure 4.2: Confocal microscopy and corresponding SEM images of the coaxial electrospun microfibers. The core of the coaxial fibers is an aqueous mixture of PEG and FITC (hence appears green in the confocal images) and the sheath is an organic mixture of PCL (3:1 CHCl_3 : CH_3OH) and DiI (hence appears red). Yellow arrows represent sections of fibers not in focus, whereas the grey arrows are sections in focus. Images are labeled according to the combination of variables used, (e.g. “PWCn” stands for “high” PCL wt %, “high” PEG MW, “high” PEG concentration, and “low” NaCl concentration). The scale bars represent 5 μm for confocal images and 10 μm for SEM images.

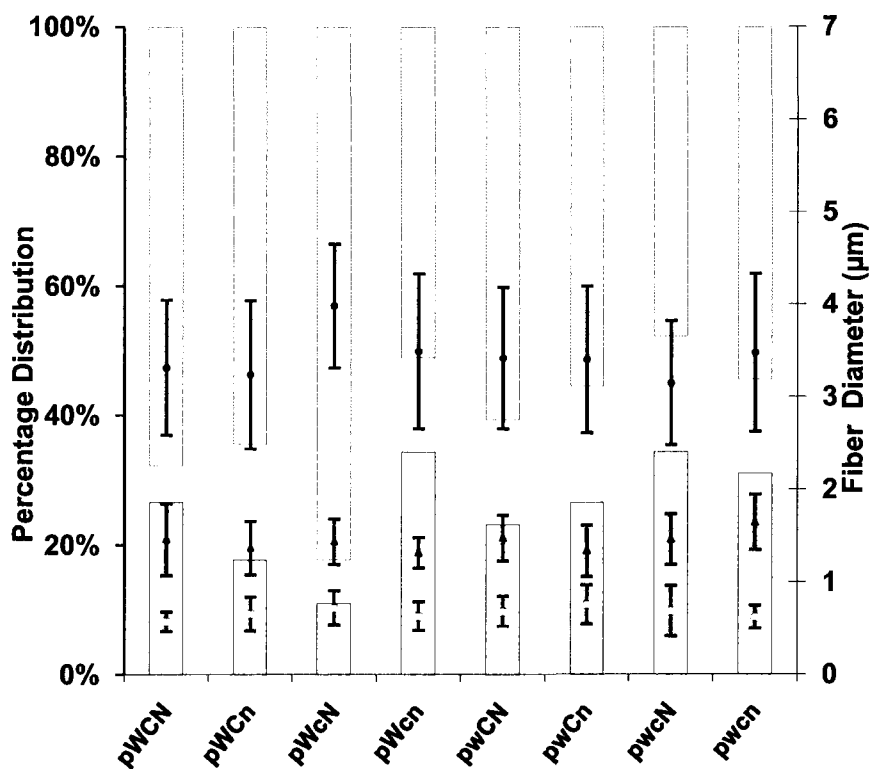
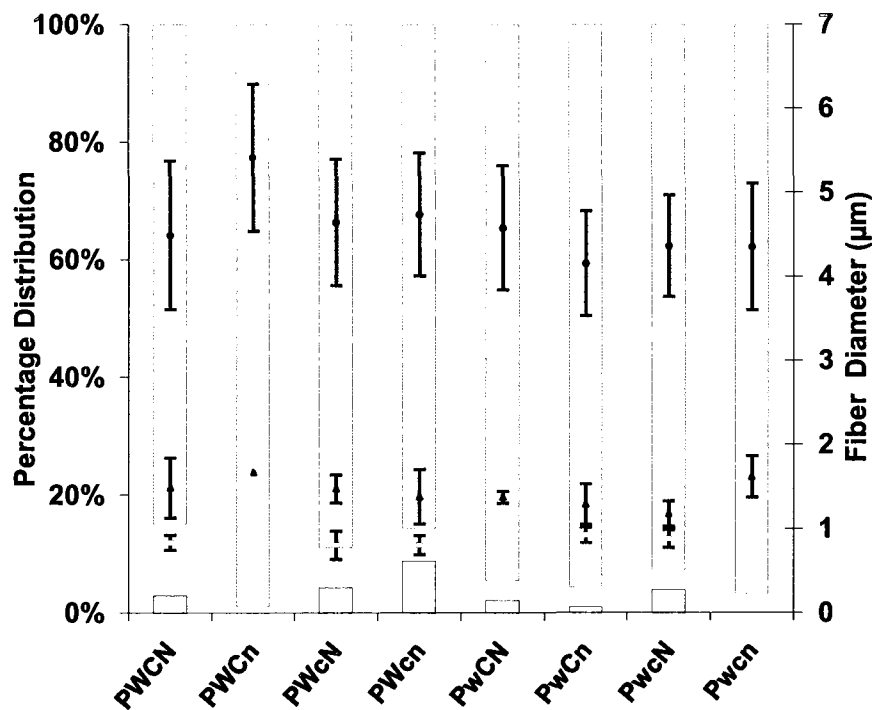


Figure 4.3: Distribution of coaxial electrospun PCL/PEG fibers. The percentage of submicron ($<1\ \mu\text{m}$, red) and micron fibers $<2\ \mu\text{m}$ (yellow) increases when the PCL (sheath) concentration changes from 11 wt % to 9wt %. Fibers greater than $2\ \mu\text{m}$ in total diameter are represented in the orange sections of the bar graphs. The circles (●) represent the average diameter of the micron fiber $> 2\ \mu\text{m}$, triangles (▲) represent average diameter of fibers between 1-2 μm and squares (■) represent average fiber diameter of submicron fibers ($< 1\ \mu\text{m}$), each with their respective standard deviations.

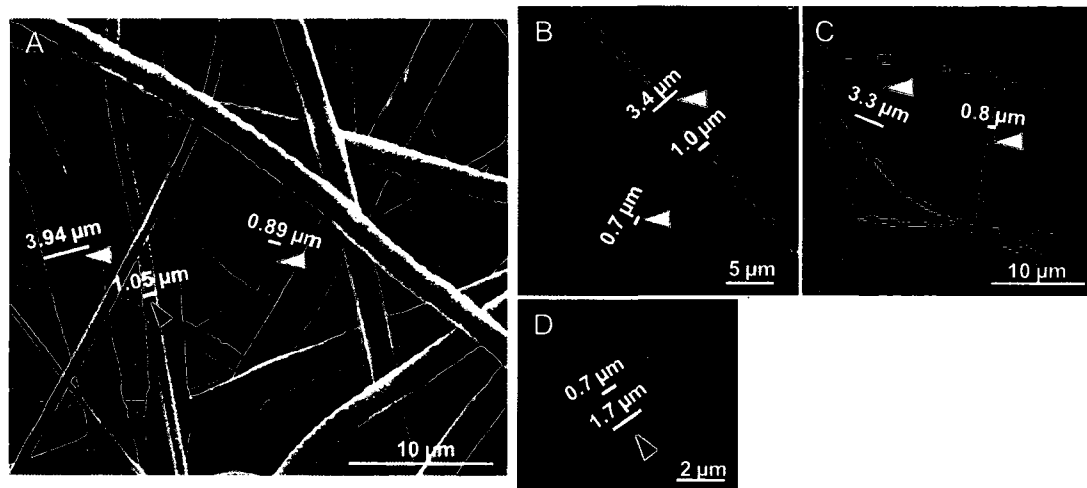


Figure 4.4: Distribution of coaxial electrospun PCL/PEG fibers. SEM (A) and confocal (B,C,D) images of 9 wt % coaxial electrospun PCL/PEG fibers displaying 3 populations of fibers based on coaxial morphology. Submicron fibers ($< 1 \mu\text{m}$) (B, C) are indicated by white arrows. Fibers between 1-2 μm have a thin PCL sheath and are largely comprised of PEG as indicated by the black arrows, and fibers $> 2 \mu\text{m}$ comprise the majority of the population of the coaxial fibers and have a thicker sheath as indicated by the yellow arrows. Scale bars are indicated on their respective images.

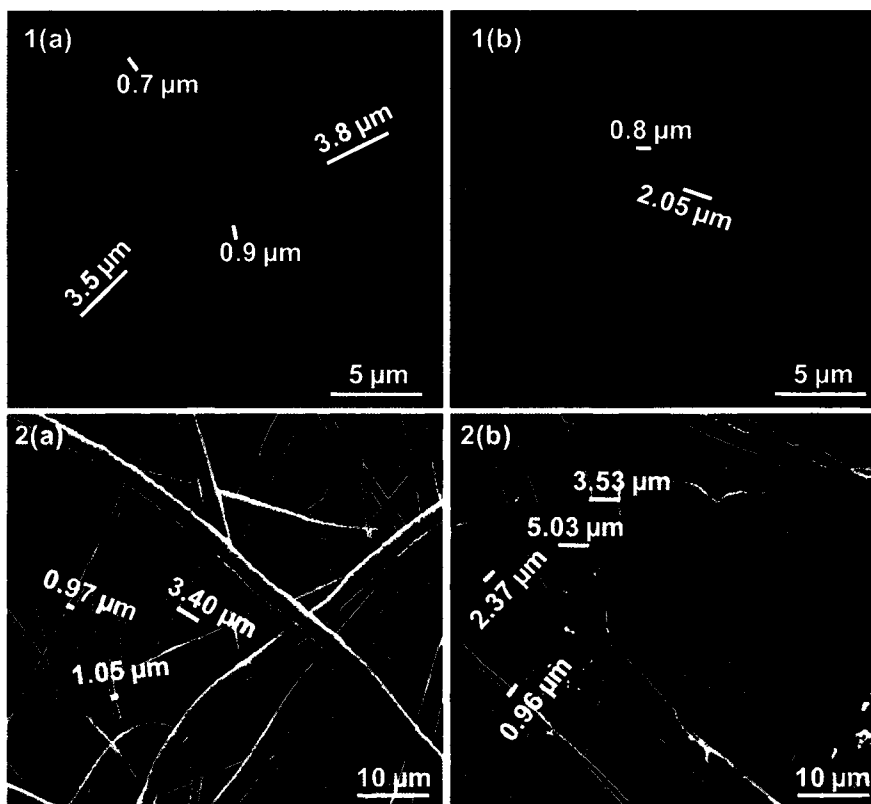


Figure 4.5: Effect of immersion in PBS on coaxial fibers. Confocal 1(a) and 1(b) and SEM 2(a) and 2(b) images of coaxial fibers made from 9 wt% PCL before (1(a) and 2(a)) and after (1(b) and 2(b)) incubation in PBS for 3 days.

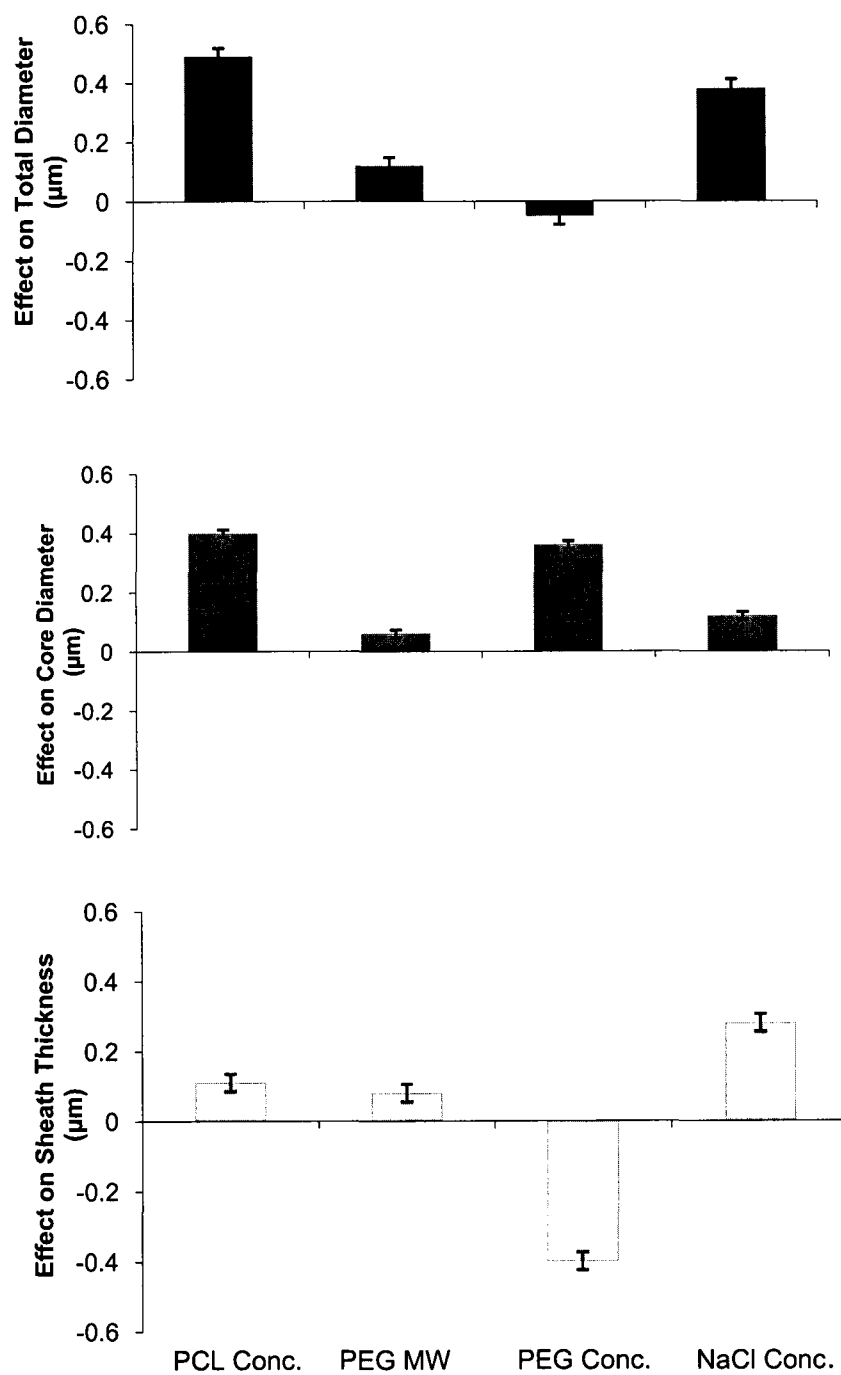


Figure 4.6: Main effects of processing parameters on fiber diameters. Effect of the variable processing parameters PCL concentration, PEG molecular weight, PEG concentration and NaCl concentration within the core solution on total fiber diameter (A), sheath thickness (B) and core diameter (C). Error bars represent standard error.

Tables

<i>Variables</i>	<i>PCL Concentration (wt%)</i>	<i>PEG Molecular Weight (kDa)</i>	<i>PEG Concentration (mg/ml)</i>	<i>NaCl Concentration (mM)</i>
<i>High</i>	<i>11 (P)</i>	<i>4.6 (W)</i>	<i>400 (C)</i>	<i>500 (N)</i>
<i>Low</i>	<i>9 (p)</i>	<i>1 (w)</i>	<i>200 (c)</i>	<i>0 (n)</i>

Table 4.1: Values of parameters used in formulating the experimental design. 24 factorial design to evaluate the influence of PCL concentration, PEG molecular weight, PEG concentration and NaCl concentration on coaxial electrospun fibers. Two levels of each of the 4 factors were used for evaluation; the levels are denoted as “high” for higher concentrations and “low” for lower of the two concentrations of each of the factors. The letters next to the values denote the symbol used for representing each of the conditions in subsequent explanation of results and discussion.

	Day 0			Day 3 (after immersion in PBS)		
	< 1 μm	1-2 μm	> 2 μm	< 1 μm	1-2 μm	> 2 μm
Group: pWCn						
Average Diameter (μm)	0.65 \pm 0.19	1.37 \pm 0.29	3.42 \pm 0.81	0.70 \pm 0.18	1.44 \pm 0.30	3.45 \pm 0.8
% prevalence	17.78 \pm 2.34	17.90 \pm 4.01	64.44 \pm 3.89	11.44 \pm 1.72	15.60 \pm 3.90	74.36 \pm 4.08
Group: pwcN						
Average Diameter (μm)	0.62 \pm 0.13	1.64 \pm 0.30	3.48 \pm 0.85	0.64 \pm 0.16	1.48 \pm 0.30	3.41 \pm 0.79
% prevalence	31.11 \pm 2.11	14.44 \pm 1.89	54.44 \pm 3.24	20.5 \pm 1.68	15.5 \pm 0.80	64.84 \pm 3.44

Table 4.2: Distribution of coaxial fiber diameters before and after immersion in PBS. Fiber distribution and average diameters of 2 types (pWCn and pwcN) of coaxial fibers made from 9 wt% PCL before and after incubation in PBS for 3 days.

	PCL Conc. (μm)	PEG MW (μm)	PEG Conc. (μm)	NaCl Conc. (μm)
Total Diameter	0.49 ± 0.03	0.12 ± 0.03	$- 0.05 \pm 0.03$	0.38 ± 0.03
Core Diameter	0.4 ± 0.01	0.06 ± 0.01	0.36 ± 0.01	0.12 ± 0.01
Sheath Thickness	0.11 ± 0.03	0.08 ± 0.03	$- 0.4 \pm 0.03$	0.28 ± 0.03

Table 4.3: Main effects of evaluated parameters on coaxial fiber diameters. Quantitative summary of the effect of variable parameters (PCL concentration, PEG molecular weight, PEG concentration and NaCl concentration) on total fiber diameter, core diameter and sheath thickness.

Chapter V

Regulated Non-Viral Gene Delivery from Coaxial Electrospun Fiber Mesh Scaffolds⁴

Abstract

In an effort to add to the versatility of three-dimensional scaffolds for tissue engineering applications, recent experimental designs are incorporating biological molecules such as plasmids and proteins within the scaffold structure. Such scaffolds act as reservoirs for the biological molecules of interest while regulating their release over various durations of time. Here, we describe the use of coaxial electrospinning as a means for the fabrication of fiber mesh scaffolds and the encapsulation and subsequent release of a non-viral gene delivery vector over a period of up to 60 days. Various fiber mesh scaffolds containing plasmid DNA (pDNA) within the core and the non-viral gene delivery vector poly(ethylenimine)-hyaluronic acid (PEI-HA) within the sheath of coaxial fibers were fabricated based on a fractional factorial design that investigated the effects of four processing parameters at two levels. Poly(ϵ -caprolactone) sheath polymer concentration, poly(ethylene glycol) core polymer molecular weight and concentration, and the concentration of pDNA were investigated for their effects on average fiber

⁴This chapter has been submitted for publication as follows: Saraf A, Baggett LS, Raphael RM, Kasper FK, Mikos AG, "Regulated Non-Viral Gene Delivery from Coaxial Electrospun Fiber Mesh Scaffolds" to the Journal of Controlled Release.

diameter, release kinetics of PEI-HA, and transfection efficiency. It was determined that increasing the values of each of the investigated parameters caused an increase in the average diameter of the fibers. The release kinetics of PEI-HA from the fibers were affected by the loading concentration of pDNA (with PEI-HA concentration adjusted accordingly to maintain a constant nitrogen to phosphorous (N:P) ratio within the complexes). Two-dimensional cell culture experiments with model fibroblast-like cells demonstrated that complexes of pDNA with PEI-HA released from fiber mesh scaffolds could successfully transfect cells and induce expression of enhanced green fluorescent protein (EGFP). Peak EGFP expression varied with the investigated processing parameters, and the average transfection observed was a function of poly(ethylene glycol) (core) molecular weight and concentration. Furthermore, fibroblast-like cells seeded directly onto coaxial fiber mesh scaffolds containing PEI-HA and pDNA showed EGFP expression over 60 days, which was significantly greater than the EGFP expression observed with scaffolds containing pDNA alone. Hence, variable transfection activity can be achieved over extended periods of time upon release of pDNA and non-viral gene delivery vectors from electrospun coaxial fiber mesh scaffolds, with release and subsequent transfection controlled by tunable coaxial fiber mesh fabrication parameters.

Abbreviations

CMV:	Cytomegalovirus
DMEM:	Dulbecco's Modified Eagle Medium
DMSO:	Dimethyl Sulfoxide

EDTA:	Ethylenediaminetetraacetic Acid
EGFP:	Enhanced Green Fluorescent Protein
GAM:	Gene Activated Matrix
HA:	Hyaluronic Acid
LSM:	Least Squares Mean
MEM:	Minimum Essential Medium
NEAA:	Non Essential Amino Acids
N:P:	Nitrogen : Phosphorus Ratio
PBS:	Phosphate Buffered Saline
PCL:	Poly(ϵ -Caprolactone)
pDNA:	Plasmid Deoxyribonucleic Acid
PEG:	Poly(Ethylene Glycol)
PEI:	Poly(Ethylenimine)
PEI-HA:	Poly(Ethylenimine)-Hyaluronic Acid
r-PEI-HA:	Rhodamine-Poly(Ethylenimine)-Hyaluronic Acid

Introduction

Traditionally, the role of tissue engineering scaffolds has been to provide mechanical support to damaged or excised tissue while facilitating the infiltration and attachment of cells. However, the development of novel processing techniques has significantly broadened their scope by allowing the incorporation and subsequent release of bioactive molecules, thus transforming the scaffolds into multifunctional bioactive factor delivery

units. The scaffold can operate as a reservoir for biological molecules, the release of which can be modulated by controlling the scaffold processing parameters. Such scaffolds have shown sustained release of a variety of proteins¹⁶¹ as well as plasmids^{162,163}. It has become increasingly feasible to deliver plasmid DNA (pDNA) to cells so as to facilitate in situ production of the encoded growth factors, signaling molecules and insoluble bioactive molecules of interest. This approach carries a significant advantage over the direct delivery of these biological agents, as intracellular expression of the delivered plasmids can be sustained over a period of days, thus mitigating the drawbacks of limited bioactivity associated with short half-lives of most biological factors. Furthermore, concerns related to gene delivery, such as low transfection efficiencies and the general requirement of high plasmid doses are gradually being mitigated with the development of new non-viral vectors and improved delivery strategies.

Tissue engineering scaffolds that entrap and release plasmid DNA have been adapted by various groups^{162,164}, and such scaffolds are popularly referred to as gene activated matrices (GAMs). The release of pDNA encoding a protein from three-dimensional biodegradable scaffolds has resulted in greater expression of the encoded protein than a similar amount of pDNA delivered to two-dimensional cell culture systems¹⁶⁵⁻¹⁶⁷. The enhancement in expression has been attributed to the close proximity of the cells to the gene delivery reservoir, as well as the sustained release of the plasmid over time^{165,168}. Scaffolds similar in concept to GAMs created by gas foaming¹⁶², emulsion^{169,170}, or electrospinning¹⁶⁶ have all been shown to successfully incorporate

pDNA, release it over an extended period of days to weeks, and preserve plasmid bioactivity over the duration of release. Successful expression of pDNA released from biodegradable scaffolds has been demonstrated using plasmids encoding reporter proteins such as luciferase^{167,171,172}, beta-galactosidase¹⁷²⁻¹⁷⁴ and enhanced green fluorescent protein^{165,169} as well as functional genes such as parathyroid hormone-1¹⁷⁵ and bone morphogenetic protein-4¹⁷⁶.

Coaxial electrospinning has previously not been employed to produce scaffolds for gene delivery in the context of tissue engineering. Coaxial fiber mesh scaffolds have a sheath/core fiber morphology where individual fibers can be fabricated from two separate immiscible polymer solutions, which allows for physical separation of aqueous-based biological molecules from the organic solvents essential for scaffold fabrication and minimizes the interaction between the two to the order of microseconds^{177,178}. Furthermore, electrospinning allows for the fabrication of multi-layered scaffolds, as demonstrated by previous experiments in our laboratory¹⁷⁹, where each layer can potentially incorporate and release a plasmid encoding a unique protein. Hence it is essential to determine the processing parameters that control the incorporation of pDNA into and release kinetics from such coaxial electrospun fiber meshes.

In this study we have incorporated a non-viral gene delivery vector previously developed in our laboratory, a hyaluronic acid (HA) derivative of poly(ethylenimine) (PEI) (PEI-HA) into non-woven coaxial electrospun fiber meshes. We incorporated pDNA into an aqueous poly(ethylene glycol) (PEG) solution to fabricate the core section of the fiber and the gene delivery vector PEI-HA into an organic sheath polymer solution

of poly(ϵ -caprolactone) (PCL) in chloroform and methanol. The coaxial electrospinning method not only minimized the interaction of the plasmid with the organic solvents, but also allowed the integration of pDNA without the need to process it through methods such as lyophilization, which in some cases has been shown to reduce the plasmid bioactivity^{180,181}. Furthermore, the volatile sheath polymer solution facilitated the processing and solidification of the fibers into non-woven fiber meshes. The plasmid was incorporated within the core of the fibers and the gene delivery vector was contained within the sheath. The hypothesis in generating these scaffolds was that, as the electronegative plasmids diffused out of the fiber cores, they would complex with the positively charged PEI-HA released from the fiber sheath and transfect cells present on the fiber surface.

To this end, we formulated a fractional factorial design to investigate the effects of various processing parameters, including (a) core polymer concentration and (b) molecular weight, (c) sheath polymer concentration, and (d) pDNA concentration, on fiber diameter distribution, PEI-HA release kinetics, and transfection efficiency. The gene delivery vector was tagged with a fluorescent molecule, rhodamine-B-isothiocyanate, to monitor its release, whereas the plasmid release was indirectly monitored through its reporter protein (EGFP) activity.

Materials and Methods

Materials

Chemicals for PEI-HA synthesis, namely, sodium borate, PEI (Mw = 25kDa) and sodium cyanoborohydrate, were purchased from Sigma-Aldrich (St. Louis, MO). Rhodamine-B-isothiocyanate for fluorescence tagging of PEI-HA was also purchased from Sigma. Sodium hyaluronate (Mw= 2.3 kDa) was generously provided by Genzyme Corp. (Cambridge, MA). Solvents used for electrospinning, namely, chloroform and methanol, were purchased at ACS grade from Fisher Scientific (Pittsburgh, PA). Chemicals used for tissue culture purposes such as Phosphate Buffered Saline (PBS), Dulbecco's Modified Eagle Medium (DMEM) with high glucose, Minimum Essential Medium (MEM) Amino Acid Solution (50X), MEM Non Essential Amino Acids (NEAA) (100X), L-Glutamine (200 mM), MEM Vitamin solution (100X) and sodium pyruvate (100 mM) were purchased from Gibco (Carlsbad, CA). Plasmid DNA encoding enhanced green fluorescent protein (EGFP) with a cytomegalovirus (CMV) promoter (pCMV-EGFP) was generously donated by Dr. Michael Barry from Mayo Clinic (Rochester, MN). Qiagen Plasmid Giga Kits for pCMV-EGFP amplification and purification were purchased from Qiagen (Valencia, CA).

Synthesis of Rhodamine Tagged PEI-HA

The synthesis of PEI-HA has previously been described by our laboratory¹⁸². For the current study, the published protocol was adapted for increased quantities of reactants. 500 mg of PEI and 1 g of HA were mixed in a 3-neck flask in the presence of 0.2 M

sodium borate buffer (pH 8.5) maintained at 40°C. The solution was stirred continuously after addition of 0.27 g of sodium cyanoborohydrate on initiation of the reaction and an additional 0.20 g 30 hrs after the initiation of the reaction. The reaction was carried out over 120 hrs, after which the product was dialyzed against 0.02 M of sodium borate buffer, and the dialysis solution was gradually transitioned to water. The product was lyophilized, and the chemical structure was confirmed with ¹H NMR as previously described. Based on NMR analysis, $11.67 \pm 0.45\%$ of the amine groups within PEI were chemically modified due to reductive amination with HA.

Lyophilized PEI-HA was dissolved in 0.2 M sodium bicarbonate buffer at 10 mg/mL concentration at pH 9.0. 10 mg of rhodamine-B-isothiocyanate was dissolved in 1 mL dimethyl sulfoxide (DMSO), and the mixture was added to 50 mL of the PEI-HA solution. The reaction solution was placed on a rotating table for 2 hrs, after which the solutions were dialyzed initially with 0.1 M sodium bicarbonate solution. The dialysis process was repeated until the dialysate showed a steady fluorescence reading during three consecutive dialysis cycles. The dialysis solution was then switched to water for three dialysis cycles. The product obtained at the end of dialysis, rhodamine-PEI-HA (r-PEI-HA), was lyophilized and stored at 4°C.

Plasmid Amplification

Plasmid DNA encoding EGFP with a CMV promoter was amplified as described previously¹⁸². Briefly, pCMV-EGFP (4.7 kb) was amplified in E. Coli bacterial cultures. Plasmids were extracted and purified using standard protocols with the Qiagen Plasmid

Giga Kit. The total plasmid yield was determined from the UV absorbance at a wavelength of 260 nm (A260). The plasmid was dissolved in Millipore water at 5 mg/mL and stored at -20°C. The ratio of A260/A280 was determined to be between 1.8 and 2.0 to assess purity of the plasmid produced.

Fabrication of Coaxial Electrospun Scaffolds

(A) Experimental Design

A two-level fractional factorial design with 4 parameters was formulated to evaluate the release and the related transfection efficiency of r-PEI-HA and pDNA from electrospun coaxial fiber mesh scaffolds. The parameters tested were (1) PCL concentration (Conc.), (2) PEG molecular weight (MW), (3) PEG Conc., and (4) pDNA Conc. within the core fiber. Hence, 8 different types of scaffolds were formulated using all the parameters described above at either a high (+1) or low (-1) concentration. The concentration of r-PEI-HA was also modified with changes in pDNA concentration so as to maintain the same N:P ratio across all formulations. Table 5.1 summarizes the combination of parameters examined in this study. The range of values used with each of these parameters was predetermined by an elimination process, where a variety of combinations of PEG and PCL polymer concentrations and molecular weights were electrospun together, to determine the values that produced a stable Taylor cone over a period of several minutes. r-PEI-HA release from the scaffolds as well as transfection

ability of the released supernatant containing r-PEI-HA and pDNA were studied over a period of 60 days.

(B) Coaxial Electrospinning Setup

The setup for coaxial electrospinning was developed and described in detail previously¹⁸³. The syringes containing PCL/r-PEI-HA in the setup for the present study were covered to prevent fluorescence bleaching.

(C) Fabrication of Coaxial Electrospun Scaffolds

PCL sheath and PEG core solutions were made according to parameters described in Table 5.1. PCL was dissolved in 2:1 chloroform: methanol solution (v/v), whereas PEG solution was made in 150 mM of NaCl solution prepared with Millipore water. r-PEI-HA was ground into a fine powder in the dark using a mortar and pestle and added to the PCL solutions. The amount of r-PEI-HA to be incorporated was calculated at a 7.5:1 N:P ratio of vector polymer to pDNA, assuming that the electrospinning process would be carried out for 50 min with each scaffold type. Hence,

$$\left(\begin{array}{c} \text{Theoretical} \\ \text{amount of pDNA} \\ \text{incorporated within} \\ \text{fiber mat} \end{array} \right) = \left(\begin{array}{c} \text{Concentration} \\ \text{of pDNA in core} \\ \text{polymer solution} \end{array} \right) \times \left(\begin{array}{c} \text{Volumetric} \\ \text{flow rate} \\ \text{of core} \\ \text{polymer} \\ \text{solution} \end{array} \right) \times \left(\begin{array}{c} \text{Duration of} \\ \text{electrospinning} \end{array} \right)$$

The r-PEI-HA/PCL solution was protected from light with an aluminum foil wrap, vortexed thoroughly and left on an orbital shaker overnight. Similarly, aqueous PEG solution was added drop-wise to pDNA solution to a final pDNA concentration of either 4 mg/mL or 2 mg/mL, based on the spinning parameters. An outer (sheath) flow rate of 8

mL/hr and an inner (core) flow rate of 0.1 mL/hr were used for the fabrication of the scaffolds for a period of 50 min. The schematic of the scaffolds produced with the respective location of its components is described in Supplemental Figure 5.1.

Scanning Electron Microscopy Analysis of Fiber Diameters

Three scaffolds of 1 mm diameter each were punched out from the coaxial fiber mesh mats and mounted on a steel stage above insulating tape. Samples were sputter coated with gold for 1 min at 100 mA, after which the scaffolds were observed with SEM (FEI Quanta 400, Hillsboro, OR). A total of 90 fibers were measured from 3 scaffolds from each group, as described previously by our laboratory^{179,183}.

Release and Quantification

(A) Release and Quantification of r-PEI-HA

Circular scaffolds of 10 mm diameter were punched out of each fiber mat and weighed. Amount of r-PEI-HA and pDNA within each scaffold of 10 mm diameter was estimated from the theoretical amount of pDNA incorporated within the fiber mat and the fractional weight of the scaffold compared to that of the fiber mat.

Amount of r-PEI-HA per scaffold was further determined with the assumption that the N:P ratio between r-PEI-HA and pDNA was maintained at 7.5:1. Scaffolds of weights between 10.5 and 12.8 mg were selected from each fiber mat group and placed in 5 mL polypropylene tubes covered with aluminum foil. The scaffolds were sterilized with ethylene oxide over a period of 14 hrs. The samples were then individually submerged in

1 mL of PBS and placed on a shaker table rotating at 115 rpm at 37 °C. The PBS supernatant was collected at predetermined time points and replaced with fresh PBS. The collected supernatant was lyophilized over 48 hrs, and the residue was resuspended in either 1.0 mL or 0.5 mL of PBS, determined by sampling the amount of fluorescence present in the sample. 100 µL of the resuspended solution was added into opaque 96-well plates and fluorescence was measured using a plate reader, Spectra Max M2 (Molecular Devices, Downingtown, PA) at Ab/Em 555/592 nm, with the emission cut-off wavelength of 590 nm. These wavelengths were determined as optimal based on a spectral frequency sweep of wavelengths ranging from 350 nm to 700 nm. Fluorescence values were compared to a standard curve generated using known concentrations of r-PEI-HA/DNA complexes of 7.5:1 N:P ratio to determine the concentration of r-PEI-HA/DNA complexes in solution, with the assumption that there was no significant difference between the fluoresce emitted by r-PEI-HA and r-PEI-HA/pDNA complexes of different N:P ratios. Data obtained was analyzed using Softmax Pro (v 4.6, Molecular Devices, Downingtown, PA).

(B) Release and Preparation of Solutions for Transfection

To assess the transfection ability of the pDNA in the release solution of the scaffolds, additional 10 mm diameter scaffolds of weights between 10.5 and 12.8 mg were placed individually in 5 mL polypropylene tubes. The samples were similarly submerged in 1 mL of PBS and placed on a shaker table at 115 rpm at 37°C. The PBS supernatant was obtained at predetermined time points and replaced with fresh PBS. The supernatant was

lyophilized over 48 hrs and resuspended in transfection medium composed of MEM Amino Acid solution, MEM NEAA and MEM Vitamins diluted to 1X concentration, 1000 mg/L of glucose, sodium pyruvate (final concentration 1 mM) and L-glutamine (final concentration 2 mM), approximately 1 hr before transfection. The resuspended solutions were centrifuged at 2000 rpm for 10 min, and the samples were allowed to stand for 50 min.

Cell Line and Cell Culture

Fischer rat fibroblast cell line (CRL 1764) was obtained from American Type Culture Collection (Manassas, VA). Cells were expanded in T75 flasks with complete medium, (DMEM supplemented with 10 vol. % FBS, 100 µg/mL penicillin, 100 U/mL streptomycin, and 0.5 µg/mL amphotericin B) and cultured at 37°C in 5% CO₂ and 95% humidity.

Cell Transfection and Reporter Gene Expression

After expansion of the cells in T75 flasks, cells were trypsinized with 0.025% Trypsin EDTA, centrifuged, quantified, and replated onto 6-well cell culture plates at 250,000 cells per well. The cells were suspended in 2 mL of tissue culture media overnight to facilitate attachment, after which the media was removed and replaced with the transfection solutions described above. The plates were covered in foil and allowed to sit in the incubator overnight. The next morning 1.5 mL of cell culture medium was added to the cells, and the cells were incubated at 37°C for 48 hrs. To assess transfection

by flow cytometry, the cells on the 6-well plates were treated with 0.5% trypsin EDTA for 5 min, after which the cells were collected in their respective 5 mL tubes and centrifuged at 2000 rpm for 10 min. The supernatant was decanted, and the cells were washed with PBS. The PBS was further replaced with 2% chilled formaldehyde solution in PBS, and the cells were allowed to fix on ice for 1 hr. The cell solution was further centrifuged (2000 rpm, 10 min), and the formaldehyde was replaced with PBS solution. Cell fluorescence was quantified using a Becton Dickinson FACS Scan instrument (BD Biosciences, San Jose, CA) at high flow and CellQuest Pro software (BD Biosciences, San Jose, CA, v. 5.1). Base-line fluorescence was quantified using cells treated with complete medium alone throughout the cell culture and transfection duration. A total of 2000 events were counted for each sample, and fluorescent cells were determined using a marker at 5% of the untreated cell population.

Reporter Gene Expression of Cells Seeded on Coaxial Fiber Meshes

Cells expanded in T75 flasks were trypsinized as described above. A cell suspension of 100,000 cells/mL was prepared in cell culture medium and 1 mL added to each 5 mL polypropylene tube. Ethylene oxide-sterilized 10 mm scaffolds were added to the tubes, and negative pressure was applied until no bubbles were observed to facilitate infiltration of the cells into the scaffolds. The cell suspension and the scaffold were then placed into 24-well plates and incubated up to predetermined time points, with media changes every 2-3 days. Expression of EGFP within CRL 1764 cells was observed using confocal microscopy at 10X and 20X magnification using a Zeiss LSM 510 confocal microscope

(Thornwood, NY). Scaffolds were excited with an argon laser (488 nm, 6% power). Emission wavelengths were monitored between 510-550 nm. Images thus obtained were further visualized using LSM 5 Image Browser (v 3,2,0,115).

Statistics

The influence of changing values of the main parameters PCL Conc., PEG MW, PEG Conc., and DNA Conc. on fiber diameter, release kinetics and transfection efficiency were analyzed using analysis of variance with SAS JMP software (v. 7.0.1, Cary, NC). The analysis evaluated means as well as least squares mean (LSM) values with the standard error associated with the computations. Further differences between specific results were evaluated using Tukey's honestly significant differences (HSD) test. To determine the influence of the main parameters at the 2 levels evaluated, LSM values at the low parameter value (-1) were subtracted from the high value (+1). Significance was determined at $p < 0.05$ unless otherwise specified.

Results

Fiber Distribution of Electrospun Coaxial Scaffolds

Eight different scaffold types were formulated based on a fractional factorial design with parameters summarized in Table 5.1. Electrospun coaxial fiber mesh mats had approximate dimensions of 10 x 10.8 cm. Theoretical calculations estimated that the amount of pDNA present per scaffold in the form of a disk of 1 mm diameter was approximately 2 μg for Groups 2, 3, 5 and 8, which contained the high pDNA loading

concentrations and approximately 1 μg for the remaining groups that had low pDNA loading concentrations. Fiber diameters were assessed with SEM, as described in the “*Methods and Materials*” section. The formulations showed a distribution of fiber diameters ranging from about 200 nm to 4 μm across 8 groups of scaffolds. Assessing the main effects of the parameters on fiber diameter showed that all four parameters, namely, PCL Conc., PEG MW, PEG Conc., and DNA Conc. significantly increased total fiber diameter when the value was increased from low (-1) to high (+1) as shown in Figure 5.1. The maximum effect on fiber diameter was observed with PCL Conc. ($0.52 \pm 0.06 \mu\text{m}$), followed by PEG MW ($0.31 \pm 0.06 \mu\text{m}$), PEG Conc. ($0.28 \pm 0.06 \mu\text{m}$), and pDNA Conc. ($0.27 \pm 0.06 \mu\text{m}$). A previous study involving electrospun coaxial fibers that did not contain any bioactive molecules suggested that some of the fibers within the meshes were composed entirely of the core polymer, which is hydrophilic and easily soluble in aqueous medium¹⁸³. To test if the meshes fabricated with the non-viral vector and pDNA showed fibers with similar properties, the meshes were immersed in PBS with agitation at 115 rpm at 37 °C for 7 days. Figure 5.2A shows the fiber diameter distribution of fibers directly after fabrication and 2B after immersion in water for 7 days. Groups that had a significant percentage of fibers within the smallest fiber diameter distribution range (100-300 nm), i.e., Groups 1 and 2, showed a decrease of 25.1 and 11.5%, respectively, in the percentage distribution of these fibers after 7 days in PBS. Other groups showed a decrease in fiber diameter across different fiber distributions. Taken together, these results suggest that, based on the values of parameters used, some fibers composed

predominantly of the core polymer PEG were distributed at various diameters within the coaxial fiber meshes.

Release of r-PEI-HA

The release of fluorescence tagged r-PEI-HA was monitored with a fluorescence plate reader over a period of 60 days. The 60 day duration for monitoring r-PEI-HA release was further divided into four groups; burst release (0-24hrs), Phase 1 (2-10 days), Phase 2 (11-28 days), and Phase 3 (35-60 days). Burst release during the first 24 hrs ranged from $9.3 \pm 1.8\%$ for Group 6 to $47.3 \pm 13.3\%$ for Group 7, as described in Table 5.2 and Figure 5.3. The main effects of the parameters on the average release of r-PEI-HA are illustrated in Figure 5.4. The concentration of pDNA (with the concentration of r-PEI-HA scaled accordingly, to maintain the same N:P ratio) was the only parameter that significantly affected the kinetics of r-PEI-HA released. Sheath PCL Conc., core PEG Conc., and PEG MW did not significantly affect the release kinetics of r-PEI-HA. Cumulative release at the end of 60 days ranged from $35.2 \pm 5.7\%$ of theoretical loading for Group 6 to $144.1 \pm 14.0\%$ for Group 5, as stated in Table 5.2.

There were significant differences between groups related to the burst release of r-PEI-HA, as stated in Table 5.2. However, there were no statistical differences between groups with respect to the r-PEI-HA released per day between Phases 1 to 3.

Transfection Efficiency of Released pDNA in 2D Cultures

Compared to the control (Group 9) that carried only pDNA within the fiber core and had no r-PEI-HA, all the experimental groups showed a significant increase in

transfection efficiency as compared to the cells treated with media alone. A graphical representation of transfection efficiencies across 60 days for all groups is shown in Figure 5.5. Although there were specific differences in average transfection efficiencies between groups as shown in Table 5.3, transfection efficiencies were not statistically different from each other after day 21. Across the groups over a period of 60 days, only PEG MW and PEG Conc. had a significant effect on transfection at $p = 0.09$ and $p = 0.10$ respectively as represented in Figure 5.6.

Transfection of Cells Seeded onto Coaxial Electrospun Fiber Mesh Scaffolds

Compared to the pDNA only group, CRL 1764 cells seeded onto scaffolds with both r-PEI-HA within the fiber sheath and pDNA within the fiber core showed a significant number of cells expressing EGFP as shown in Figure 5.7. EGFP expression by the cells was observed over the duration of the experiment, with qualitative differences in transfection efficiencies observed between groups and time points, as shown in Figure 5.7.

Discussion

The study described here was designed to determine the effect of certain processing parameters on electrospun fiber diameter distribution, PEI-HA release kinetics, and transfection efficiencies of pDNA released from electrospun coaxial fiber mesh scaffolds incorporating pDNA and PEI-HA, a non-viral gene delivery vector. Coaxial electrospinning has thus far not been employed for delivery of pDNA, and factors

influencing the formation of coaxial fiber meshes and their release properties are largely unknown. The experimental plan was formulated with the goal of establishing parameters that allowed for the formation of coaxial electrospun fiber meshes and determining if the examined values of these parameters could dictate the release kinetics of pDNA and r-PEI-HA, as well as the associated transfection efficiencies. Just as the process of electrospinning is dependent on the interaction of multiple factors, including the dielectric properties of the solvents used^{144,142}, flow rates of polymer solutions during extrusion¹⁴⁶, the electric potential and quantity of charge circulating through the electrospinning circuit¹³⁹, and the distance between the needle and collecting plate¹⁴⁷; the coaxial electrospinning process has a similar set of complex governing interactions.

In the experimental design implemented here, pDNA was incorporated within the core polymer (PEG) solution, whereas r-PEI-HA was pulverized and dissolved within the sheath polymer (PCL) solution. We had previously described experiments where a set of coaxial electrospun fiber mesh scaffolds were fabricated based on a full factorial design using parameters similar to those described in this study¹⁸³. These common parameters included sheath (PCL) Conc., core (PEG) Conc., and (PEG) MW. It was observed that the range of the parameters tested had to be limited significantly to allow the coaxial electrospinning of polymer solutions incorporating the cationic gene delivery vector and anionic pDNA, thus limiting the versatility of the coaxially electrospun groups. Furthermore, despite the formation of a stable Taylor cone during fabrication of the fiber meshes for all the formulations, the coaxial fibers showed a greater distribution of fiber diameters, as shown in Figure 5.2 and discussed in "*Fiber Distribution of Electrospun*

Coaxial Scaffolds". Previously, DNA has been incorporated into uniaxial electrospun fibers by Luu et al.¹⁶⁶, and the fibers obtained had a significant variation in fiber diameters. Both these observations suggest that the inclusion of highly charged moieties, such as a cationic gene delivery vector and anionic pDNA, significantly affect the electrospinning properties of polymer jets.

The assessed parameters showed a similar effect of increasing sheath polymer concentration and core polymer molecular weight on fiber diameter, as was previously observed in the absence of the vector and plasmid. The average fiber diameter increased with the increase in sheath (PCL) Conc. and PEG MW. In addition, an increase in the concentration of PEG, pDNA and r-PEI-HA also caused a similar increase in the average fiber diameter. To determine if all fibers within the mesh were truly coaxial, we immersed them in PBS for 7 days. Analysis showed a significant number of fibers across various groups that completely dissolved in a period of 7 days, which suggested that these fibers were composed predominantly of PEG and were prevalent in various size ranges within different groups. However, there was also a significant and larger population of fibers that did not change in prevalence across subgroups of fiber diameters, suggesting that these fibers were indeed coaxial.

As one of the goals of this experiment, we attempted to characterize the release of incorporated r-PEI-HA from the sheath of coaxial fibers. The direct release of pDNA could not be monitored in this case, as r-PEI-HA significantly decreased binding of pDNA to dyes such as PicoGreen or ethidium bromide during complex formation. Hence, the release of r-PEI-HA was monitored via fluorescence. In the case of uniaxial

electrospinning Luu et al.¹⁶⁶ observed that most of the burst release occurred at 2 hrs, after which pDNA release decreased precipitously. Similar to observations made by Luu et al., r-PEI-HA contained within the sheath fibers of the present study displayed a burst release within 24 hrs after immersion in PBS. However, in the fibers fabricated here, there was also a significant amount of r-PEI-HA released between days 2 to 10, ranging from 1.75 ± 0.39 to $6.30 \pm 1.60\%$ of theoretical loading. Only the loading concentration of pDNA (and subsequently that of r-PEI-HA, which was increased to maintain a constant N:P ratio among groups) appeared to significantly influence the release kinetics of r-PEI-HA. Some of the burst release observed here could be attributed to the dissolution of fibers made predominantly from PEG as described above.

The release kinetics were also significantly influenced by the location of PEI-HA and DNA within the coaxial fibers. The initial design of the experiments described here attempted to electrospin r-PEI-HA/pDNA complexes entirely within the core of the coaxial fibers by preassembling the complexes before mixing them with the core polymer solution. To accommodate for the solubility of PEI-HA/pDNA complexes, dextran (instead of PEG) was used as a core polymer and the optimal viscosity for spinning was attained at concentrations noted in the table in the supplemental section (Supplemental Table 5.1). However, the core polymer containing the complexes showed negligible release of PEI-HA/pDNA complexes (Supplemental Figure 5.2). Although we could not determine the cause behind the absence of release of PEI-HA/pDNA complexes, a possible reason could be that the interactions between the core and sheath polymer limited the incorporation of the PEI-HA/pDNA complexes within the coaxial fibers.

Some of the coaxial fiber mesh scaffold groups in the study where PEI-HA was incorporated within the polymer sheath and pDNA was incorporated within the fiber core showed greater than 100% cumulative release over the duration of the study. Although, during the fabrication of the scaffolds, the r-PEI-HA and pDNA were loaded such that the N:P ratio between them was constant at 7.5:1, it is feasible that the ratio at which r-PEI-HA and pDNA were released was not constant over the duration of the experiment. The r-PEI-HA/pDNA release values were calculated using a calibration curve generated from known concentrations of r-PEI-HA/pDNA in solution (constant N:P ratio of 7.5:1), with the assumption that there was no significant difference between the fluorescence of r-PEI-HA and r-PEI-HA/pDNA complexes of differing N:P ratios. However, it was found that calibration curves generated by measuring the fluorescence corresponding with known concentrations of r-PEI-HA alone (N:P ratio of 1:0) and r-PEI-HA/pDNA complexes (N:P ratio of 7.5:1) in solution were significantly different from each other, as illustrated in Supplemental Figure 5.3. The inability of the detection method employed in the release study to differentiate between free r-PEI-HA and r-PEI-HA/pDNA complexes of different N:P ratios in solution was a limitation of the study and taken together with the differences in fluorescence for a given concentration of free r-PEI-HA versus r-PEI-HA/pDNA complexes, may account for the greater than 100% cumulative release observed for some groups.

The temporal differences between peaks of r-PEI-HA/pDNA complex release (Table 2) and maximum EGFP expression in CRL 1764 cell lines (Figure 5.5) further suggests a potential variation in the ratios of r-PEI-HA and pDNA in the duration of the release. In

general, EGFP expression could be more directly correlated to the release of pDNA rather than r-PEI-HA. However, pDNA release could not be directly detected in this experimental design and is a limitation associated with this study. However, transfection efficiencies with scaffolds containing r-PEI-HA were significantly higher than with those containing pDNA alone, suggesting that the presence of r-PEI-HA in the fibers did enhance transfection, relative to pDNA alone in the fibers. Transfection efficiency seemed to be most influenced by core polymer parameters; PEG MW and concentration. Changing PEG concentration from low to high values decreased the observed transfection of cells. The decrease in transfection could be related to a potential decrease in the amount of pDNA released due to the increase in PEG concentration, as has been observed in other controlled release systems with proteins and peptides¹⁸⁴. The lower release observed in other studies has been attributed to an increase in the matrix density of the polymer holding the bioactive molecule of interest. However, pDNA release was not directly measured in the present study, so the effects of PEG Conc. on pDNA release are not known in the context of this study.

A similar phenomenon can be expected when the core polymer MW is increased. The increase in PEG MW, however, caused an increase in transfection, which is counter to expectations. However, this effect can be attributed to a number of factors. Increase in the MW of PEG has been reported to increase condensation of pDNA in the presence of NaCl, which is present within the core fiber¹⁸⁵. pDNA with a more compact structure would potentially have less retention within the coaxial fiber, which could lead to an increase in release and subsequently in transfection. Furthermore, any interaction

between the r-PEI-HA and pDNA within the coaxial fiber may also influence release kinetics, due to a differential degree of condensation of pDNA after its interaction and complexation with r-PEI-HA.

We observed a significant effect of PEG Conc. and MW on transfection efficiencies at days 14 and 21. There were significant differences in transfection between groups up to day 21. However, after day 21 there were no significant differences in transfection between groups. It can be surmised that the observed transfection efficiency is dependent on the core polymer properties, i.e., molecular weight and concentration. Further changing the amount of r-PEI-HA loaded within the sheath fibers, which in turn would affect the N:P ratio at which complexes are formed, may give additional insight into the change in release kinetics of r-PEI-HA and the effect on pDNA transfection efficiency.

Lastly, cells directly seeded onto the fabricated coaxial fiber mesh scaffolds showed successful expression of EGFP, and this expression was significantly higher than that observed on meshes containing pDNA alone. The increase in EGFP expression in meshes containing both PEI-HA and pDNA suggests that, despite separating the pDNA and the gene delivery vector (r-PEI-HA) in different components of the coaxial fibers, the pDNA and r-PEI-HA are able to form complexes, be it inside or outside of the coaxial fibers, which are able to transfect cells with a greater efficiency than released pDNA alone.

Conclusions

We have successfully designed coaxial electrospun fiber mesh scaffolds containing a non-viral gene delivery vector (r-PEI-HA) and pDNA within the sheath and core of the fiber, respectively. These studies elucidate the role of the processing parameters used to fabricate fiber meshes, i.e., (A) PCL sheath polymer Conc., (B) PEG core polymer MW, (C) PEG core polymer Conc., and (D) Conc. of pDNA within the fiber core, using a fractional factorial design. The results suggest that increasing the parameters above increases the average diameter of the fiber across all groups. Furthermore, the release of r-PEI-HA from the fiber sheath is dependent upon the concentration of pDNA, and the associated concentration of r-PEI-HA, embedded within the fibers. Most of the fabricated scaffolds show extended release of the gene delivery vector over a period of 60 days. Additionally, the transfection efficiency of the pDNA released from scaffolds also incorporating r-PEI-HA was sustained up to 60 days, and the transfection efficiency was dependent upon the concentration and MW of the core polymer, (PEG). Since statistical differences in transfection were observed between groups at different time points, it can be surmised that coaxial fiber mesh scaffolds with differential transfection properties can be fabricated by changing the parameters examined in this study. Such scaffolds with variable and sustained transfection properties can be applied for tissue engineering and other gene delivery applications involving gene therapy.

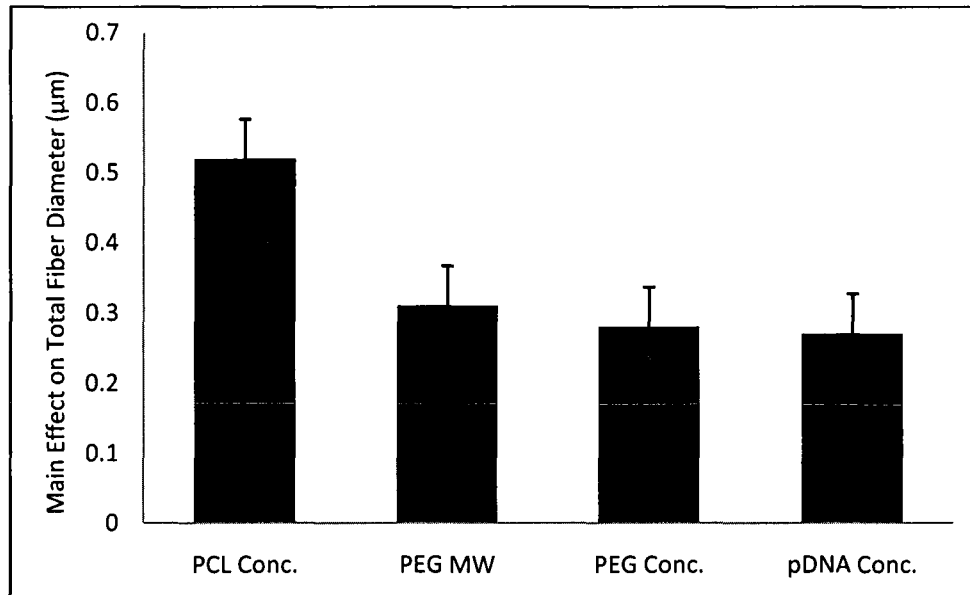
Figures

Figure 5.1: Main effects of PCL Conc., PEG MW, PEG Conc., and pDNA Conc. on average total fiber diameter of electrospun coaxial fiber meshes. A positive number represents an increasing effect of the particular parameter as its value increases from low (-1) to high (+1); the low (-1) and high (+1) values of the respective parameters are listed in Table 5.1. Error bars represent standard error of the effect for n=3 per scaffold type (and thirty fibers per scaffold).

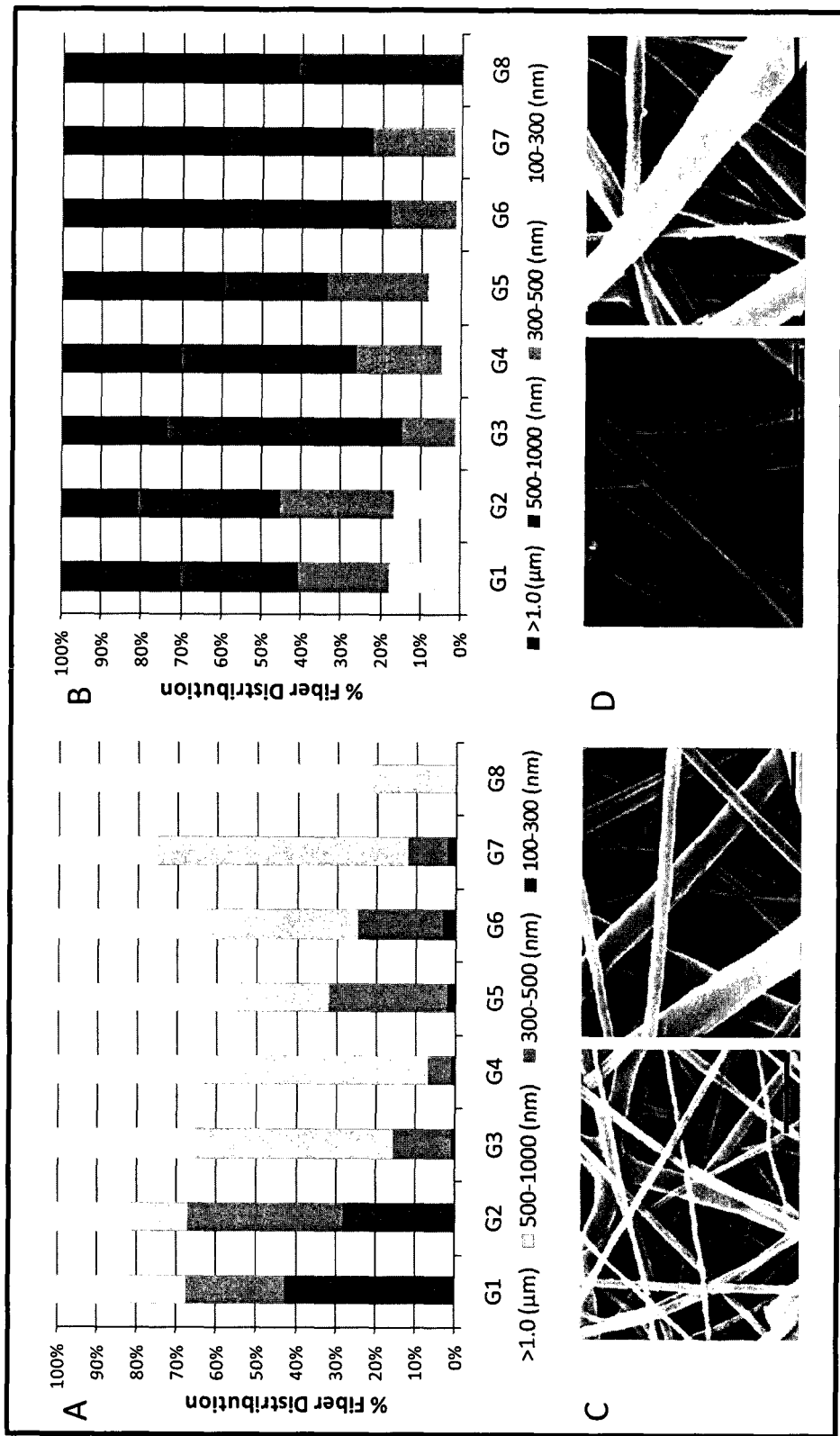


Figure 5.2: Fiber diameter distribution within electrospun coaxial meshes immediately after fabrication (A) and after immersion and agitation in PBS for 7 days (B), with their respective SEM images (C and D). Horizontal bars represent 2 μm.

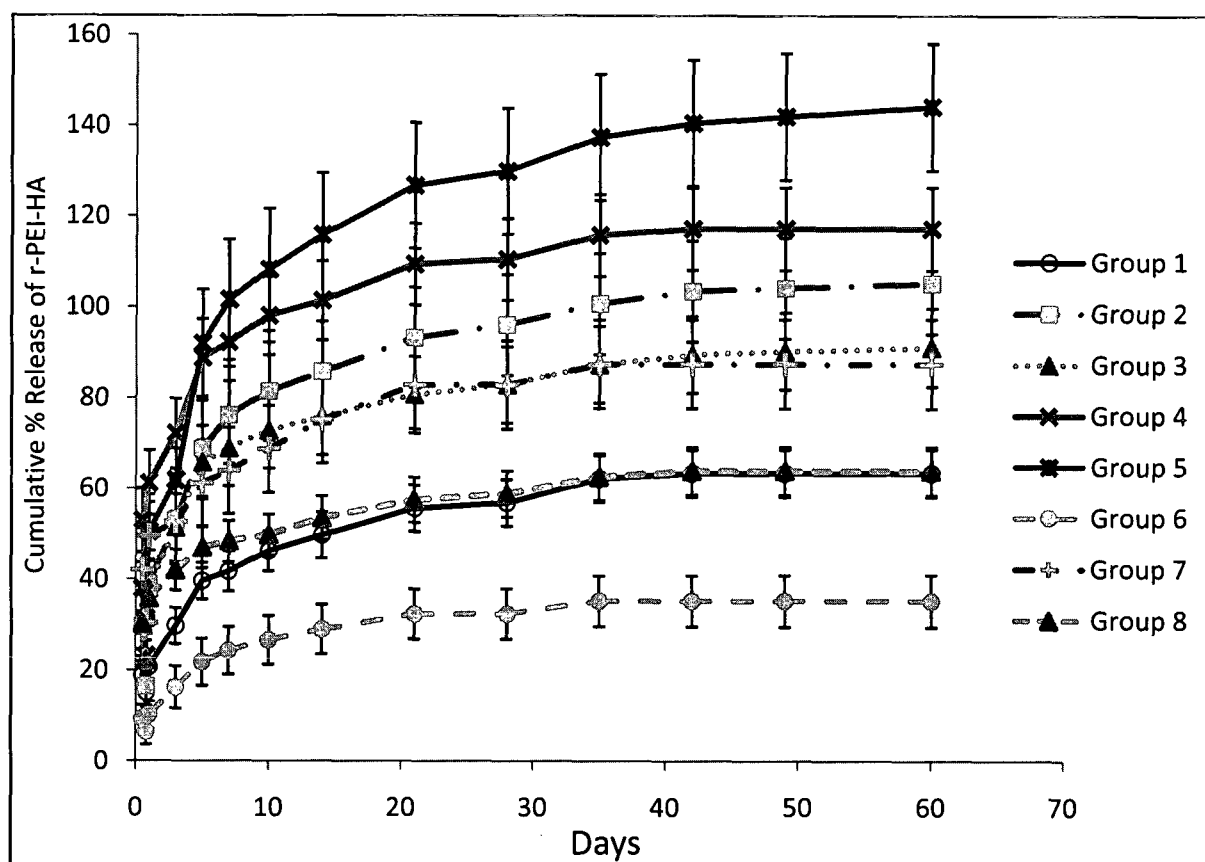


Figure 5.3: Cumulative release of rhodamine-tagged PEI-HA (r-PEI-HA) from electrospun coaxial fiber meshes at 37 °C in PBS with agitation at 115 rpm. Error bars represent standard deviation for n=4.

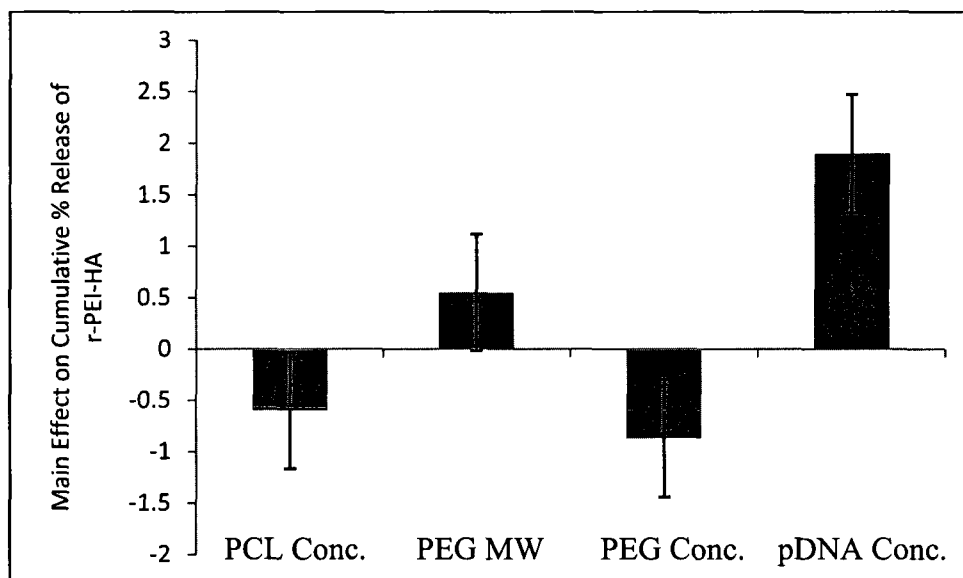


Figure 5.4: Main effects of PCL Conc., PEG MW, PEG Conc., and pDNA Conc. on r-PEI-HA release. A positive number represents an increasing effect of the particular parameter as its value increases from low (-1) to high (+1); the low (-1) and high (+1) values of the respective parameters are listed in Table 5.1. Error bars represent standard error of the effect for $n = 4$.

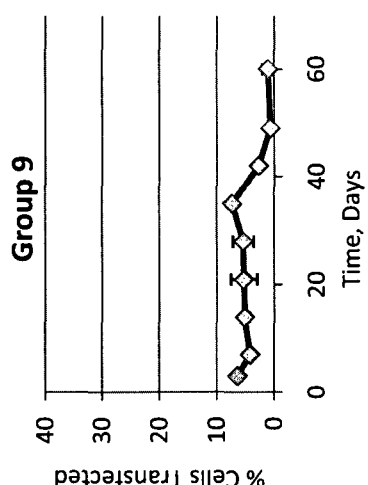
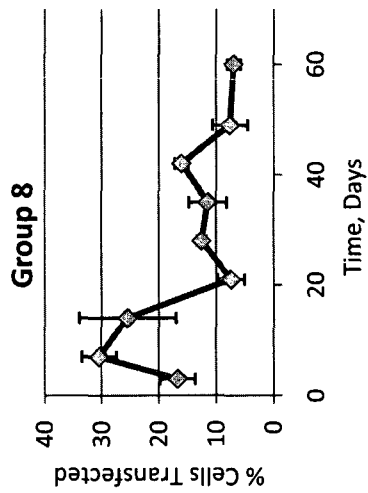
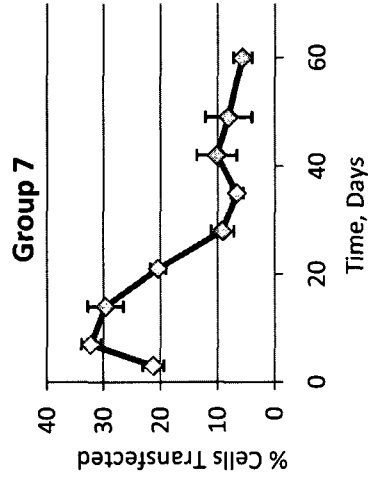
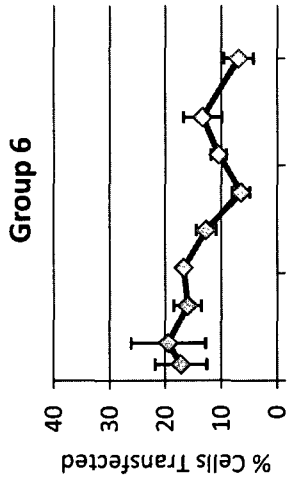
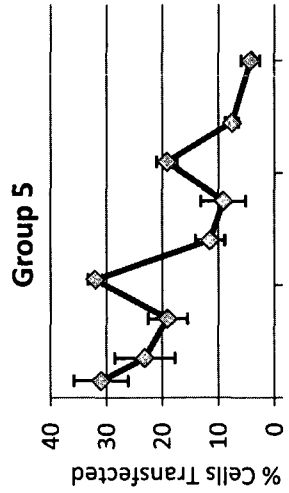
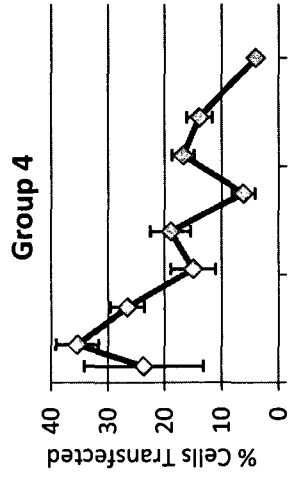
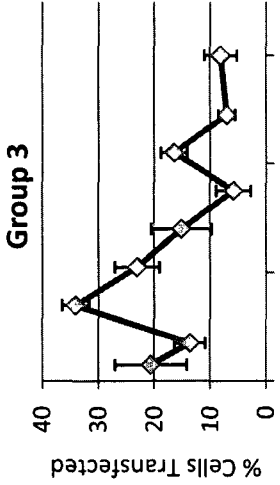
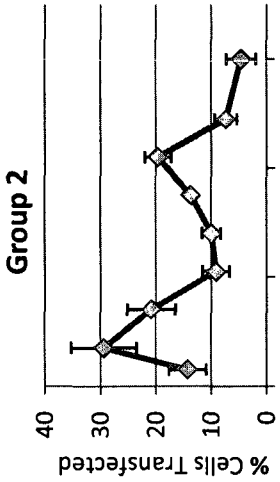
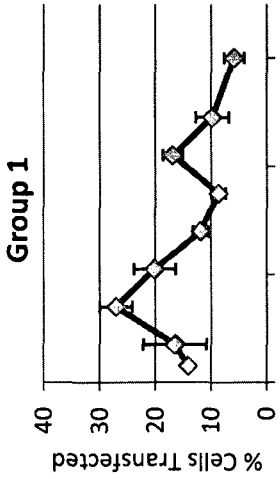


Figure 5.5: Transfection efficiency of released pDNA in 2D cultures of fibroblast-like cells (CRL 1764) over a period of 60 days. Formulation parameters of the Groups 1 to 8 are described in Table 5.1. Group 9 is composed of scaffolds containing pDNA within the fiber core and no r-PEI-HA during fabrication. Error bars represent standard deviation for $n = 4$.

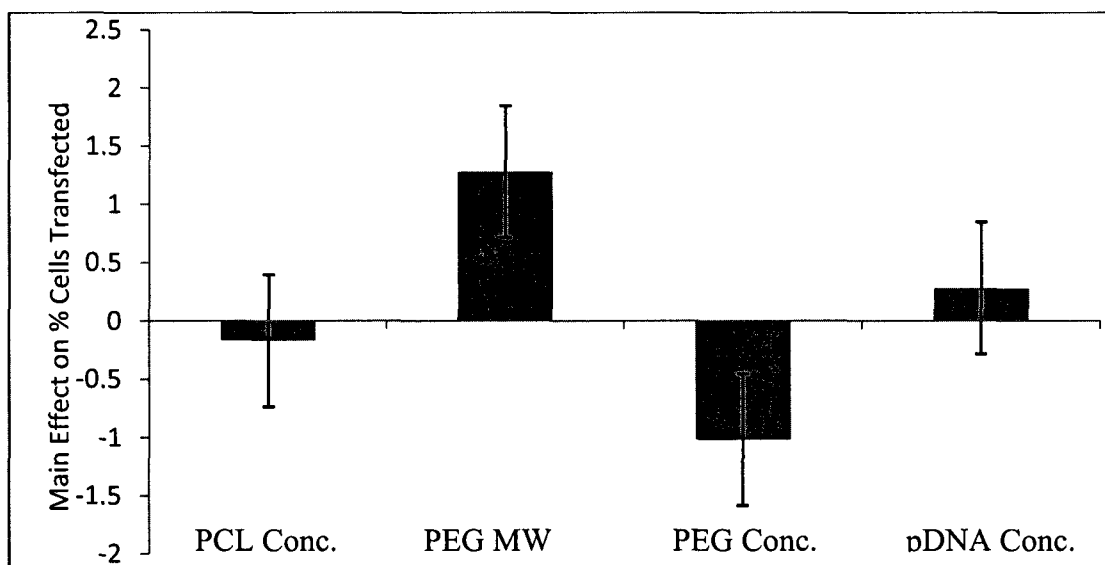
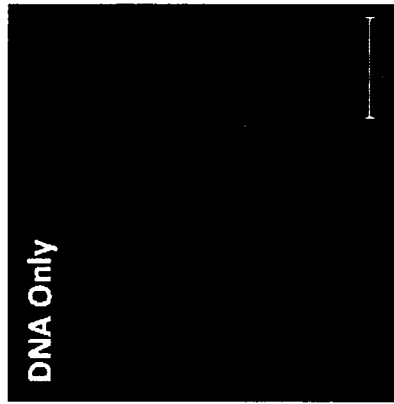
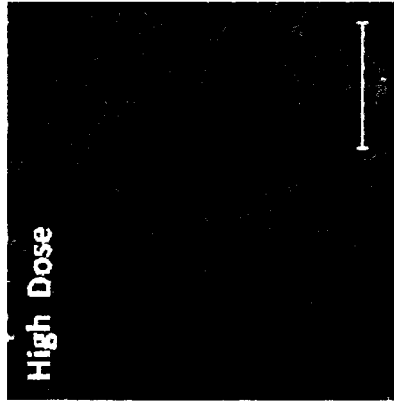
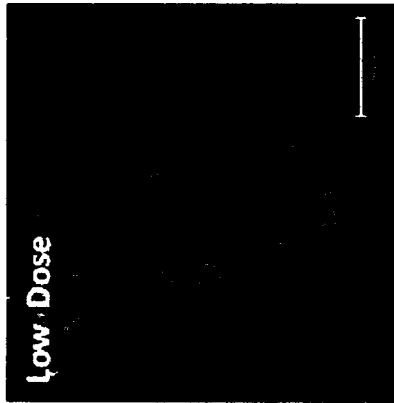
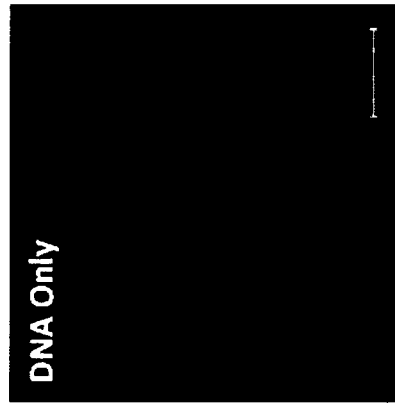
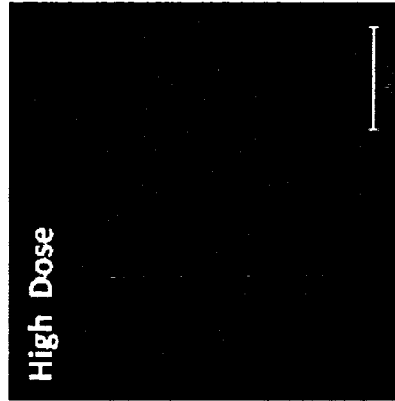
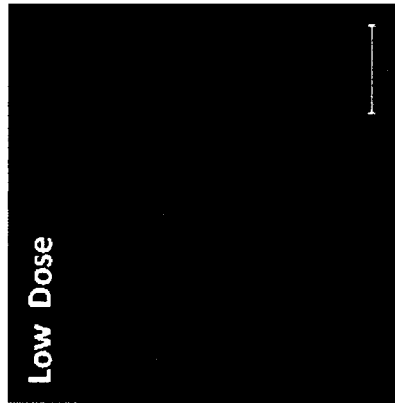


Figure 5.6: Main effects of PCL Conc., PEG MW, PEG Conc., and pDNA Conc. on cell transfection efficiency. A positive number represents an increasing effect of the particular parameter as its value increases from low (-1) to high (+1); the low (-1) and high (+1) values of the respective parameters are listed in Table 5.1. Error bars represent standard error of the effect for $n=4$.

Day 3



Day 28



Day 60

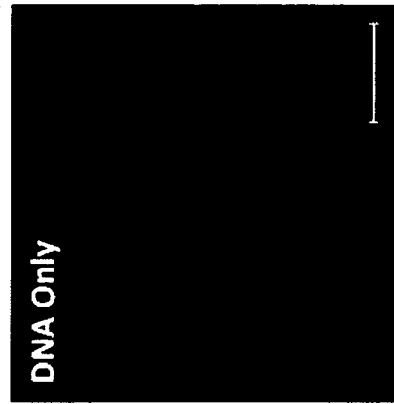
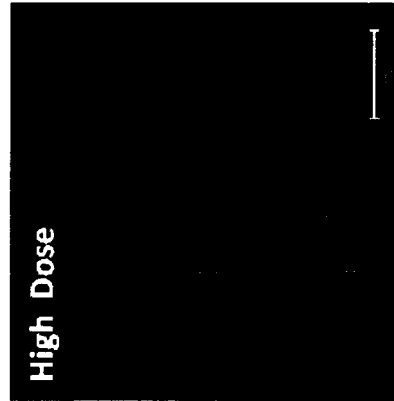
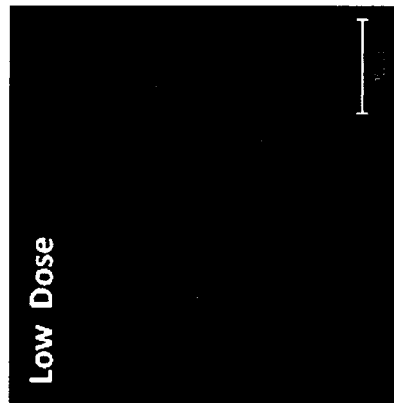


Figure 5.7: Expression of EGFP by cells seeded on electrospun fiber mesh scaffolds at Day 0, Day 28 and Day 60. Horizontal bars represent 100 μm .

Tables

Parameters	PCL Concentration	PEG Molecular Weight	PEG Concentration	pDNA Concentration
Group 1	-1	-1	-1	-1
Group 2	-1	-1	1	1
Group 3	-1	1	-1	1
Group 4	-1	1	1	-1
Group 5	1	-1	-1	1
Group 6	1	-1	1	-1
Group 7	1	1	-1	-1
Group 8	1	1	1	1
High (+1)	16 wt%	4.6 kDa	300 mg/mL	4 mg/mL
Low (-1)	14 wt%	3.3 kDa	150 mg/mL	2 mg/mL

Table 5.1: Fractional factorial experimental design for fabrication of coaxial electrospun fiber mesh scaffolds.

	Burst Release (0 - 24 hrs)	Phase 1 (2 - 10 days) %/day	Phase 2 (11 - 28 days) %/day	Phase 3 (35 - 60 days) %/day	Cumulative % Theoretical Loading
Group 1	22.6 ± 1.9 ^{#†}	3.1 ± 0.4	0.7 ± 0.2	0.2 ± 0.0	63.4 ± 5.2 ^{††}
Group 2	34.5 ± 9.4 ^{††}	4.6 ± 1.4	0.9 ± 0.1	0.3 ± 0.1	105.2 ± 11.1 [#]
Group 3	37.8 ± 7.6 [*]	4.4 ± 0.7	0.6 ± 0.1	0.3 ± 0.1	91.1 ± 8.6 ^{#††}
Group 4	43.1 ± 14.7 [*]	4.9 ± 0.3	0.7 ± 0.2	0.2 ± 0.0	117.2 ± 9.2 [#]
Group 5	46.7 ± 10.4 [*]	6.3 ± 1.6	1.2 ± 0.4	0.4 ± 0.2	144.1 ± 14.0 [*]
Group 6	9.3 ± 1.8 [#]	2.1 ± 0.7	0.3 ± 0.0	0.1 ± 0.1	35.2 ± 5.7 [†]
Group 7	47.3 ± 13.3 [*]	2.1 ± 0.5	0.8 ± 1.0	0.2 ± 0.1	87.5 ± 9.8 ^{#††}
Group 8	35.0 ± 0.5 ^{*†}	1.8 ± 0.4	0.5 ± 0.3	0.2 ± 0.1	63.9 ± 5.4 ^{††}

Table 5.2: Percentage of r-PEI-HA released per day during burst (0-24hrs), Phase 1 (2-10 days), Phase 2 (11-28 days) and Phase 3 (35-60 days). Data are presented as means ± standard deviation. Groups having similar symbols are not statistically significant from each other within groups. There was no significant difference in release between Phase 1, Phase 2 and Phase 3.

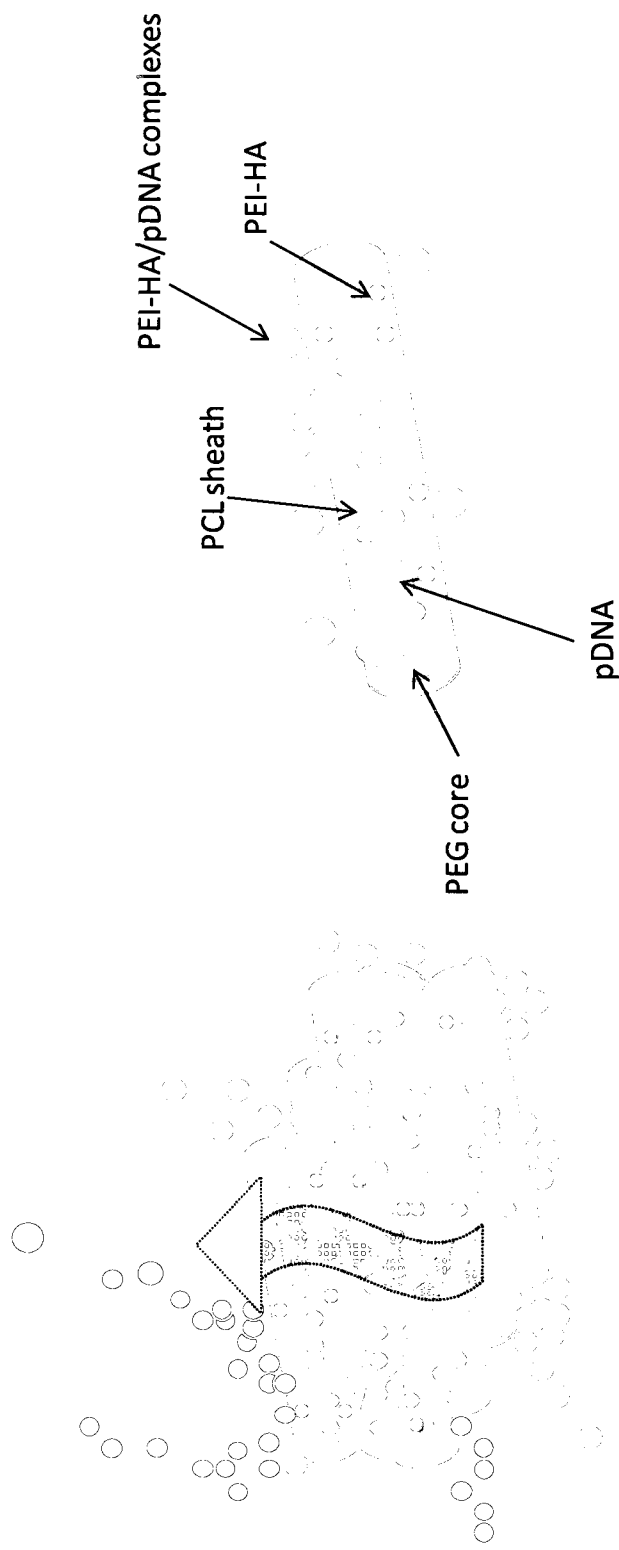
Group #	Mean \pm Standard Error
Group 1	14.45 \pm 0.62 ^{†¶}
Group 2	13.46 \pm 0.60 ^{†¶}
Group 3	16.23 \pm 0.60 ^{*#‡}
Group 4	17.54 \pm 0.60 [*]
Group 5	17.37 \pm 0.60 ^{*#}
Group 6	13.25 \pm 0.61 [¶]
Group 7	15.45 \pm 0.62 ^{*#‡}
Group 8	14.54 \pm 0.60 ^{#‡¶}

Table 5.3: Average transfection efficiencies over 60 days for 8 groups of coaxial electrospun fiber mesh scaffolds. Data are presented as means \pm standard error for n=4. Groups with similar symbols are not statistically different from each other.

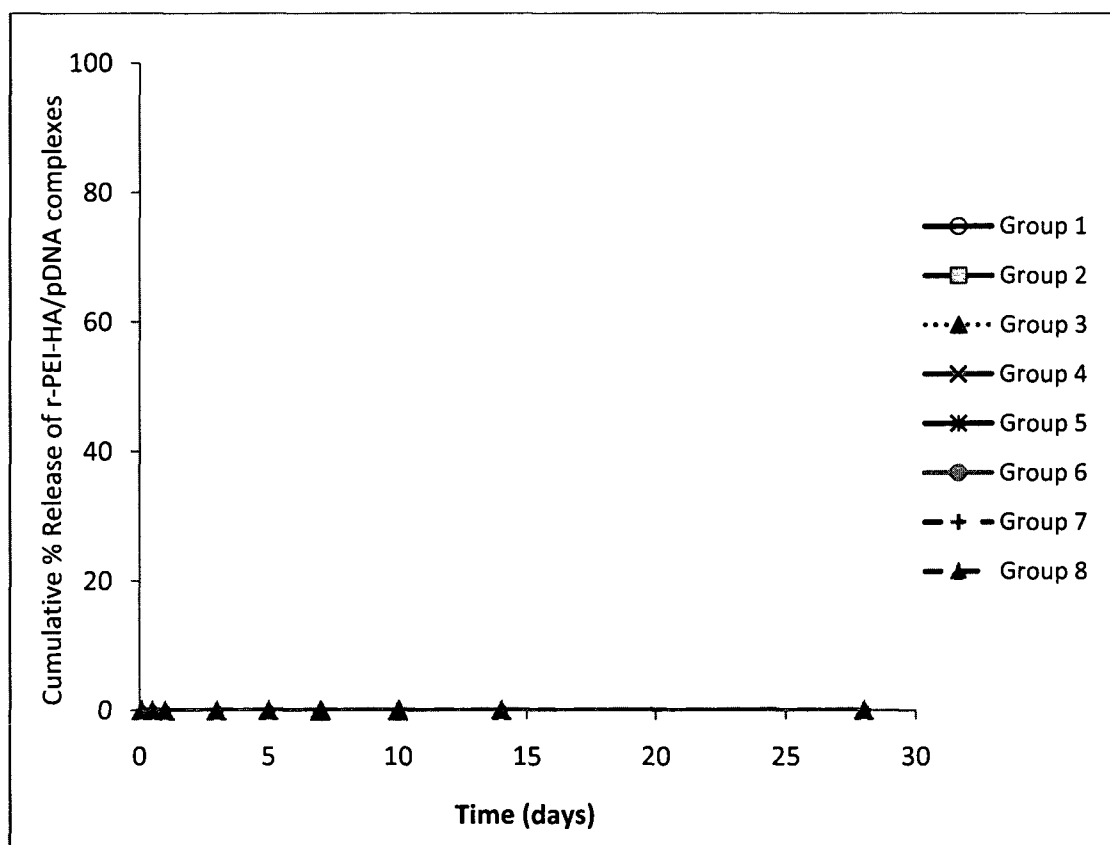
Supplemental Data

	PCL Conc.	Dextran MW	Dextran Conc.	pDNA Conc.
High	16 wt %	200 kDa	200 mg/mL	1.5 mg/mL
Low	14 wt %	68 kDa	100 mg/mL	0.5 mg/mL

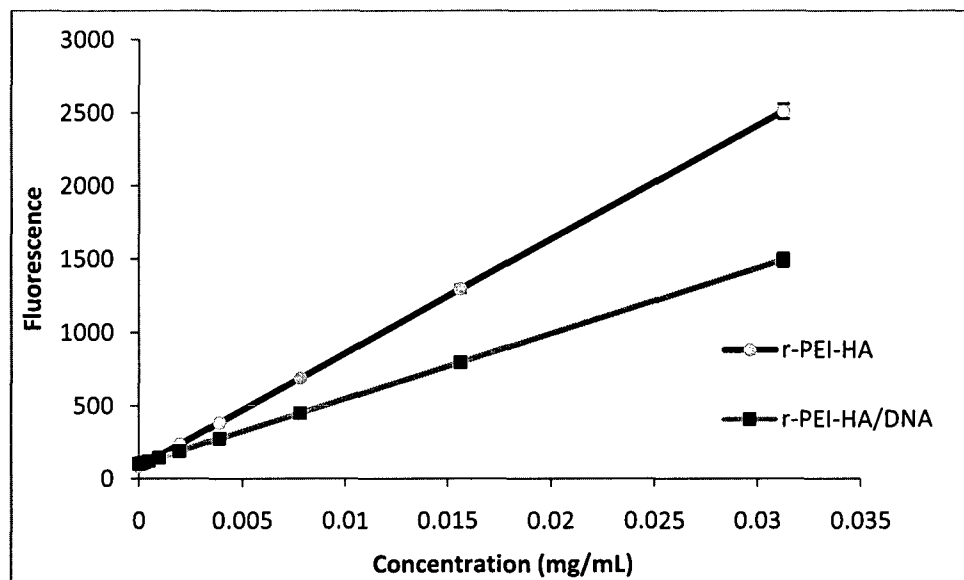
Supplemental Table 5.1: Values of parameters tested in a fractional factorial design in which PEI-HA/pDNA complexes were incorporated in the fiber core, with dextran as the core polymer.



Supplemental Figure 5.1: Schematic of the coaxial scaffolds loaded with PEI-HA and pDNA (left). Eight scaffold types were fabricated by changing four different factors (PEG Conc., PEG MW, PEG Conc., DNA Dose) at two different parameter levels as indicated in Table 5.1. Individual fiber of the coaxial scaffold indicating the location of the PCL sheath, PEG core, pDNA and PEI-HA (right). Studies described here suggest that PEI-HA and pDNA form complexes before transfecting fibroblast cells.



Supplemental Figure 5.2: Cumulative release of rhodamine-tagged PEI-HA (r-PEI-HA) from coaxial electrospun fiber meshes, where r-PEI-HA/pDNA complexes were preassembled and incorporated within the coaxial fiber core. Release samples were placed at 37 °C in PBS with agitation at 115 rpm. Error bars represent standard error for n=4.



Supplemental Figure 5.3: Representative fluorescence calibration curves for r-PEI-HA and r-PEI-HA/pDNA complexes at N:P ratio 7.5:1. Error bars represent standard deviation for n=3.

Chapter VI

Summary

The work presented in this thesis aims at adapting existing biomaterials to create novel and creative solutions for the purpose of tissue engineering. This was achieved by focusing on two application related to tissue engineering; firstly, non-viral gene delivery vectors that can effectively transfect multi-potent cells and secondly, novel three dimensional scaffolds that can present biological factors such as plasmids over extended durations.

A novel non-viral gene delivery vector was created by chemically conjugating PEI, a potent, inexpensive and widely used polymeric gene delivery vector, with HA a ubiquitous extracellular matrix molecule. A zwitterionic polymer containing a cationic PEI and anionic HA was thus synthesized. The novel vector thus created displayed significantly reduced cytotoxicity and better transfection efficiency on multipotent hMSCs. Further experiments with this novel polymer elucidated the role of ions in controlling the conformational dynamics of this vector, which provide significant insight into the behavior and optimization of zwitterionic polymers. This has implications in determining transfection efficiencies of non-viral gene delivery vectors.

In addition to non-viral gene delivery, biomaterials were used for the fabrication of three dimensional scaffolds through the process of coaxial electrospinning. PCL and PEG

were dissolved in organic and aqueous solvents respectively and spun together under the influence of the electric field to form sheath and core components (respectively) of a coaxial fiber mesh. A full factorial design evaluated the influence of PCL concentration, PEG concentration and molecular weight and the presence of salt within the aqueous core polymer solution. This study provided insights into the influence processing parameters have in fabricating fibers with variable morphologies.

Finally, PEI-HA and plasmid DNA were incorporated within the coaxial fibers and a fractional factorial design was implemented in understanding the role of processing parameters on fiber diameters, release kinetics and transfection efficiencies. Introduction of charged moieties such as PEI-HA and DNA significantly influenced the fiber diameters and morphologies of the fibers produced. Furthermore, the dose of PEI-HA or DNA influenced the release kinetics of the vector, whereas the core polymer properties influenced the transfection efficiencies observed. In summary, tunable release kinetics could be achieved by modulating the processing parameters used for the fabrication of coaxial electrospun fibers.

Although these scaffolds were synthesized with gene delivery in mind, the scaffolds are versatile in their applications. Similar results can be expected with the incorporation of other biological molecules. Furthermore, extended bioactivity observed with these scaffolds is an added bonus for tissue engineering and other applications related to gene delivery.

Future Direction

Although these studies provide a significant insight into the fabrication and application of three dimensional scaffolds for gene delivery purposes, numerous aspects of these experiments can be elaborated upon to optimize this gene delivery system. Firstly, the experiments described here utilize a single molecular weight of HA (2.3 kDa) conjugated to PEI at a single concentration. The influence of varying the molecular weight and percentage of chemical conjugation can potentially have an influence on the transfection efficiency and release kinetics. Furthermore, different molecular weights of HA oligomers have varied intracellular signaling effects which can be examined in the context of chondrogenesis or osteogenesis.

The potential of non-viral gene delivery applications are also numerous in the context of tissue engineering. Although traditional signaling molecules including TGF- β and BMPs can be encoded into plasmids and delivered with a potential increase in the efficacy of gene delivery with the system described here, it would also be interesting to investigate the feasibility of delivering plasmids encoding transcription factors such as Sox-5, Sox-6, Sox-9 and Runx-2 for chondrogenesis and osteogenesis applications. Since transcription factors initiate a signaling cascade that promote multi-potent cells along a specific differentiation pathway, the strategy of delivering transcription factors can be more effective than delivery of individual cytokines or signaling molecules from a tissue engineering perspective.

Lastly, it would be important to investigate the influence of the different types of scaffolds described here (i.e., with varying fiber diameters and fiber morphologies) on their ability to initiate and preserve chondrogenesis and osteogenesis in multi-potent cells such as hMSCs. Since fiber diameters play an important role in defining the porosity of these scaffolds, the pore size and porosity can potentially have an influence on gene expression, extracellular matrix production as well as the morphology of the cells seeded onto these scaffolds.

Chapter VII

Bibliography

1. Racial/ethnic differences in the prevalence and impact of doctor-diagnosed arthritis - United States 2002. *MMWR Morb Mortal Wkly Rep* **54**, 119-123(2005).
2. Madry, H. et al. Enhanced repair of articular cartilage defects in vivo by transplanted chondrocytes overexpressing insulin-like growth factor I (IGF-I). *Gene Ther* **12**, 1171-9(2005).
3. Laurencin, C.T. et al. Tissue engineering: orthopedic applications. *Annu Rev Biomed Eng* **1**, 19-46(1999).
4. Mason, J.M. et al. Cartilage and bone regeneration using gene-enhanced tissue engineering. *Clin Orthop Relat Res* S171-8(2000).
5. Kofron, M.D. & Laurencin, C.T. Orthopaedic applications of gene therapy. *Curr Gene Ther* **5**, 37-61(2005).
6. Visna, P. et al. Treatment of deep cartilage defects of the knee using autologous chondrograft transplantation and by abrasive techniques—a randomized controlled study. *Acta Chir Belg* **104**, 709-14(2004).
7. Bachmann, G. et al. MRI in the follow-up after MACI® or microfracture . *Radiologe* **44**, 773-782(2004).
8. Kolettas, E. et al. Chondrocyte phenotype and cell survival are regulated by culture conditions and by specific cytokines through the expression of Sox-9 transcription factor. *Rheumatology (Oxford)* **40**, 1146-56(2001).
9. Hardingham, T., Tew, S. & Murdoch, A. Tissue engineering: chondrocytes and cartilage. *Arthritis Research and Therapy* **4**, S63-S68(2002).
10. Young, A.A. et al. Regional assessment of articular cartilage gene expression and small proteoglycan metabolism in an animal model of osteoarthritis. *Arthritis Res Ther* **7**, R852-61(2005).

11. Wakitani, S. et al. Mesenchymal cell-based repair of large, full-thickness defects of articular cartilage. *J Bone Joint Surg Am* **76**, 579-92(1994).
12. Solchaga, L.A., Goldberg, V.M. & Caplan, A.I. Cartilage regeneration using principles of tissue engineering. *Clin Orthop Relat Res* S161-70(2001).
13. Jorgensen, C., Gordeladze, J. & Noel, D. Tissue engineering through autologous mesenchymal stem cells. *Curr Opin Biotechnol* **15**, 406-10(2004).
14. Saxer, R.A. et al. Gene mediated insulin-like growth factor-I delivery to the synovium. *J Orthop Res* **19**, 759-67(2001).
15. Nixon, A.J. et al. Insulinlike growth factor-I gene therapy applications for cartilage repair. *Clin Orthop Relat Res* S201-13(2000).
16. Sellers, R.S., Peluso, D. & Morris, E.A. The effect of recombinant human bone morphogenetic protein-2 (rhBMP-2) on the healing of full-thickness defects of articular cartilage. *J Bone Joint Surg Am* **79**, 1452-63(1997).
17. Gelse, K. et al. Articular cartilage repair by gene therapy using growth factor-producing mesenchymal cells. *Arthritis Rheum* **48**, 430-41(2003).
18. Djouad, F. et al. Immunosuppressive effect of mesenchymal stem cells favors tumor growth in allogeneic animals. *Blood* **102**, 3837-44(2003).
19. Le Blanc, K. et al. Mesenchymal Stem Cells Inhibit and Stimulate Mixed Lymphocyte Cultures and Mitogenic Responses Independently of the Major Histocompatibility Complex. *Scandinavian Journal of Immunology* **57**, 11-20(2003).
20. Evans, C.H. et al. Gene therapy for rheumatic diseases. *Arthritis Rheum* **42**, 1-16(1999).
21. Trippel, S.B., Ghivizzani, S.C. & Nixon, A.J. Gene-based approaches for the repair of articular cartilage. *Gene Ther* **11**, 351-9(2004).
22. Gouze, E. et al. In vivo gene delivery to synovium by lentiviral vectors. *Mol Ther* **5**, 397-404(2002).

23. Evans, C.H. et al. Clinical trials in the gene therapy of arthritis. *Clin Orthop Relat Res* **S300-7**(2000).
24. Makarov, S.S. et al. Suppression of experimental arthritis by gene transfer of interleukin 1 receptor antagonist cDNA. *Proc Natl Acad Sci U S A* **93**, 402-6(1996).
25. Bakker, A.C. et al. Overexpression of active TGF-beta-1 in the murine knee joint: evidence for synovial-layer-dependent chondro-osteophyte formation. *Osteoarthritis Cartilage* **9**, 128-36(2001).
26. Mi, Z. et al. Adverse effects of adenovirus-mediated gene transfer of human transforming growth factor beta 1 into rabbit knees. *Arthritis Res Ther* **5**, R132-9(2003).
27. Tuli, R. et al. Transforming growth factor-beta-mediated chondrogenesis of human mesenchymal progenitor cells involves N-cadherin and mitogen-activated protein kinase and Wnt signaling cross-talk. *J Biol Chem* **278**, 41227-36(2003).
28. Shuler, F.D. et al. Increased matrix synthesis following adenoviral transfer of a transforming growth factor beta1 gene into articular chondrocytes. *J Orthop Res* **18**, 585-92(2000).
29. Alvarez, J. et al. TGFbeta2 mediates the effects of hedgehog on hypertrophic differentiation and PTHrP expression. *Development* **129**, 1913-24(2002).
30. Pepper, M. et al. Chondrocytes inhibit endothelial sprout formation in vitro: Evidence for involvement of a transforming growth factor-beta. *Journal of Cellular Physiology* **146**, 170-179(1991).
31. Lee, J.Y. et al. New use of a three-dimensional pellet culture system for human intervertebral disc cells: initial characterization and potential use for tissue engineering. *Spine* **26**, 2316-22(2001).
32. Mi, Z. et al. Adverse effects of adenovirus-mediated gene transfer of human transforming growth factor beta 1 into rabbit knees. *Arthritis Res Ther* **5**, R132-R139(2003).
33. Grande, D.A. et al. Stem cells as platforms for delivery of genes to enhance cartilage repair. *J Bone Joint Surg Am* **85-A Suppl 2**, 111-6(2003).

34. Smith, P. et al. Genetic enhancement of matrix synthesis by articular chondrocytes: Comparison of different growth factor genes in the presence and absence of interleukin-1. *Arthritis and Rheumatism* **43**, 1156-1164(2000).
35. Lefebvre, V. & Smits, P. Transcriptional control of chondrocyte fate and differentiation. *Birth Defects Research Part C: Embryo Today: Reviews* **75**, 200-212(2005).
36. Lefebvre, V. et al. SOX9 is a potent activator of the chondrocyte-specific enhancer of the pro alpha1(II) collagen gene. *Mol. Cell. Biol* **17**, 2336-2346(1997).
37. Ng, L.J. et al. SOX9 binds DNA, activates transcription, and coexpresses with type II collagen during chondrogenesis in the mouse. *Dev. Biol* **183**, 108-121(1997).
38. Bridgewater, L.C., Lefebvre, V. & de Crombrughe, B. Chondrocyte-specific enhancer elements in the Col11a2 gene resemble the Col2a1 tissue-specific enhancer. *J. Biol. Chem* **273**, 14998-15006(1998).
39. Bi, W. et al. Sox9 is required for cartilage formation. *Nat. Genet* **22**, 85-89(1999).
40. Ikeda, T. et al. The combination of SOX5, SOX6, and SOX9 (the SOX trio) provides signals sufficient for induction of permanent cartilage. *Arthritis Rheum* **50**, 3561-73(2004).
41. Lefebvre, V., Behringer, R.R. & de Crombrughe, B. L-Sox5, Sox6 and Sox9 control essential steps of the chondrocyte differentiation pathway. *Osteoarthr. Cartil* **9 Suppl A**, S69-75(2001).
42. Hoffmann, A. et al. The T-box transcription factor Brachyury mediates cartilage development in mesenchymal stem cell line C3H10T1/2. *J Cell Sci* **115**, 769-81(2002).
43. Apparailly, F. et al. Adenovirus-mediated transfer of viral IL-10 gene inhibits murine collagen-induced arthritis. *J Immunol* **160**, 5213-20(1998).
44. Bessis, N. et al. Encapsulation in hollow fibres of xenogeneic cells engineered to secrete IL-4 or IL-13 ameliorates murine collagen-induced arthritis (CIA). *Clin Exp Immunol* **117**, 376-82(1999).

45. Bakker, A. et al. Overexpression of active TGF-beta-1 in the murine knee joint: Evidence for synovial-layer-dependent chondro-osteophyte formation. *Osteoarthritis and Cartilage* **9**, 128-136(2001).
46. Verma, I.M. & Somia, N. Gene therapy — promises, problems and prospects. *Nature* **389**, 239-42(1997).
47. Lubberts, E. et al. IL-4 gene therapy for collagen arthritis suppresses synovial IL-17 and osteoprotegerin ligand and prevents bone erosion. *J Clin Invest* **105**, 1697-710(2000).
48. Gelse, K. et al. Fibroblast-mediated delivery of growth factor complementary DNA into mouse joints induces chondrogenesis but avoids the disadvantages of direct viral gene transfer. *Arthritis Rheum* **44**, 1943-53(2001).
49. Goomer, R.S. et al. Nonviral in vivo gene therapy for tissue engineering of articular cartilage and tendon repair. *Clin Orthop Relat Res* S189-200(2000).
50. Baragi, V.M. et al. Transplantation of adenovirally transduced allogeneic chondrocytes into articular cartilage defects in vivo. *Osteoarthritis Cartilage* **5**, 275-82(1997).
51. Mason, J. et al. Cartilage and bone regeneration using gene-enhanced tissue engineering. *Clinical Orthopaedics and Related Research* (2000).
52. Ng, K.W. et al. A layered agarose approach to fabricate depth-dependent inhomogeneity in chondrocyte-seeded constructs. *Journal of Orthopaedic Research* **23**, 134-141(2005).
53. Saxer, R. et al. Gene mediated insulin-like growth factor-I delivery to the synovium. *Journal of Orthopaedic Research* **19**, 759-767(2001).
54. Adachi, N. et al. Muscle derived, cell based ex vivo gene therapy for treatment of full thickness articular cartilage defects. *J Rheumatol* **29**, 1920-30(2002).
55. Ho, Y.C. et al. Highly efficient baculovirus-mediated gene transfer into rat chondrocytes. *Biotechnol Bioeng* **88**, 643-51(2004).
56. Dinser, R. et al. Comparison of long-term transgene expression after non-viral and adenoviral gene transfer into primary articular chondrocytes. *Histochem Cell Biol* **116**, 69-77(2001).

57. Doherty, P.J. et al. Resurfacing of articular cartilage explants with genetically-modified human chondrocytes in vitro. *Osteoarthritis Cartilage* **6**, 153-9(1998).
58. Goomer, R. et al. Nonviral in vivo gene therapy for tissue engineering of articular cartilage and tendon repair. *Clinical Orthopaedics and Related Research* (2000).
59. Bakker, A. et al. Prevention of murine collagen-induced arthritis in the knee and ipsilateral paw by local expression of human interleukin-1 receptor antagonist protein in the knee. *Arthritis and Rheumatism* **40**, 893-900(1997).
60. Godbey, W.T., Wu, K.K. & Mikos, A.G. Poly(ethylenimine) and its role in gene delivery. *J Control Release* **60**, 149-60(1999).
61. Grosse, S. et al. Lactosylated polyethylenimine for gene transfer into airway epithelial cells: role of the sugar moiety in cell delivery and intracellular trafficking of the complexes. *J Gene Med* **6**, 345-56(2004).
62. Zanta, M.A. et al. In vitro gene delivery to hepatocytes with galactosylated polyethylenimine. *Bioconjug Chem* **8**, 839-44(1997).
63. Kunath, K. et al. Galactose-PEI-DNA complexes for targeted gene delivery: degree of substitution affects complex size and transfection efficiency. *J Control Release* **88**, 159-72(2003).
64. Kassem, M. Stem cells: potential therapy for age-related diseases. *Ann. N. Y. Acad. Sci* **1067**, 436-442(2006).
65. Caplan, A.I. & Bruder, S.P. Mesenchymal stem cells: building blocks for molecular medicine in the 21st century. *Trends Mol Med* **7**, 259-264(2001).
66. Incani, V. et al. Palmitic acid substitution on cationic polymers for effective delivery of plasmid DNA to bone marrow stromal cells. *J Biomed Mater Res A* **81**, 493-504(2007).
67. Kim, S. et al. Efficacy and cytotoxicity of cationic-agent-mediated nonviral gene transfer into osteoblasts. *J Biomed Mater Res A* **71**, 308-315(2004).
68. Aluigi, M. et al. Nucleofection is an efficient nonviral transfection technique for human bone marrow-derived mesenchymal stem cells. *Stem Cells* **24**, 454-461(2006).

69. Nakashima, S. et al. Highly efficient transfection of human marrow stromal cells by nucleofection. *Transplant Proc* **37**, 2290-2(2005).
70. Lisignoli, G. et al. Hyaluronan-based polymer scaffold modulates the expression of inflammatory and degradative factors in mesenchymal stem cells: Involvement of Cd44 and Cd54. *J Cell Physiol* **207**, 364-73(2006).
71. Knudson, C.B. Hyaluronan and CD44: strategic players for cell-matrix interactions during chondrogenesis and matrix assembly. *Birth Defects Res C Embryo Today* **69**, 174-96(2003).
72. Poulsom, R. CD44 and hyaluronan help mesenchymal stem cells move to a neighborhood in need of regeneration. *Kidney Int* **72**, 389
73. Kircheis, R. et al. Coupling of cell-binding ligands to polyethylenimine for targeted gene delivery. *Gene Ther* **4**, 409-18(1997).
74. Kichler, A. Gene transfer with modified polyethylenimines. *J Gene Med* **6 Suppl 1**, S3-10(2004).
75. Spees, J.L. et al. Internalized antigens must be removed to prepare hypoinmunogenic mesenchymal stem cells for cell and gene therapy. *Mol Ther* **9**, 747-56(2004).
76. Neu, M., Fischer, D. & Kissel, T. Recent advances in rational gene transfer vector design based on poly(ethylene imine) and its derivatives. *J Gene Med* **7**, 992-1009(2005).
77. Boussif, O. et al. Synthesis of Polyallylamine Derivatives and Their Use as Gene Transfer Vectors in Vitro. *Bioconjugate Chem.* **10**, 877-883(1999).
78. Ito, T. et al. Hyaluronic acid and its derivative as a multi-functional gene expression enhancer: Protection from non-specific interactions, adhesion to targeted cells, and transcriptional activation. *Journal of Controlled Release* **112**, 382(2006).
79. Segura, T., Chung, P.H. & Shea, L.D. DNA delivery from hyaluronic acid-collagen hydrogels via a substrate-mediated approach. *Biomaterials* **26**, 1575(2005).
80. West, D.C. et al. Angiogenesis induced by degradation products of hyaluronic acid. *Science* **228**, 1324-1326(1985).

81. Feinberg, R.N. & Beebe, D.C. Hyaluronate in vasculogenesis. *Science* **220**, 1177-1179(1983).
82. Knudson, W. et al. Hyaluronan oligosaccharides perturb cartilage matrix homeostasis and induce chondrocytic chondrolysis. *Arthritis Rheum* **43**, 1165-1174(2000).
83. Mukhopadhyay, D. et al. Specificity of the tumor necrosis factor-induced protein 6-mediated heavy chain transfer from inter-alpha-trypsin inhibitor to hyaluronan: implications for the assembly of the cumulus extracellular matrix. *J Biol Chem* **279**, 11119-28(2004).
84. Sekiya, I. et al. Expansion of human adult stem cells from bone marrow stroma: conditions that maximize the yields of early progenitors and evaluate their quality. *Stem Cells* **20**, 530-541(2002).
85. Grande-Allen, K.J. et al. Glycosaminoglycans and proteoglycans in normal mitral valve leaflets and chordae: association with regions of tensile and compressive loading. *Glycobiology* **14**, 621-33(2004).
86. Calabro, A., Hascall, V.C. & Midura, R.J. Adaptation of FACE methodology for microanalysis of total hyaluronan and chondroitin sulfate composition from cartilage. *Glycobiology* **10**, 283-93(2000).
87. Calabro, A. et al. Microanalysis of enzyme digests of hyaluronan and chondroitin/dermatan sulfate by fluorophore-assisted carbohydrate electrophoresis (FACE). *Glycobiology* **10**, 273-281(2000).
88. Sakaguchi, H. et al. Isolation of reducing oligosaccharide chains from the chondroitin/dermatan sulfate-protein linkage region and preparation of analytical probes by fluorescent labeling with 2-aminobenzamide. *J Biochem (Tokyo)* **129**, 107-18(2001).
89. Godbey, W.T., Wu, K.K. & Mikos, A.G. Size matters: molecular weight affects the efficiency of poly(ethylenimine) as a gene delivery vehicle. *J Biomed Mater Res* **45**, 268-75(1999).
90. Temenoff, J.S. et al. In vitro cytotoxicity of redox radical initiators for cross-linking of oligo(poly(ethylene glycol) fumarate) macromers. *Biomacromolecules* **4**, 1605-13(2003).

91. Colter, D.C. et al. Rapid expansion of recycling stem cells in cultures of plastic-adherent cells from human bone marrow. *Proc. Natl. Acad. Sci. U.S.A* **97**, 3213-3218(2000).
92. Georgiou, T.K. et al. Nanoscopic Cationic Methacrylate Star Homopolymers: Synthesis by Group Transfer Polymerization, Characterization and Evaluation as Transfection Reagents. *Biomacromolecules* **5**, 2221-2229(2004).
93. Kvam, B.J. et al. ¹H- and ¹³C-NMR studies of solutions of hyaluronic acid esters and salts in methyl sulfoxide: comparison of hydrogen-bond patterns and conformational behaviour. *Carbohydr Res* **230**, 1-13(1992).
94. Volpi, N. & Maccari, F. Purification and characterization of hyaluronic acid from the mollusc bivalve *Mytilus galloprovincialis*. *Biochimie* **85**, 619-625(2003).
95. Hua, Q., Knudson, C.B. & Knudson, W. Internalization of hyaluronan by chondrocytes occurs via receptor-mediated endocytosis. *J Cell Sci* **106 (Pt 1)**, 365-75(1993).
96. Maleski, M.P. & Knudson, C.B. Hyaluronan-mediated aggregation of limb bud mesenchyme and mesenchymal condensation during chondrogenesis. *Exp Cell Res* **225**, 55-66(1996).
97. Farrell, L. et al. A comparison of the effectiveness of cationic polymers poly-L-lysine (PLL) and polyethylenimine (PEI) for non-viral delivery of plasmid DNA to bone marrow stromal cells (BMSC). *Eur J Pharm Biopharm* **65**, 388-397(2007).
98. Fischer, D. et al. In vitro cytotoxicity testing of polycations: influence of polymer structure on cell viability and hemolysis. *Biomaterials* **24**, 1121-31(2003).
99. Moghimi, S.M. et al. A two-stage poly(ethylenimine)-mediated cytotoxicity: implications for gene transfer/therapy. *Mol Ther* **11**, 990-5(2005).
100. Ogris, M. et al. The size of DNA/transferrin-PEI complexes is an important factor for gene expression in cultured cells. *Gene Ther* **5**, 1425-1433(1998).
101. Ogris, M. et al. The size of DNA/transferrin-PEI complexes is an important factor for gene expression in cultured cells. *Gene Ther* **5**, 1425-33(1998).

102. Cotten, M., Wagner, E. & Birnstiel, M.L. Receptor-mediated transport of DNA into eukaryotic cells. *Methods Enzymol* **217**, 618-44(1993).
103. Tang, M.X. & Szoka, F.C. The influence of polymer structure on the interactions of cationic polymers with DNA and morphology of the resulting complexes. *Gene Ther* **4**, 823-32(1997).
104. Yoshihiro Itoh, K.A.S.S. Solution and membrane properties of zwitterionic polymers. *Die Makromolekulare Chemie* **187**, 1691-1697(1986).
105. Godbey, W.T., Wu, K.K. & Mikos, A.G. Tracking the intracellular path of poly(ethylenimine)/DNA complexes for gene delivery. *Proc Natl Acad Sci U S A* **96**, 5177-81(1999).
106. Lungwitz, U. et al. Polyethylenimine-based non-viral gene delivery systems. *Eur J Pharm Biopharm* **60**, 247-66(2005).
107. Zhu, P. et al. The Influence of Solvent and Temperature Upon the Aggregation of Poly(ethylene glycol). *Macromolecular Chemistry and Physics* **202**, 1380-1383(2001).
108. Ali, A.A. New generation of super absorber nano-fibres hybrid fabric by electrospinning. *Journal of Materials Processing Technology* **199**, 193-198(2008).
109. Dersch, R. et al. Electrospinning of Nanofibres: Towards New Techniques, Functions, and Applications. *Aust. J. Chem.* **60**, 719-728 (2007).
110. Kang, Y. et al. Application of electrospun polyurethane web to breathable water-proof fabrics. *Fibers and Polymers* **8**, 564-570(2007).
111. Tan, K. & Obendorf, S.K. Fabrication and evaluation of electrospun nanofibrous antimicrobial nylon 6 membranes. *Journal of Membrane Science* **305**, 287-298(2007).
112. Goldberg, M.[., Langer, R.[. & Jia, X.[. Nanostructured materials for applications in drug delivery and tissue engineering. *Journal of Biomaterials Science, Polymer Edition* **18**, 241-268(2007).
113. Kenawy, E. et al. Controlled release of ketoprofen from electrospun poly(vinyl alcohol) nanofibers. *Materials Science and Engineering: A* **459**, 390-396(2007).

114. Tungprapa, S., Jangchud, I. & Supaphol, P. Release characteristics of four model drugs from drug-loaded electrospun cellulose acetate fiber mats. *Polymer* **48**, 5030-5041(2007).
115. Vaseashta, A. & Stamatina, I. Electrospun polymers for controlled release of drugs, vaccine delivery, and system-on-fibers. *Journal of Optoelectronics and Advanced Materials* **9**, 1606-1613(2007).
116. Yang, D., Li, Y. & Nie, J. Preparation of gelatin/PVA nanofibers and their potential application in controlled release of drugs. *Carbohydrate Polymers* **69**, 538-543(2007).
117. Hong, Y. et al. Generating Elastic, Biodegradable Polyurethane/Poly(lactide-co-glycolide) Fibrous Sheets with Controlled Antibiotic Release via Two-Stream Electrospinning. *Biomacromolecules* **9**, 1200-1207(2008).
118. Zhou, Y. et al. Electrospun Water-Soluble Carboxyethyl Chitosan/Poly(vinyl alcohol) Nanofibrous Membrane as Potential Wound Dressing for Skin Regeneration. *Biomacromolecules* **9**, 349-354(2008).
119. Kim, G.H. & Yoon, H. A direct-electrospinning process by combined electric field and air-blowing system for nanofibrous wound-dressings. *Applied Physics A: Materials Science & Processing* **90**, 389-394(2008).
120. Chen, J., Chang, G. & Chen, J. Electrospun collagen/chitosan nanofibrous membrane as wound dressing. *Colloids and Surfaces A: Physicochemical and Engineering Aspects* **313-314**, 183-188(2008).
121. Duan, Y. et al. Preparation of antimicrobial poly(ϵ -caprolactone) electrospun nanofibers containing silver-loaded zirconium phosphate nanoparticles. *Journal of Applied Polymer Science* **106**, 1208-1214(2007).
122. Han, I. et al. Effect of Poly(3-hydroxybutyrate-co-3-hydroxyvalerate) Nanofiber Matrices Cocultured With Hair Follicular Epithelial and Dermal Cells for Biological Wound Dressing. *Artificial Organs* **31**, 801-808(2007).
123. Silva, S.Y. et al. Double blind, randomized, placebo controlled clinical trial for the treatment of diabetic foot ulcers, using a nitric oxide releasing patch: PATHON. *Trials*. **8**, 26(2007).

124. Li, W. et al. Electrospun nanofibers immobilized with collagen for neural stem cells culture. *Journal of Materials Science: Materials in Medicine* **19**, 847-854(2008).
125. Moroni, L. et al. 3D Fiber-Deposited Electrospun Integrated Scaffolds Enhance Cartilage Tissue Formation. *Advanced Functional Materials* **18**, 53-60(2008).
126. Powell, H.M. & Boyce, S.T. Fiber density of electrospun gelatin scaffolds regulates morphogenesis of dermal-epidermal skin substitutes. *Journal of Biomedical Materials Research Part A* **84A**, 1078-1086(2008).
127. Andrews, K.D., Hunt, J.A. & Black, R.A. Technology of electrostatic spinning for the production of polyurethane tissue engineering scaffolds. *Polymer International* **57**, 203-210(2008).
128. Srouji, S. et al. 3-D Nanofibrous electrospun multilayered construct is an alternative ECM mimicking scaffold. *Journal of Materials Science: Materials in Medicine* **19**, 1249-1255(2008).
129. Mieszawska, A. et al. The Synthesis and Fabrication of One-Dimensional Nanoscale Heterojunctions. *Small* **3**, 722-756(2007).
130. Jin, M. et al. Large-scale fabrication of Ag nanoparticles in PVP nanofibres and net-like silver nanofibre films by electrospinning. *Nanotechnology* **18**, 075605(2007).
131. Nie, H. & Wang, C. Fabrication and characterization of PLGA/HAp composite scaffolds for delivery of BMP-2 plasmid DNA. *Journal of Controlled Release* **120**, 111-121(2007).
132. Fu, Y. et al. Optimized bone regeneration based on sustained release from three-dimensional fibrous PLGA/HAp composite scaffolds loaded with BMP-2. *Biotechnology and Bioengineering* **99**, 996-1006(2008).
133. Chew, S. et al. Aligned Protein-Polymer Composite Fibers Enhance Nerve Regeneration: A Potential Tissue-Engineering Platform. *Advanced Functional Materials* **17**, 1288-1296(2007).
134. Zeng, J. et al. Influence of the drug compatibility with polymer solution on the release kinetics of electrospun fiber formulation. *Journal of Controlled Release* **105**, 43-51(2005).

135. Qi et al. Encapsulation of Drug Reservoirs in Fibers by Emulsion Electrospinning: Morphology Characterization and Preliminary Release Assessment. *Biomacromolecules* **7**, 2327-2330(2006).
136. Zhang, Y.Z. et al. Coaxial Electrospinning of (Fluorescein Isothiocyanate-Conjugated Bovine Serum Albumin)-Encapsulated Poly(ϵ -caprolactone) Nanofibers for Sustained Release. *Biomacromolecules* **7**, 1049-1057(2006).
137. Jiang, H. et al. Modulation of protein release from biodegradable core-shell structured fibers prepared by coaxial electrospinning. *Journal of Biomedical Materials Research Part B: Applied Biomaterials* **79B**, 50-57(2006).
138. Liao, I.C., Chew, S.Y. & Leong, K.W. Aligned core-shell nanofibers delivering bioactive proteins. (2006)
139. Deitzel, J.M. et al. The effect of processing variables on the morphology of electrospun nanofibers and textiles. *Polymer* **42**, 261-272(2001).
140. Thompson, C. et al. Effects of parameters on nanofiber diameter determined from electrospinning model. *Polymer* **48**, 6913-6922(2007).
141. Zong, X. et al. Structure and process relationship of electrospun bioabsorbable nanofiber membranes. *Polymer* **43**, 4403-4412(2002).
142. Hohman, M.M. et al. Electrospinning and electrically forced jets. I. Stability theory. *Phys. Fluids* **13**, 2201-2220(2001).
143. Hohman, M.M. et al. Electrospinning and electrically forced jets. II. Applications. *Phys. Fluids* **13**, 2221-2236(2001).
144. Shin, Y.M. et al. Experimental characterization of electrospinning: the electrically forced jet and instabilities. *Polymer* **42**, 09955-09967(2001).
145. Casper, C.L. et al. Controlling Surface Morphology of Electrospun Polystyrene Fibers: Effect of Humidity and Molecular Weight in the Electrospinning Process. *Macromolecules* **37**, 573-578(2004).
146. Katti, D.S. et al. Bioresorbable nanofiber-based systems for wound healing and drug delivery: Optimization of fabrication parameters. *Journal of Biomedical Materials Research Part B: Applied Biomaterials* **70B**, 286-296(2004).

147. Wang, C. et al. Effect of concentration, voltage, take. *Pigment & Resin Technology* **35**, 278 - 283(2006).
148. Katti, D.S. et al. Bioresorbable nanofiber-based systems for wound healing and drug delivery: Optimization of fabrication parameters. *Journal of Biomedical Materials Research Part B: Applied Biomaterials* **70B**, 286-296(2004).
149. Zhang, Y. et al. Preparation of Core–Shell Structured PCL-r-Gelatin Bi-Component Nanofibers by Coaxial Electrospinning. *Chemistry of Materials* **16**, 3406-3409(2004).
150. Wang, M. et al. Production of Submicron Diameter Silk Fibers under Benign Processing Conditions by Two-Fluid Electrospinning. *Macromolecules* **39**, 1102-1107(2006).
151. Pham, Q.P., Sharma, U. & Mikos, A.G. Electrospun poly(epsilon-caprolactone) microfiber and multilayer nanofiber/microfiber scaffolds: characterization of scaffolds and measurement of cellular infiltration. *Biomacromolecules* **7**, 2796-2805(2006).
152. Sun, Z. et al. Compound Core-Shell Polymer Nanofibers by Co-Electrospinning. *Advanced Materials* **15**, 1929-1932(2003).
153. Yu, J., Fridrikh, S. & Rutledge, G. Production of Submicrometer Diameter Fibers by Two-Fluid Electrospinning. *Advanced Materials* **16**, 1562-1566(2004).
154. Huang, Z. et al. Encapsulating drugs in biodegradable ultrafine fibers through coaxial electrospinning. *Journal of Biomedical Materials Research Part A* **77A**, 169-179(2006).
155. Koski, A., Yim, K. & Shivkumar, S. Effect of molecular weight on fibrous PVA produced by electrospinning. *Materials Letters* **58**, 493-497(2004).
156. Eda, G., Liu, J. & Shivkumar, S. Flight path of electrospun polystyrene solutions: Effects of molecular weight and concentration. *Materials Letters* **61**, 1451-1455(2007).
157. Fridrikh, S.V. et al. Controlling the Fiber Diameter during Electrospinning. *Phys. Rev. Lett.* **90**, 144502(2003).

158. Hou, H. et al. Poly(p-xylylene) Nanotubes by Coating and Removal of Ultrathin Polymer Template Fibers. *Macromolecules* **35**, 2429-2431(2002).
159. Reneker, D.H. & Chun, I. Nanometre diameter fibres of polymer, produced by electrospinning. *Nanotechnology* **7**, 216-223(1996).
160. Rueda, N. et al. Factorial design for the evaluation of the influence of preparation parameters upon the properties of dispersed molybdenum sulfide catalysts. *Applied Catalysis A: General* **215**, 81-89(2001).
161. Tessmar, J.K. & Göpferich, A.M. Matrices and scaffolds for protein delivery in tissue engineering. *Adv. Drug Deliv. Rev* **59**, 274-291(2007).
162. Shea, L.D. et al. DNA delivery from polymer matrices for tissue engineering. *Nat Biotech* **17**, 551-554(1999).
163. Storrie, H. & Mooney, D.J. Sustained delivery of plasmid DNA from polymeric scaffolds for tissue engineering. *Adv. Drug Deliv. Rev* **58**, 500-514(2006).
164. Bonadio, J. Tissue engineering via local gene delivery. *Journal of Molecular Medicine* **78**, 303-311(2000).
165. Liang, D. et al. In vitro non-viral gene delivery with nanofibrous scaffolds. *Nucleic Acids Res* **33**, e170(2005).
166. Luu, Y.K. et al. Development of a nanostructured DNA delivery scaffold via electrospinning of PLGA and PLA-PEG block copolymers. *J Control Release* **89**, 341-53(2003).
167. Heyde, M. et al. Development of a slow non-viral DNA release system from PDLLA scaffolds fabricated using a supercritical CO technique. *Biotechnology and Bioengineering* **98**, 679-693(2007).
168. Lim, S.H., Liao, I. & Leong, K.W. Nonviral Gene Delivery from Nonwoven Fibrous Scaffolds Fabricated by Interfacial Complexation of Polyelectrolytes. *Mol Ther* **13**, 1163-1172(2006).
169. Luo, D. et al. Controlled DNA Delivery Systems. *Pharmaceutical Research* **16**, 1300-1308(1999).

170. Tinsley-Bown, A.M. et al. Formulation of poly(-lactic-co-glycolic acid) microparticles for rapid plasmid DNA delivery. *Journal of Controlled Release* **66**, 229-241(2000).
171. Cohen-Sacks, H. et al. Delivery and expression of pDNA embedded in collagen matrices. *Journal of Controlled Release* **95**, 309-320(2004).
172. Jang, J.H. et al. Surface adsorption of DNA to tissue engineering scaffolds for efficient gene delivery. *J Biomed Mater Res A* **77**, 50-8(2006).
173. Shea, L.D. et al. DNA delivery from polymer matrices for tissue engineering. *Nat Biotech* **17**, 551-554(1999).
174. Huang, Y. et al. Long-term in vivo gene expression via delivery of PEI-DNA condensates from porous polymer scaffolds. *Hum. Gene Ther* **16**, 609-617(2005).
175. Fang, J. et al. Stimulation of new bone formation by direct transfer of osteogenic plasmid genes. *Proc Natl Acad Sci U S A.* **93**, 5753-5758(1996).
176. Huang, Y. et al. Bone regeneration in a rat cranial defect with delivery of PEI-condensed plasmid DNA encoding for bone morphogenetic protein-4 (BMP-4). *Gene Ther* **12**, 418-426(2005).
177. Sun, Z. et al. Compound Core-Shell Polymer Nanofibers by Co-Electrospinning. *Advanced Materials* **15**, 1929-1932(2003).
178. Yu, J., S. V. Fridrikh & G. C. Rutledge Production of Submicrometer Diameter Fibers by Two-Fluid Electrospinning. *Advanced Materials* **16**, 1562-1566(2004).
179. Pham, Q.P., Sharma, U. & Mikos, A.G. Electrospun poly(epsilon-caprolactone) microfiber and multilayer nanofiber/microfiber scaffolds: characterization of scaffolds and measurement of cellular infiltration. *Biomacromolecules* **7**, 2796-805(2006).
180. Allison, S.D., Molina, M.C. & Anchordoquy, T.J. Stabilization of lipid/DNA complexes during the freezing step of the lyophilization process: the particle isolation hypothesis. *Biochim Biophys Acta* **1468**, 127-38(2000).
181. Allison, S.D. & Anchordoquy, T.J. Mechanisms of protection of cationic lipid-DNA complexes during lyophilization. *Journal of Pharmaceutical Sciences* **89**, 682-691(2000).

182. Saraf, A. et al. Synthesis and conformational evaluation of a novel gene delivery vector for human mesenchymal stem cells. *Biomacromolecules* **9**, 818-27(2008).
183. Saraf, A. et al. Fabrication of Nonwoven Coaxial Fiber Meshes by Electrospinning. *Tissue Eng Part C Methods* (2009).doi:10.1089/ten.tec.2008.0422
184. Caliceti, P. et al. Effective protein release from PEG/PLA nano-particles produced by compressed gas anti-solvent precipitation techniques. *Journal of Controlled Release* **94**, 195-205(2004).
185. Ramos, de Vries, R. & Ruggiero Neto, J. DNA Ψ -Condensation and Reentrant Decondensation: Effect of the PEG Degree of Polymerization. *The Journal of Physical Chemistry B* **109**, 23661-23665(2005).